The Stress Corrosion Cracking of Maraging Steels

A thesis submitted as a requirement for the degree of Doctor of Philosophy at the University of Newcastle upon Tyne.

P. M. Haigh, B.Sc.,

Department of Metallurgy,

University of Newcastle upon Tyne.

July, 1970.

CONTENTS

Cont.. 2.

----0----

SYNOPSIS

The stress corrosion cracking of 18% Ni maraging steel has been investigated in 0.6 N sodium chloride solutions. The principal aim was to determine the dependence of the cracking process on structural and environmental variables.

The susceptibility towards intergranular stress corrosion cracking was found to be associated with the state of the prior austenite grain boundary network. Processing variables which produce changes in the size or chemical nature of the grain boundaries were found to have the greatest effect on susceptibility. The cracking propensity was found to be effected by solution pH and the process appeared to be under cathodic control. Crack initiation was associated with the formation of structurally independent surface fissures, whose growth depend on the solution condition rather than the pH value.

Investigations were carried out into the environmental conditions required to produce stress corrosion and hydrogen embrittlement failures. The evidence produced indicates that these two mechanisms can be characterised by the

potential range under which they occur and by the associated fracture surfaces. As a result the failures obtained for Maraging Steels in 0.6 N sodium chloride solutions under naturally corroding conditions, can be considered to be due to a stress corrosion cracking mechanism.

Introduction

The increasing development of the aerospace industry over the last fifteen years has produced a demand for materials which can withstand extremely high loads and adverse environmental conditions. Yield strengths of up to 100 t.s.i. can be obtained using medium-carbon low alloy steels, but these may be inadequate in other properties, e.g. ductility, fatigue strength, corrosion resistance and ease of fabrication, especially by welding. This demand for better overall properties in ultra-high strength materials lead to the development of the maraging steels (1, 2, 3, 4) the first series of which were developed by Beiber in 1958, being simple Fe - Ni - Ti - Al alloys, having high strength/toughness values obtained with a simple heat treatment. This involves age hardening of an iron-nickel martensite to produce strengths of up to 135 t.s.i. The steels have developed to provide a range of properties, but their application has been limited somewhat by their susceptibility towards stress corrosion cracking and

hydrogen embrittlement especially in the highest strength versions. Investigations have been carried out in these fields, but largely by ad hoc testing and results have been general in nature and largely incomplete. Throughout the present work an attempt has been made to rationalise the various factors governing susceptibility towards stress corrosion cracking and where possible identify the mechanisms involved.

PHYSICAL METALLURGY

1.1. Composition

Since the development of the first alloys (5) there has been a marked increase in the number of grades of maraging steels available. Commercial versions have certain common features (6); unwanted elements being kept as low as possible e.g. carbon = 0.03% (max.), silicon and manganese = 0.20% (max. total), sulphur and phosphorus each less than 0.01%. The alloy additions made depend upon the properties desired, the major grades falling within the composition ranges:-

Ni	12	-	25%
Co	8	-	10%
Mo	3	-	5%
Al	0.1	-	0.7%
Ti	0.2	-	1.6%

balance Fe

Recent trends have been towards a stainless maraging steel, possessing good corrosion resistant

properties with adequate strength and toughness. These tend to be cobalt-free, with the chromium and nickel contents balanced to give complete martensite transformation above room temperature, and the austenite reversion temperature above 480°C to permit aging of the matrix.

A typical composition is:-

6% Ni 15% Cr 0.75% Ti 0.03% C

which resembles the traditional precipitation hardenable 18/8 steels. Grades based on systems other than iron-nickel have been developed, in particular the copper maraging steels (7) containing 1 - 6% Cr, with additions of Ni, Si, and Cr, as required. These alloys, however, do not possess the same attractive range of properties as the nickel maraging steels and only have U.T.S. values of up to 70 t.s.i. in the fully aged condition.

Owing to the great variety of maraging steels, the following sections will only be concerned with the

effects specific to the 18 Ni grade.

The maraging steels offer several advantages in addition to those of high strength and toughness. Weldability is an attractive feature, as both fully aged and annealed material can be welded without preheat, and the joint given a simple post-weld age to produce a high strength section. Fatigue properties are as good as steels of equivalent strength, but corrosion resistance is often significantly worse, (the latter is covered in detail in a later section).

1.2 Heat Treatment

The standard treatment of commercial material involves age hardening of an iron-nickel martensite (8), the latter being produced by a solution treatment for 1 hour at 800°C, followed by air cooling to room temperature. This results in a b.c.c. martensite which is soft and ductile. Age hardening is achieved

by heating for 3 hours at 480°C, followed by air cooling. The overall dimensional changes are small and this enables machining to be carried out in the annealed condition. More complex heat treatments (9, 10) have been studied to produce specific properties, but these do not appear to have had significant practical use so far.

1.3 Microstructure

1.3.1 Austenite/Martensite formation

The iron-nickel equilibrium diagram is shown in Fig. 1. The indicated decomposition of austenite into ferrite in the relevant composition range does not occur in practice even with prolonged heat treatment, b.c.c. martensite forming a cooling. The amount of martensite formed is a function of nickel content (fig 2.) and is independent of the cooling rate employed. Several forms of martensite have been identified in other maraging steels, but in the 18 Ni grade the only form known at present is "massive" martensite, forming in long elongated platelets.

The original austenite grain size determines the size of the martensite platelets, which form with a wavy interface and have a high dislocation density, and the final strength of the steel depends to some extent upon the form of these platelets. Low M_s temperatures are to be avoided as these give a twinned martensite (13), which does not yield as tough a material as that formed with higher M_s temperatures. Alloying elements affect the M_s temperatures in much the same way as in conventional steels, i.e. cobalt raises, and molybdenum lowers the M_s temperature while nickel stabilises the austenite.

Reheating the martensite can lead to several reactions (14,15):-

(a) above the A_s temperature the martensite transforms by a shear mechanism back to austenite.

(b) below the A_s temperature martensite transforms

to alpha' and gamma'; where alpha' is a low nickel form of b.c.c. martensite and gamma' is a high nickel form of f.c.c. austenite. Cooling from regions where (a) or (b) occur produces martensite from the austenite and alpha' but the gamma' contains enough nickel to be stable at room temperature. Other elements affect the reversion reactions in similar ways according to their tendency to stabilise austenite or ferrite (16). Titanium, for example, retards reversion owing to the formation of Ni_3 Ti, which lowers the nickel content of the matrix; molybdenum has the opposite effect by enriching the nickel content as a result of Fe_2 Mo replacing Ni_3 Mo on prolonged aging (7).

Studies (18,19) on the work-hardening behaviour, the temperature and strain-rate dependence of the flow stress in these massive martensites indicate behaviour similar to those observed in low alloy steels.

1.3.2 Ausaging

This describes aging treatments carried out with material in the fully austenitic condition, and several workers (20, 21) have investigated the precipitation reactions occuring in the region of 700°C - i.e. above the normal maraging range and below the austenitising region. The alloys considered were the higher nickel maraging steels (22), from 25 - 28% and some possessed higher Ti, Al and Nb contents than usual. Ausaging at 700°C produced small spherical precipitates uniformly distributed and a cellular grain boundary precipitate, both believed to be gamma' Ni_3 (Ti, Al). These effects were only produced after prolonged aging of up to 100 hours. The effect of the precipitation is chiefly found in the M_s temperature, as removing elements from the solution causes the M_s temperature to rise, depending upon the amount of precipitation and the nature of the precipitates.

Steels which are ausaged, then subsequently maraged, tend to have higher final strengths than conventionally treated material, although the increase is only slight for the large increase in treatment time.

1.3.3 Maraging

The degree of hardening in these steels depends not only upon the minor additional elements, but also upon the nickel content, and the kinetics of the aging and reversion reactions. The elements which produce hardening can be classified into three principal groups:

(a) strong hardening - Be, Ti,

(b) medium hardening - Al, Nb, Mn, Mo, Si, Ta, V,

(c) weak hardening - Co, Cu, Zr.

These individual effects, however, may differ considerably when two or more elements are present in one alloy (section 1.4).

The identification of precipitates formed during maraging has been the subject of a great deal of work and comment, as a large number have been identified and

reported (Table 1.) Structural determinations are difficult owing to the small precipitate sizes, and several methods, e.g. X-Ray and electron microscope may involve extraction of precipitates from an overaged matrix, which could yield precipitates different from those found in the "normally" aged matrix, or introduce "foreign" diffraction lines e.g. fron oxide inclusions. The interpretation of the diffraction patterns is often confusing, as several phases believed to be present have similar standard patterns. The results, to date, however, do indicate certain trends in the 18 nickel grades. Aging for several hours at approximately 480°C produces Ni_3 Mo, and with prolonged aging, (or, at higher temperatures) Fe_2 Mo, laves or sigma phases have been detected. Work by Marcus et al (29) (using Mossbauer Spectroscopy) showed the Ni_3 Mo precipitate to be replaced by Fe_2 Mo after 41 hours at 480°C, and Detert (26) also indicates the equilibrium phases to be of the form A_2B, A_7B_6 or sigma phase, and not Ni_3(Mo, Ti).

T A B L E I

INVESTIGATOR	PRECIPITATE	HEAT TREATMENT	
		Aging	Temp/Time
Baker & Swann (23)	Ni_3Mo/Ni_3Ti	-	-
Bandi et al. (27)	Ni_3Mo(or Ni_2FeMo)	various	
	Fe_2Mo		
	TiC,TiN by extraction		
Banerjee et al. (5)	Ni_3Mo or Ni_3Ti	485	8
Banerjee,Hauser (5)	σFeMo-alloy no Ti	540	6
	η Ni_3Ti-alloy no Co,Mo	"	"
	σFeMo -alloy no Co,Ti	"	"
Barelly (5)	Ni_3Mo	480	14
Chilton & Barton (25)	Ni_3Mo,σFeTi	485	8
Detert (26)	Ni_3Ti,Ni_3Mo		
	Equilibrium phases A_2B,	-	-
	A_7B_6 or σ		
Florcen & Speich (24)	Ni_3Mo,Ni_3Ti	-	-
Hammond & Ansell (28)	Ni_3AI-Ti	-	-
Marcus et al. (29)	Ni_3Mo,	480	3
	Fe_2Mo	480	41
Mihalisim (30)	Coarse & Fine ppts.	485	3
Miller & Mitchell (31)	ηNi_3Ti alloy no Co,Mo	600	3
	ηNi_3Ti " " Co	600	3
	Fe_2Mo " " Co,Ti	550	16
	Fe_2Mo " " Ti	550	16
Reisdorf (20)	Ni_3Mo	485	3
	$(NiFeCo)_3Mo$		
Reisdorf & Baker (5)	Ni_3Mo or Ni_3Ti	485	8
	σFeMo, Ni_3Ti	485	8
	σFeMo alloy no Co	485	30

The identification of cobalt and titanium in precipitates is more difficult and their actual role in the alloys somewhat uncertain. Analyses of higher nickel alloys indicate eta Ni_3Ti present and it has been suggested that this is also present in the 18 nickel grades, owing to the similarity between the structures of Ni_3Mo and eta Ni_3Ti. Chilton and Barton (25) have found titanium present as a sigma phase, and it may be present in the molybdenum as $Ni_3(Mo, Ti)$. Reisdorf (20) identified titanium as Ti (C, N.), using extraction replicas, and recent work by Bandi et al (27) using E.G.A. and D.T.A.,[+] also find TiC or $TiC_x N_y$ in both annealed, and aged materials.

The uncertainty in precipitate identification is accompanied with doubt as to the correct morphology, the major precipitates being rod or ribbon-like Ni_3Mo and spherical sigma phase, each having maximum dimensions of a few hundred angstroms.

[+] Effluent Gas and Differential Thermal analyses.

Precipitation occurs uniformly on dislocations or at martensite platelet boundaries, whilst grain boundary precipitates are not normally visible. Preferred orientations of the precipitate particles have been reported and some particles are believed to be coherent with the matrix, as strain fields have been seen by several workers, (21,25,31). Garwood and Jones (22) indicate that the preferred orientation may be due to the preferred orientation of the dislocations within the matrix (along the (111) b.c.c. direction) and subsequent precipitation on the dislocations. Double maraging, as employed by Floreen (32) has little additional effect on the precipitation reactions, as the majority of imperfections are "tied up" during the first aging treatment.

1.3.4 Maraging Kinetics

The kinetics of the maraging process have been studied chiefly by comparison with binary and ternary systems of a similar nature.

Initial investigations (9) showed that the incubation time before precipitation commenced was very small, or non-existent, as significant hardness increases were obtained for a few minutes of aging at 480°C. Resistivity (33) and internal friction (34) measurements also indicate little or no incubation period (less than 1 min.) The hardness/time curve shows an effect after 0.1 hour (which is said to be due to precipitation of residual carbon) and thereafter a continuous increase until overaging occurs after about 100 hours treatment, (Fig. 1.3). Later work by Peters (35) suggests that below 450°C there are two possible forms of molybdenum - containing precipitate - a dislocation and a matrix nucleated precipitate, the latter tending to dissolve above this temperature.

Conventional plots involving the variation of some kinetically dependent parameter, e.g. hardness or electrical resistivity, can yield activation energy values for the reactions.

The general relationship is of the form,

$$\frac{\Delta X}{\Delta X_o} = kt^n$$

X - parameter at time t

X_o - "annealed" value of parameter

k - temperature dependent constant

n - time " "

- hence plots of X v.s. time gives the constant n, and Arrhenius type plots of the time to reach a given value of X v.s. ^{1}/maraging temperature give values of activation energies. Values (5,37) of n obtained (0.2 - 0.4) differ from those for diffusion controlled processes (0.5) and similarly activation energies (20 - 40 Kcal/mole) are less than those of substitutional element diffusion in ferrite (60 Kcal/mole). These values suggest that the reactions are governed by the large number of lattice imperfections provided by the martensitic transformation. The absence of any incubation period (38) is indicative of a very small free energy of nucleation under conditions of high supersaturation and precipitation on dislocations. Reports of recent work, however, on ferrite and martensite matrices (5) treated to similar conditions, produce activiation energies of approximately 65 Kcal/mole - i.e. similar to those for diffusion of a substitutional element.

These results tend to contradict the initial work, and the correct mechanism has yet to be enunciated.

The effect of mechanical working before or after maraging has been reported to have several effects (9,16,39-40). Ausforming produces only minor improvements in strength, whereas working during the martensite transformation produces a greater increase in strength for a similar amount of work. Cold working before maraging produces the largest increase in strength and has a marked effect on the kinetics of hardening, e.g. a two hour treatment after 40% cold work produces a hardness similar to that from a normal three hour treatment (39). This appears to be a result of the increase in density of dislocations, which provide more nucleation sites and increase the diffusion rates.

1.4 Mechanisms of Strengthening

1.4.1 Elemental Contributions

Alloying elements affect the strengthening processes in various ways and these are sometimes expressed in the form of an empirical equation. Detert (39) suggests, for example, for 18% nickel maraging steels,

0.2% proof stress = 26.7 + 6.2%Co + 15.8%Mo + 61.4%Ti

(in kg/mm^2)

The nickel content governs the amount of martensite produced on cooling, 18% Ni giving the maximum amount. As can be seen the greatest single effect is that due to titanium - approximately 45 t.s.i. for each per cent addition (42). The disadvantage of high titanium contents is in reduced N.T.S./TS ratio for above 0.14% Ti. This may be due to the neutralising effect of titanium on carbon, producing a precipitate at the grain boundaries (43). The effect of cobalt alone is on the stacking fault energy of the matrix (44), and does not appear to be a result of long range ordering or precipitation as suggested by certain workers(30).

The cobalt with a stacking fault energy of 20 ergs/cm^2 lowers that of the matrix (75 ergs/cm^2) so hindering cross-slip, which results in an increase in average dislocation density and hence strengthening. For Fe/Ni/Co alloys the strength increases linearly with cobalt content producing increases of up to 18 t.s.i. The addition of molybdenum, however, produces a marked increase in strength, greater than that produced by either cobalt or molybdenum alone; as shownin Fig 1.4. The optimum strength conditions are obtained by additions of 9% Co and 5%Mo; higher strengths can be obtained with minimum loss in N.T.S. by increasing the cobalt content, whereas increasing the molybdenum results in the disadvantage of having to use higher annealing temperatures for solution of all phases. In the presence of molybdenum, the effect of cobalt has been suggested (24,31) to be in reducing the solubility limit of molybdenum, and so increasing the amount of Ni_3Mo. This has been confirmed by electron microscopy, where cobalt can be seen to produce a finer dispersion of precipitates than in its absence.

The effects of other alloying elements is chiefly found in the variations in toughness values (46). Molybdenum prevents grain boundary precipitates in much the same way as it effects the temper brittleness of steels, and small additions (42) of boron and zirconium (less than 0.01%) also retard grain boundary precipitation, improving toughness and stress corrosion resistance. Elements such as Al, Mn, Si, Be, Cb, produce a decrease in notch toughness with increase in yield strength; aluminium having a similar effect to titanium (45). The presence of a third element in an Fe - 18% Ni martensite produces variations in yield strength as can be seen in Fig. 1.5. No systematic correlation can be made between hardening produced and size or electronegativity of the element (24), although generally the more potent hardeners are those differing greatly in size from the Fe - Ni matrix.

The carbon content of these steels is kept as low as possible - the term steel being a misnoma as carbon is unwanted, and, if present in quantites greater than 0.03

atomic % is detrimental to the properties. It is present as TiC or Ti C_X Ny, which has been shown to precipitate at the prior austenite grain boundaries (47,48), and produces a notch (and stress corrosion) sensitive material.

1.4.2 Strengthening Theories

One of the most attractive features of maraging steels is the combination of high strength and toughness. The strength of conventional age-hardened materials has been explained in numerous ways by several workers (9,23,24, 26,37,45,49), and these theories have been applied to maraging steels.

The strength of an Fe - Ni martensite is in the region of 36 t.s.i., and that of a commercial grade unaged maraging steel approximately 68 t.s.i. This difference can be accounted for by the solid solution hardening produced by the alloying elements Co, Mo, and Ti (45). Aging the steel produces increases of 45 - 90 t.s.i. and this has been explained by two mechanisms.

In the initial stages of precipitation the strength of the individual particles has to be considered. Work by Ansell (50,51) produced formulae to include the shear stength of the particles, where,

$\sigma_y = f_n.(f ; \tau_p)$ $\quad$ f - volume fraction

τ_p - shear strength of particles

Assuming particles to be spheres

$$\sigma_y = \frac{\tau_p}{4} \cdot \frac{f^{1/3}}{0.83 - f^{1/3}}$$

and above a critical diameter d_c

$$\sigma_y = \sqrt{\frac{Gb}{2\lambda} \tau_p}$$ $\quad$ λ - interparticle spacing.

so giving

$$d_c = \frac{8Gb}{\tau_p} \cdot \frac{0.83 - f^{1/3}}{f^{1/3}}$$

Fitting values to the above, and assuming the point where $d = d_c$; $f \sim 5\%$; $d_c \sim 200$ Å so $\lambda \sim 250$ Å

$G = 7.3.\ 10^3$ kg/mm^2 $\quad$ $b = 2.5$ Å

so $\tau_p = 1.10^3$ kg/mm^2 $\quad$ (630 t.s.i)

$\sigma_y = 200$ kg/mm^2 $\quad$ (130 t.s.i)

This is of the order obtained in these steels, and Detert, (26,37) suggests that during the initial stages this

mechanism holds.

The later stages of aging have been explained by an Orowan relationship (23).

$$\sigma = \sigma_o + \alpha \frac{Gb}{\lambda}$$

σ - total strength

σ_o - matrix strength

The particle spacing is approximately 300Å, which gives value of sigma in the region of 90 t.s.i. This appears to be the most likely explanation of the strengthening process, as various workers (52) have observed dislocations bowing, and also dislocation tangles around precipitate particles.

Several reports (9,53) base explanations on ordering mechanisms of hardening, but these are not concerned with the precipitates now known to be present and tend to be of minor importance. Conrad (49) investigated the temperature dependence of the flow stress, and found that the variation was of a similar nature to that in mild steels,

$$\sigma = \sigma^* (T, \dot{\varepsilon}) + \sigma_\mu$$

The major strengthening, σ_p is due to long range internal stress fields, which can be developed by a fine dispersion of particles.

The superior toughness obtained is explained less readily and appears to be the cumulative result of certain factors. The nature of these steels i.e. being alloys free from unwanted residual elements, and the uniform distribution of precipitate, contribute significantly to the toughness. Alloying elements have their various effects ; (section 1.4.1) and additions of nickel may reduce the tendency towards clevage due to hydrogen embrittlement, by producing microscopic regions of austenite, hence local areas of high ductility (37). These could occur at the grain boundaries or around precipitate particles, so increasing the resistance to void formation at the matrix/particle interface. However, the precise reasons for the toughness of the 18% nickel grade still remain obscure, as other maraging steels with equivalent strengths do not appear to possess such high toughness values.

CORROSION CRACKING

1.5 Introduction

The phenomenon known as stress corrosion cracking may be considered to be the effect produced by the conjoint action of stress and corrosion, which is greater than that produced by either acting alone. In certain cases failures could be more precisely defined, such as, corrosion assisted brittle failure, or stress assisted dissolution, and reviews on stress corrosion cracking tend to consider failures as a wide range of specific cases. It is convenient to summerise this range and to categorise certain groups according to their predominant features:-

(a) Where corrosion is predominant, and occurs along a pre-existing anodic path. Stress in this case may only assist the process in a secondary manner, e.g. intergranular failure of mild steels in nitrates.

(b) Where corrosion occurs along strain generated active paths, stress produces repeated fracture of protective films and exposes the underlying metal

to the corrosive environment, e.g. the transgranular failure of brasses in ammoniacle environments, or the plastic yielding that may accompany stress application which assists depolarisation and permits the passage of relatively high current densities.

(c) where stress is predominant, and specific cases of adsorption produces catastrophic failures, e.g. hydrogen embrittlement of high strength steels.

Failures produced in many materials could be classed in more than one group and great care has to be taken to fully consider the environmental and structural conditions involved.

The published literature dealing with the corrosion cracking aspects of maraging steels is in many cases inconsistent and inadequate. Several authors suggest that the stress corrosion cracking is a special instance of hydrogen embrittlement (54,55) whilst other authors regard these two modes of failure as quite different, (56-9). In reviewing the literature it appears necessary to assume that a distinction can be made,

although the situation is complicated by the fact that both are characterised by an intergranular fracture path. The type and rate of attack is governed by structural and environmental factors and, to some extent the general corrosion rate.

1.6 Composition

The susceptibility towards stress corrosion cracking has been considered in certain cases to be dependent upon the chemical composition of the steel. Material having different carbon contents has been tested by Scharfstein (60) who concluded that reducing the carbon by a factor of seven had no effect on the susceptibility. A similar effect, however, occurs in mild steels where the susceptibility does not decrease until the carbon is reduced to very low levels. This could be the case in maraging steels as material of very low carbon content has not been the subject of any published testing programmes to date. The effect of titanium was investigated by Rubin (59), in steels of 0.23 to 1.4% Ti, who found susceptibility to increase as the titanium content increased. Small additions of zirconium and boron have the opposite effect, decreasing the susceptibility by reducing the amount of grain boundary precipitate (69).

In conditions where hydrogen embrittlement is the failure mechanism, poor resistance has been associated with high molybdenum and nickel contents, whereas high carbon contents tend to be beneficial (62).

1.7 Production Variables

Relatively little work has been published on how the prior processing history effects the susceptibility of maraging steels towards stress corrosion or hydrogen embrittlement cracking. The majority of workers have mainly considered the limiting conditions for using the steel in specific situations, with the material tested treated to optimum strength conditions. Variations in austenitising and/or aging temperatures produce strengths depending upon the prior austenite grain size and the size and amount of precipitate present. The effects are somewhat similar to those found in many other conventional materials (63), and the susceptibility would be expected to vary in a similar manner (64-8). The effect of prior austenite grain size has been investigated by Parkins and Haney (58), who

found no apparent change between 800 - 1000°C, but material austenitised at 760°C was more resistant to stress corrosion cracking. The different temperatures used produce only slight variations in strength level, and the main factor involved appeared to be the austenite grain size, which varied somewhat over the temperature range considered. Other workers (61,69) have reported that coarse austenite grain sizes are to be avoided, but no complete survey has yet been produced.

The production of martensite is unaffected by the cooling rate and normal treatments involving a comparison of quenching and furnace cooling show little effect on stress corrosion cracking. Aging the martensite produces precipitation, and, as in other materials, the amount and form vary with tempering temperature. Work on low alloy and maraging steels (59,70,71) indicates greatest susceptibility at the lower tempering temperatures, the effect decreasing with increase in temperature.

Other reports (57) show similar variations with aging temperature, although the effects of under and overaged precipitates remain unexplained.

Mechanical deformation during heat treatment has been considered in section 1.3.4 and the production of a deformed structure could influence susceptibility to stress corrosion either by altering the precipitation reactions or producing a change in the anodic paths. Work by Phelps (62) shows that austenitic stainless steels can be rendered non-susceptible to stress corrosion cracking by cold working, and Dean et al. (61) found cold working before maraging to reduce the susceptibility of maraging steels. Other mechanical treatments have a less marked effect (72), but any producing a change in the prior austenite grain boundary network would be expected to alter the susceptibility.

1.8 Stress

The conventional stress-time to failure curves can be obtained for maraging steels, where a threshold stress exists, and above which increasing loads

produce increasing susceptibility (58,73). High levels of loading require only small crack advancements before final mechanical failure occurs and can also induce other effects. Leckie and Loginow (74) indicate a strength level above which specimens fail by hydrogen embrittlement and below which they are immune, and work on pre-cracked specimens (54) shows that crack velocities depend upon the stress intensity at the crack tip.

In analysing the effects of stress the stressing systems have to be considered carefully, i.e. constant load, constant strain, etc. Many reports include mixed results quoted from various types of testing and these must be interpreted cautiously.

1.9 Environment

The majority of corrosion cracking failures in maraging steels have been produced in either saline solutions or environments containing hydrogen sulphide.

Tests have been carried out in natural sea water where possible (56,73,74) but where more stringent control is required artificial sea water (0.6N NaCl) is used. The latter was found less agressive than natural sea water (74) and increasing the flow rate produced greater general attack than under quiescent conditions. Specimens tested by Hasan (73) using alternate immersion tests in natural sea water did not appear to yield reproducible results and their general conclusions on the cracking mechanisms are limited.

Green and Haney (75) considered variations in environmental conditions and their effect on the stress corrosion cracking susceptibility. Tests were carried out using foil type specimens 0.002" thick, and thus the results may only be applicable for initiation conditions with bulk material. Using 0.6N NaCl, variations in solution pH produced minima in the time to failure/pH plot at values of 2 and 11 (Fig. 1.6). This was also accompanied by a change in general corrosion attack

across the pH range 2 - 12. In acid pH solutions, failures in maraging steels were found to be a function of the chloride ion concentration at a given pH, with long failure times where no chloride ions were present and short failure times when chloride ions were in ready supply. The effect was not produced in H11 and 4340 steels, whose failures in this range were due to hydrogen embrittlement. With alkaline pH values, however, failures were only produced when chloride ions were present. Minima were obtained for 4340, H11 and maraging steels, and to investigate this further, electrode potential measurements were made (76). These values were found to be steady after approximately 1 hour, and plots of failure time/pH and electrode potential/pH show the variations produced with different solution concentrations (Fig. 1.7 and 1.8). The results indicate passivation occuring over a range of pH from 10 to 12, the minima becoming broader and moving to higher values with increase in chloride ion concentration (76,77).

Investigations on the effect of the oxygen level of the solution (55,75,78) suggest oxygen reduction to be the major cathodic reaction under natural conditions, as lifetimes were reduced up to 30% by allowing free access of oxygen to solutions. However, many workers still consider the reduction of hydrogen ions to be involved in the cracking process.

Tests in solutions containing hydrogen sulphide have shown maraging steels to be more resistant to hydrogen embrittlement than many other high strength steels, and measurements by Snape (79) showed then to have four times the permeability for hydrogen than other steels.

1.10 Polarisation - Pourbaix Diagram

Methods for studying differences between hydrogen embrittlement or stress corrosion cracking at low pH values are limited, owing to the close association of the free corrosion potentials of maraging steels and the potentials where oxygen reduction and hydrogen ion reduction are both feasible.

Differences can be achieved by using polarisation techniques, (80) where the anodic or cathodic reactions are stimulated by anodic or cathodic polarisation. Results produced (58) favour a stress corrosion mechanism under natural and anodically polarised conditions with hydrogen embrittlement occuring at cathodic potentials below approximately 750 mv. (s.c.e.).

The types of failure at various potentials have in certain cases been associated with the Pourbaix diagram for iron (62) - at potentials more negative than the hydrogen line (less than 750 mv.) failures tend to be by hydrogen embrittlement, and above the line they are due to stress corrosion cracking. A region exists in between offering a range of potentials slightly more negative than the free corrosion potential where cathodic protection is possible. Green and Haney (76) found when failures occured at the alkaline pH values that the electrode potentials were coincident with the onset of Fe_3O_4 formation. At pH values greater than 11.4

passivation occurs at more negative values of electrode potentials and no stress corrosion failure occurs; this corresponds to an area of the Pourbaix diagram where iron may be passivated.

1.11 Theories

The cracking mechanisms fall into two categories, one involving failure by hydrogen embrittlement and the other concerned mainly with active path stress corrosion cracking.

1.11.1 Stress Corrosion Cracking

As in many other systems failure is produced in three steps:-

(a) Initiation

(b) Propagation

(c) Final mechanical failure

(a) In un-notched plain specimens the initiation process depends on the development of some form of discontinuity in the surface of the specimen. Surface films (other than air formed oxide films) are not normally present on conventionally tested material and a classical film

rupture mechanism does not occur. Green and Haney (75) suggest that initiation occurs in acid solutions as a result of a breakdown in the air formed oxide film by the chloride ions present, whereas in alkaline solutions initiation appears to be a result of the state of partial passivation which exists in the range pH 10-12 for these steels. This reduces the anodic areas and produces intense selective attack which initiates stress corrosion failure. Certain workers suggest (55) that propagation occurs immediately following any "film" breakdown, but this is not necessarily correct, as pits or surface fissures may develop. Fontana (81) observed these in stainless 403,4340 and maraging steels, the depth depending upon the tempering temperature. Fissures of a similar nature have been observed by Parkins and Haney (58) and metallographic evidence shows intergranular stress corrosion cracks propagating from the tips of these fissures. These fissures tend to be stress, rather than structurally dependant, and growth is at right angles to the tensile axis.

(b) The observations of various workers on propagation appear to be in general agreement; the crack follows a pre-existing active path along the prior austenite grain boundaries producing an intergranular failure. Transgranular cracking has been reported (82), but no explanation of the amount or nature given. The active path is a result of precipitation occuring at the austenite grain boundaries at some stage during the heat treatment, and Pellisier (48) has identified the precipitate as TiC or TiC/N. The amount of precipitation depends to some extent upon the alloy content, with additions promoting grain boundary precipitation increasing the susceptibility, and vica versa. Alloying elements which produce a change in the austenite: martensite ratio present in the matrix could also alter the susceptibility, although little evidence exists in support of this. Mechanical deformation during heat treatment has been found (61,62,72) to reduce susceptibility and this appears to be a result of a change in the state of the prior austenite grain boundaries. This may be a simple effect of producing a

more tortuous anodic path or could be associated with dispersion of segregate away from the grain boundaries, as is the case in certain mild steels.

Classical theories of stress corrosion suggest that cracks can propagate along active paths by pure electrochemical dissolution or by a combined electrochemical - mechanical mechanism. The literature on maraging steels tends to favour the electrochemical - mechanical explanation, on the basis of the crack propagation rates observed. The calculated current density required to maintain rates of the order of 10^{-1} mm/hr. is approximately 0.5 A/cm^2 for pure electrochemical dissolution (58). Current densities of this magnitude could lead to marked polarisation of the anode and as a result many workers conclude that to maintain the observed cracking rates an intermittent electrochemical-mechanical process must occur. Examination of fracture surfaces, however, indicate clean intergranular failures, with no indication of alternate stress corrosion and mechanical rupture areas, as might be expected.

Stress could have a marked effect here, as several workers suggest (83) that, in dealing with anodic dissolution of metal in the highly stressed region of a crack tip, current densities of the order of 0.5 A/cm^2 can be sustained by the yielding material. This, plus the depolarisation effects of stress in producing crack opening, could readily explain crack propagation rates by pure electrochemical dissolution and thus can be considered as a possible mechanism. However, recent work by Brown (84) shows that low pH values could be produced at the tip of a crack during stress corrosion cracking, as has frequently been postulated by earlier workers. In systems where hydrogen embrittlement and stress corrosion cracking occur adjacent potential regions, changes in cracking mechanism are a possible result of such a pH drop inducing a potential change at the crack tip. This could explain the high rates of crack propagation obtained, being a combination of electrochemical-hydrogen embrittlement, and not pure electrochemical or electrochemical-mechanical.

Leckie favours an explanation on this basis, but offers no practical evidence in support.

Two types of intergranular cracking have been observed in maraging steels, "fine and branched" cracks occuring in the most susceptible condition and wide blunt cracks in less susceptible material. In longer lasting tests some short transgranular secondary cracks have also been observed (58) but these tend to be of minor importance. Cracking has been produced in various environments (85), humid air and argon (62), distilled water (75), salt water and a whole range of industrial fluids (57). In all cases the cracking remains intergranular, except with investigations using sheet material where confusion between surface fissures and transgranular cracking could arise.

(c) The cracks propagate across the specimen and lead to mechanical failure, or arrest, according to the type of testing system used. Where mechanical failure does occur it is by void coalescence, producing a ductile

rupture, and fractrographic examination reveals a typical dimple topography.

1.11.2 Hydrogen Embrittlement

Failure readily occurs by this mechanism when specimens are subjected to certain environmental conditions (86). Doubt arises in deciding some form of "boundary values" where either stress corrosion or hydrogen embrittlement cracking occur for a given experiment. Observations of fracture surfaces (79) indicate similar failures to those of stress corrosion cracking, the differences being the general absence of corrosion product and surface fissures. Cracking rates due to hydrogen embrittlement have received little attention, other than expressing the rapid failures which can be achieved, and the process is thought to be stress dependent, with failures not occuring below a threshold stress as in stress corrosion cracking(55).

The mechanisms suggested involve two principle effects, both resulting from the adsorption of atomic

hydrogen on the surface of the metal. Several workers suggest that the presence of this hydrogen can reduce the value of surface energy, and according to the equation for elastic fracture,

$$\frac{\sigma^2}{2E} \geqslant 2\gamma$$

decrease in the size of gamma would reduce the stress required for fracture (87). Other authors (88) indicate that the atomic hydrogen can diffuse into the metal and collect at vacancies or dislocations where it combines to form molecular hydrogen. The pressures generated by this process have been estimated to be sufficiently great to produce stress in excess of the fracture stress, and so initiate catastrophic fracture. Permeability measurements show maraging steel to have a greater capacity for hydrogen take-up than other high-strength steels, and yet they are more resistant to hydrogen embrittlement cracking. Tetelman suggests that hydrogen embrittlement cracking in conventional steels is due to diffusion of atomic hydrogen to the carbides which provide ideal sites for nucleation of molecular hydrogen and crack initiation. On this

basis the absence of large amounts of carbide in maraging steels could offer a possible explanation of their greater resistance to hydrogen embrittlement cracking than other high-strength steels.

Investigations in support of the theories have largely been concerned with pre-cracked type specimens, where crack initiation times are reduced, and the mechanisms have been related to the high crack propagation rates observed. Whilst many of the conclusions may be correct, lack of precise test results and other supporting data tend to indicate some confusion in relation to a complete understanding of the mechanisms involved.

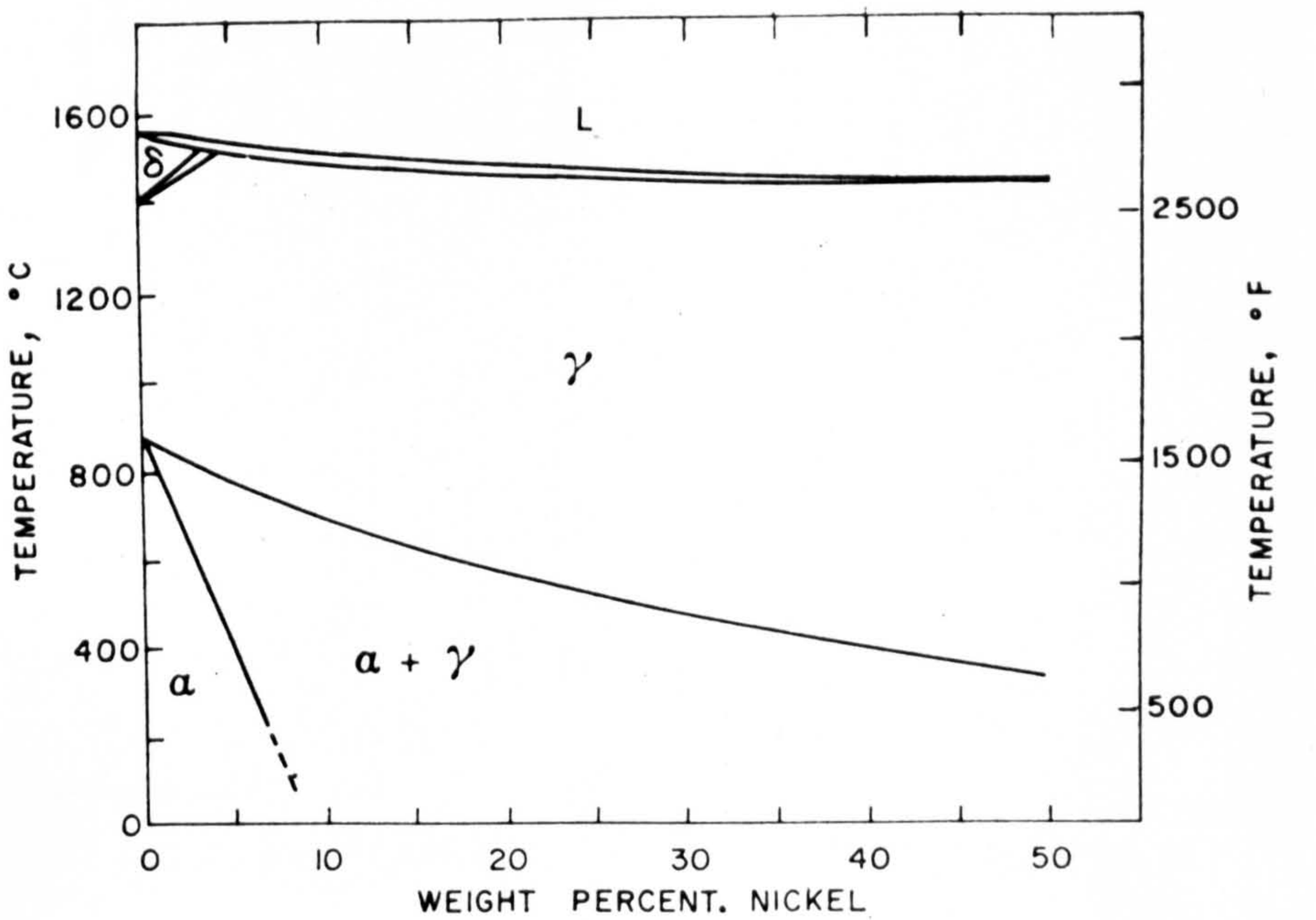

Fig. 1.1 Iron-Nickel Equilibrium diagram (11)

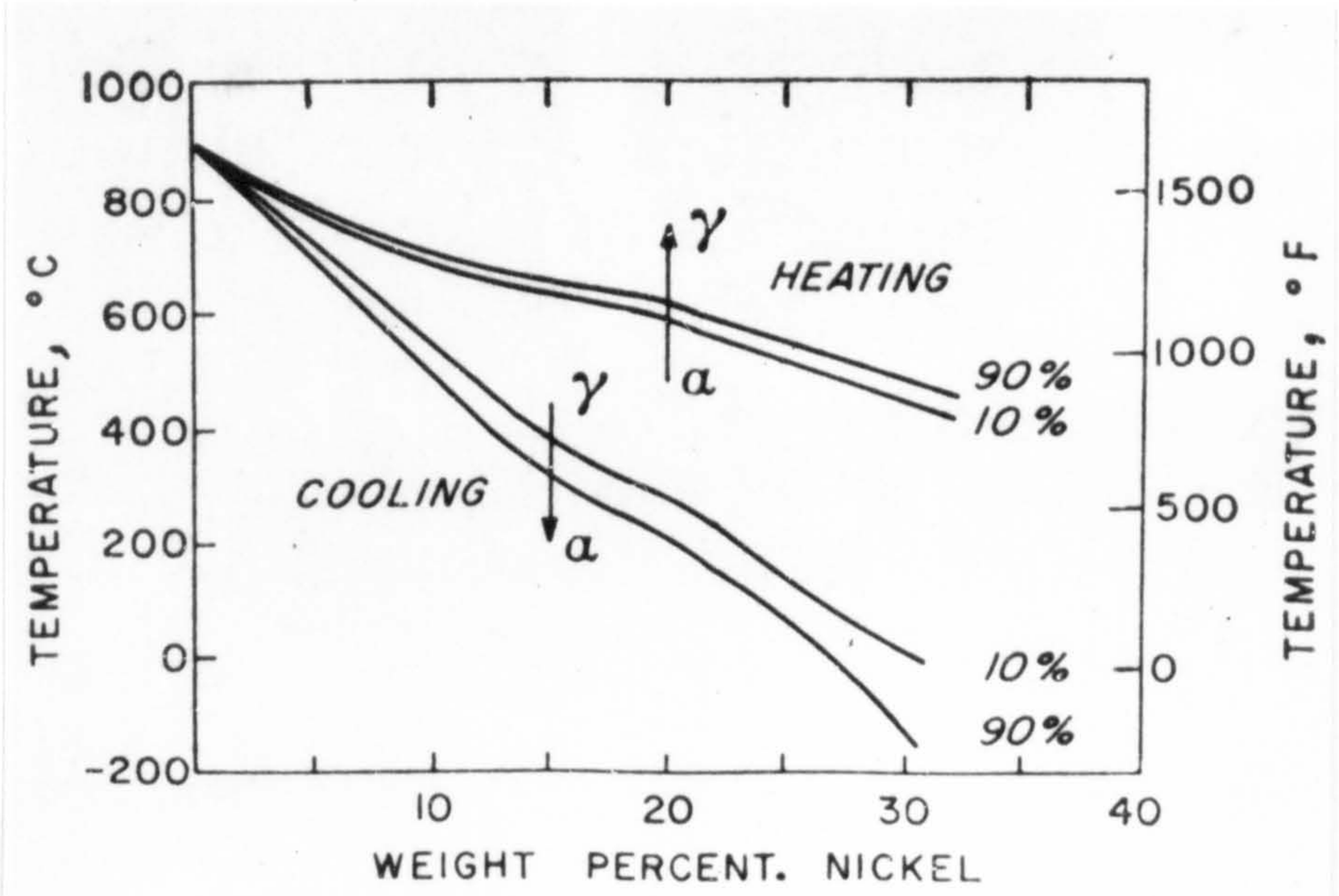

Fig. 1.2 Metastable diagram for Iron-Nickel (12)

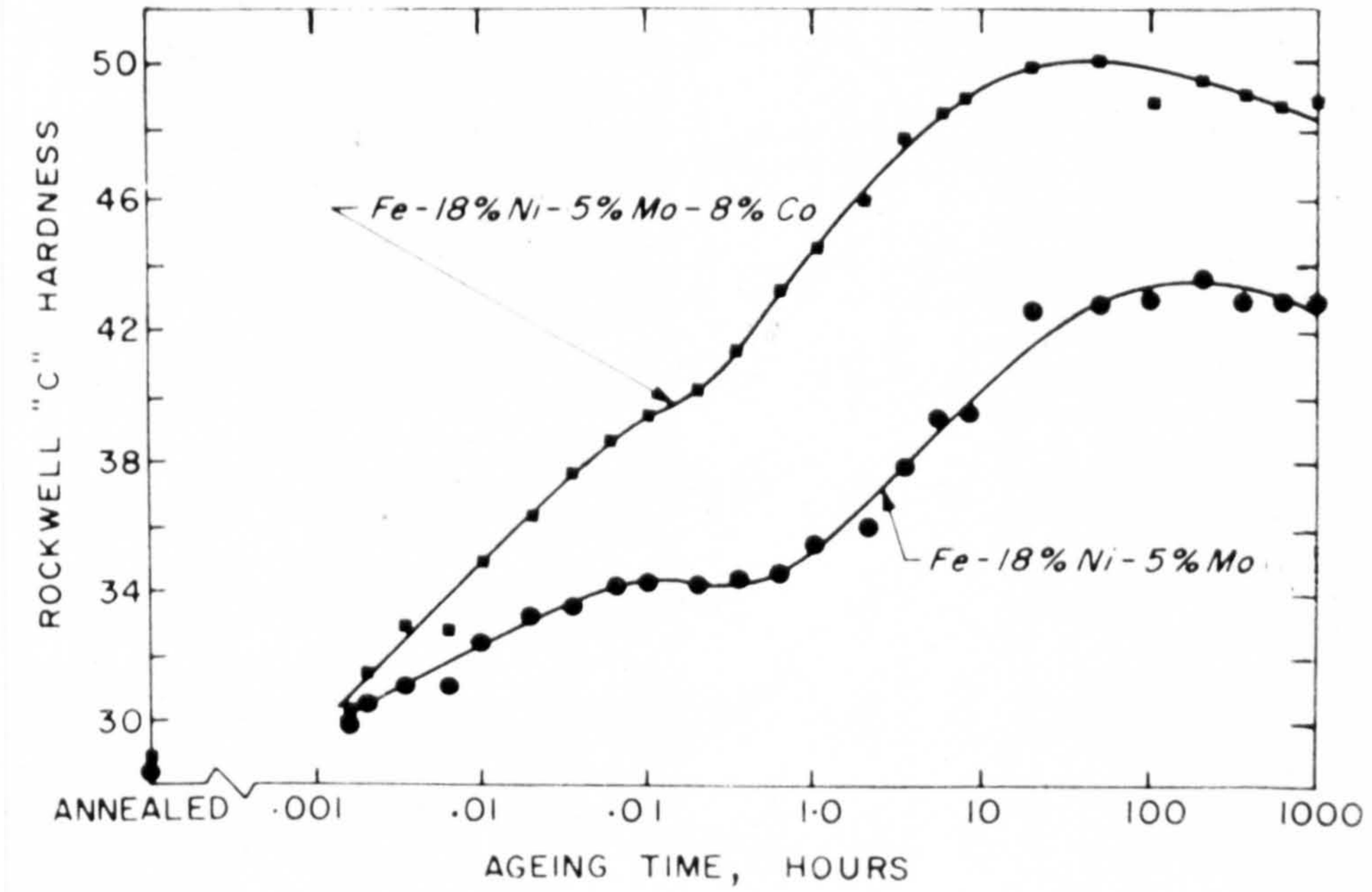

Fig. 1.3 Hardness - time curve. (5)

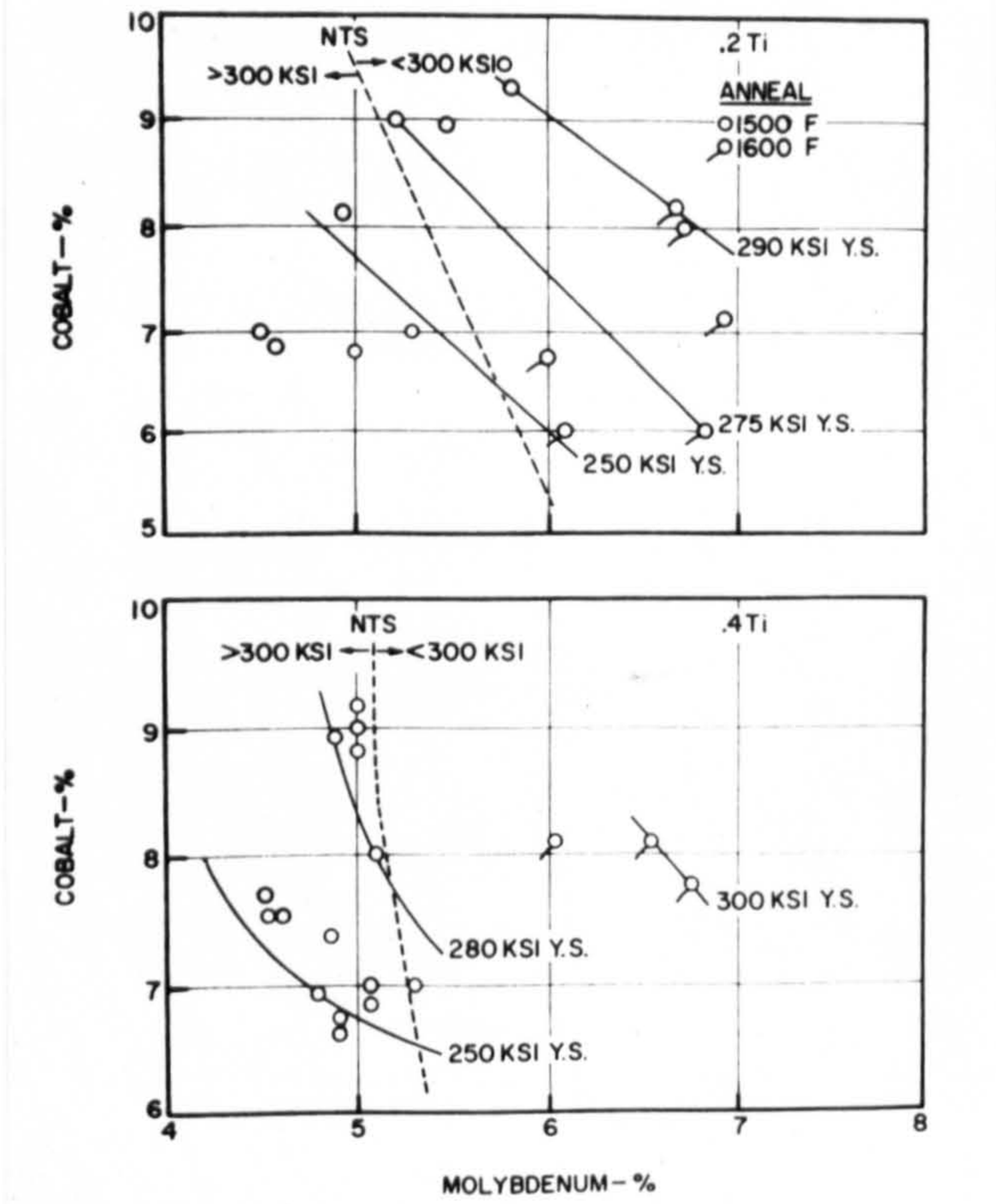

Fig. 1.4 The effect of Co and Mo on the strength of Maraging Steels (42)

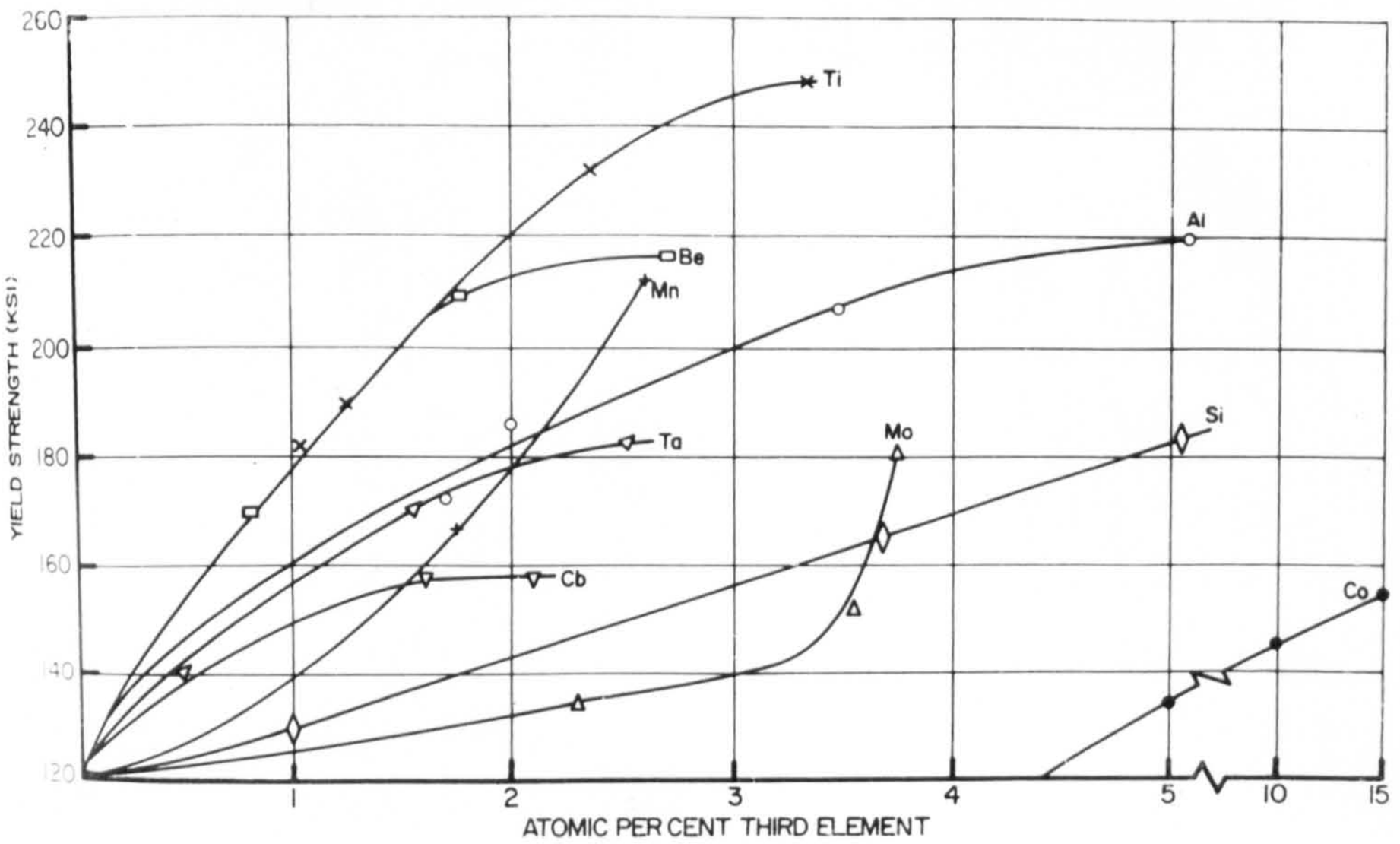

Fig. 1.5 Effect of third element on the strength of Fe-Ni martensite (45).

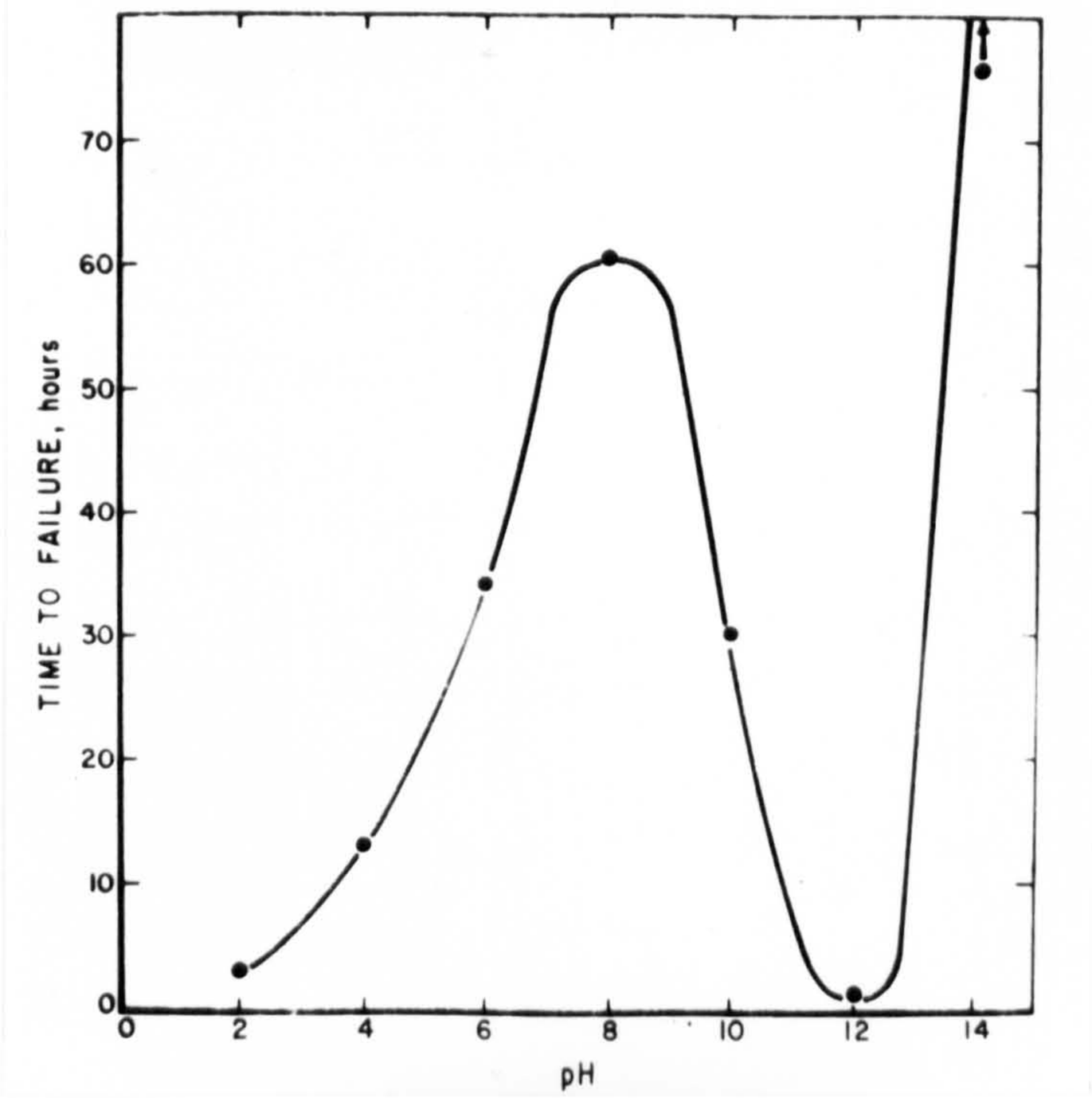

Fig. 1.6 Time to failure - pH plot.

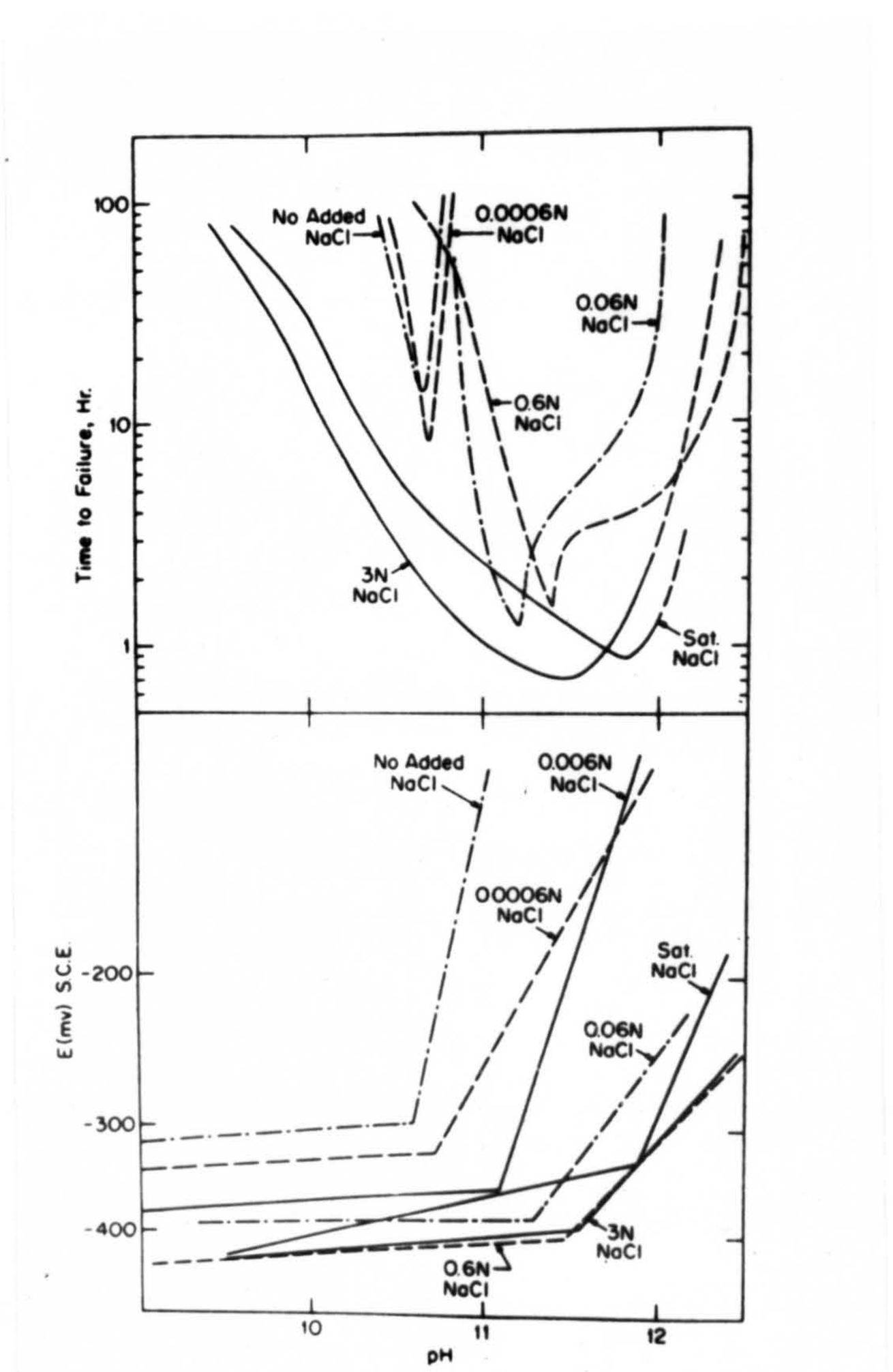

Fig. 1.7 and 1.8 Variation in failure time and electrode potential with pH values.

2. EXPERIMENTAL TECHNIQUE

2.1 Specimen Preparation

The steel was received as bar stock of various diameters (0.75 - 0.25") and of compositions shown in table 2. Stock of greater diameter was initially hot rolled to approximately 0.5" diameter at 900°C and then pickled in 40% HCl prior to cold drawing. The latter was carried out through a series of twelve dies to a final diameter of 0.1875" (85% reduction) using a proprietary lubricant (Clydoll Tanteroll No. 2.). Where appropriate interstage annealing was carried out at 800°C in an argon atmosphere. The drawn rod was cut to length and machined into stress corrosion test specimens with the form shown in figure 2.1. Over the guage length the specimens were emeried to a 000 finish, the remainder of the specimen being coated with Lacomit lacquer, and were degreased immediately prior to use.

The material for pre-cracked specimens was available

TABLE II

Analysis of Steels used:-

ELEMENT	PERCENTAGE PRESENT IN STEEL			
	A	B	C	D
C	0.004	0.0I6	0.0I0	0.009
Si	0.09	0.07	0.06	0.05
S	0.005	0.007	0.004	0.0I
Mn	0.03	0.0I	0.03	0.0I
P	0.002	0.002	0.002	0.005
Ni	I7.9	I8.32	I7.8	I8.5
Cr	-	0.02	-	-
Mo	4.55	4.85	4.50	5.30
Ti	0.68	0.68	0.66	0.55
Al	0.088	0.17	0.094	0.11
Co	8.80	8.74	8.90	7.60
Zr	0.03	0.01	0.03	0.013
B	0.005	0.004	0.004	0.003

as rod which was hot-forged to rectangular section before use. The specimens were machined to the dimensions shown in figure 2.2 and were heat treated prior to the introduction of the pre-crack by subjection to fatigue, (95,99).

2.2 Heat Treatment

Austenitising treatments were carried out in vacuum furnaces capable of attaining 1100°C (fig. 2.3). Temperatures were controlled by Ether proportional controllers, one being fitted with a programming unit. Sangamo clocks provided an automatic on-off switching mechanism and the whole treatment was recorded on an Ether Xactline chart recorder (fig. 2.4). The furnaces were in the horizontal position and consisted of an outer silica tube, wound with Nichrome wire to give a 4" long constant temperature zone, and an inner vacuum tube fitted with brass end caps and attached to diffusion and rotary pumps. The specimens were discharged from the furnace and air cooled after austenitising.

Several treatments were carried out in a vertical furnace capable of quenching specimens directly into water. Specimens were supported in the hot zone using thermocouple wire attached to a top end cap. Argon was passed through the furnace to prevent excessive oxidation, and quenching was achieved by removing the bottom end cap and the supporting pin from the top end cap.

All aging treatments were carried out in a Hereaus forced-air furnace from which specimens were air cooled.

2.3 Solutions

All material was tested in a 0.6N. sodium chloride solution made from demineralised water and analytical grade chemicals. Hydrochloric acid or sodium hydroxide were used to adjust the pH to the desired value. In some test solutions certain chemical additions were made in the following amounts:-

Anthraquinone - 2 gms. per litre

Chloroplatinic acid - 25 c.cs. per litre.

Hydrogen peroxide - 10 ccs. per litre

Sodium arsenate - 20 gms per litre

2.4 Testing Apparatus

All mechanical tensile data were produced using a Mand tensile machine with load-relaxation curves recorded automatically on a X-Y recorder.

The majority of stress corrosion tests were carried out under constant total strain conditions using a Hounsfield tensometer (Fig. 2.5), although occasionally a hardbeam tensometer (Fig. 2.6) was employed. All pre-cracked specimen testing was conducted using a Brown-type cantilever beam apparatus shown in figure 2.7.

Test cells consisted of a simple glass tube and rubber bung assembly (Fig. 2.8) with modifications introduced where controlled atmosphere tests were to be carried out. Load-relaxation phenomena and times to failure were recorded from the response of a Wheatstone Bridge arrangement of strain guages (Fig. 2.9). Two

guages were fixed to the opposite surfaces of the beam and two compensating guages were fixed to a dummy beam located adjacent to the machine. Power was provided by a 30 volt d.c. pack and the potential change produced by a change in the state of strain of the beam was recorded on a Servoscribe Potentiometric Recorder.

The hardbeam machine employed a similar arrangement of strain guages incorporated in a 5000 pound load cell. Calibration of the cell was achieved by measuring the potential outputs obtained under increasing and decreasing loads in an Amsler Tensile testing machine.

Tests on pre-cracked specimens were carried out on a cantilever beam apparatus that was designed to take up to $\frac{1}{2}$" thick specimens and loads of up to 100 lbs. suspended at a distance of 21" from the pre-crack. Solutions were contained in a polyethylene bottle (Fig. 2.10) and the specimen sealed in with Bostic Outdoor adhesive. Beam deflections were recorded using a

Honeywell linear transducer, a type CA31 amplifier and a Servoscribe recorder.

2.5 Electrochemical Measurements

Corrosion potential-time curves were determined during testing using a string bridge and calomel electrode arrangement coupled to a Pye pH-meter. The output was recorded at the same time as the load relaxation by using a two-pen Servoscribe Recorder.

Galvanostatic testing was achieved using a galvanostat built to the specifications indicated in figure 2.11, with two 12 volt batteries used as the power source. Current was applied to the specimens through a multi-range milliameter and a platinum electrode.

Potentiodynamic polarisation curves were obtained employing the cell arrangement shown in figure 2.12. The calomel electrode was suspended in an agar bridge, and specimens were mounted in the centre of the cell using a rubber bung arrangement to give an exposed area of $1cm^2$. In tests where stirring was required the cell

was supported over a magnetic stirrer and a plastic-coated magnet placed in the cell. Potential sweeps were produced by a Chemical Electronics Linear Sweep Generator coupled to a potentiostat, and the potential and current (via. a log-linear converter) were plotted automatically on a Bryans X-Y Recorder. The cell could be adapted readily to operate under controlled atmosphere conditions when required. On completion of each run the cell was dismantled, washed with distilled water, and a new solution and specimen introduced for each test.

For certain tests it was necessary to subject specimens to anodic polarisation in an unstressed condition prior to testing in the normal manner. Galvanostatic polarisation was carried out for the desired time, after which the solution was discarded and the specimen and cell ultrasonically cleaned and dried to remove corrosion products. The diameter of the specimen was then measured and the test loaded to the required stress value.

General corrosion rates were determined by conventional weight loss measurements and instantaneous corrosion rates determined using a Pulsed Current technique. Weight loss experiments were carried out on small cylindrical specimens and tests were conducted in 30 m.l. bottles. After removal the specimens were ultrasonically cleaned, dried, the weight change determined and the final solution pH measured. Instantaneous corrosion rates were obtained using a pulse generator arrangement (90) using specimens and cell similar to those in figure 2.12. $\frac{\Delta E}{\Delta I}$ values were obtained for various pulse amplitudes and frequencies of 18 and 22 c.p.s. Anodic and cathodic Tafel slopes were plotted using a Galvanostat and multi-range micro and milliameters and plotted in a log-linear manner.

2.6 Electron Microscopy

Discs approximately 1 mm. thick were cut from heat treated rod 3 mm. in diameter using a jewellers saw when possible. This proved to be unsatisfactory

for several of the higher strength conditions and consequently a high speed cut-off machine was constructed (fig. 2.13). A ⅓ h.p., sealed three-phase motor turns the water-cooled tungsten carbide wheel ($\frac{1"}{32}$ thick by 9" diameter) at 1,400 r.p.m. The specimen was clamped in a moveable arm and set to cut specimens of the required thickness, which were retrieved by use of a small permanent magnet. The latter was placed on the tip of the rod and, on cutting through, the magnet and thin disc fall into the wire basket. The discs were filed to remove lips (produced at the point of severance), and mounted on a 1" diameter brass block using a cold mounting compound. Polishing was carried out on 320 and 600 grade silicon carbide papers using a wheel built to rotate at 30 r.p.m. and fitted with an Autopol polishing head. After producing a uniform surface on one side the mounting compound was dissolved in benzene, the discs turned, remounted and ground to a thickness of approximately 0.2 mm.

Electropolishing was carried out in a solution of 90% acetic acid - 10% perchloric acid and the discs supported in platinum tipped tweezers, in an arrangement shown in figure 2.14. An electropolisher was built to provide a full-wave rectified d.c. source capable of a maximum current of 10 amps (fig. 2.15) and a two stage polishing technique was developed using a "high current" (300 mA) until the film was seen to perforate, and then a "low current" (150 mA) to enlarge the thin areas. On producing a suitably thin area the specimen was transferred (without switching-off the current) to washing solutions of acetic acid followed by dry methanol; the foils being stored under vacuum.

Carbon replicas were prepared using a two-stage acetate technique. A negative replica of the surface was produced on a strip of cellulose acetate paper and this was gold-palladium shadowed and coated with carbon in an Evaporator unit. The replica was removed from the evaporator and the desired area cut out and mounted

on a copper grid. The latter was immersed in a solution of acetone for several hours to dissolve the cellulose acetate and leave a positive replica of carbon on the grid which could then be examined in the electron microscope.

Detailed examination of fracture surfaces was carried out in the Scanning Electron Microscope (S.E.M.), rather than by the use of carbon replicas, as the latter inevitably contained artefacts. When possible specimens were produced specifically for use in the S.E.M., and all surfaces were removed from their corrosive environments, washed and dried as quickly as possible. The specimens were attached to aluminium stubs with Araldite and electrical contact was achieved through a silver paint suspension. The stub was then coated with a thin layer of gold in order to improve the emmisivity of the surfaces, and specimens were viewed at 45^{o} in a Cambridge S.E.M.

Some polished and etched microspecimens were examined in a Geoscan microscope and the instrument used to produce line and dispersion scans over chosen areas. The specimens were prepared as for optical microscopy, usually using a 2% Nital etch but occasionally a modified Fry's reagent, or a mixture of etchants (91) could be used where others were inadequate.

2.7 X-Ray Analysis

Specimens were produced in powder form and mixed with gum-tragacanth to produce a rod 1-2 mm. diameter and 15 mm. long. These were exposed for 24 hours in an 18 cm. camera, using FeK_a radiation and a LiF monochromator. The film was processed and the lines measured to give data suitable for d-spacing determinations.

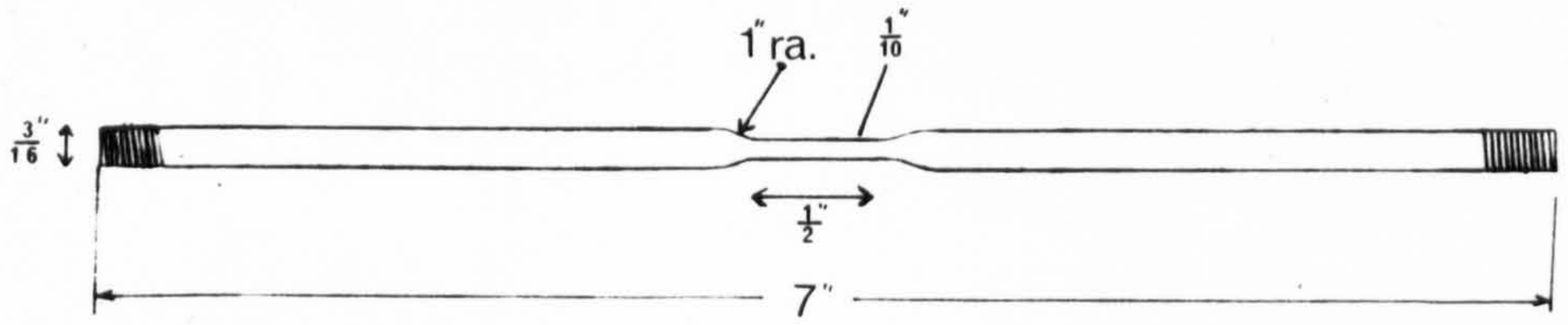

Fig. 2.1 Tensile Specimen.

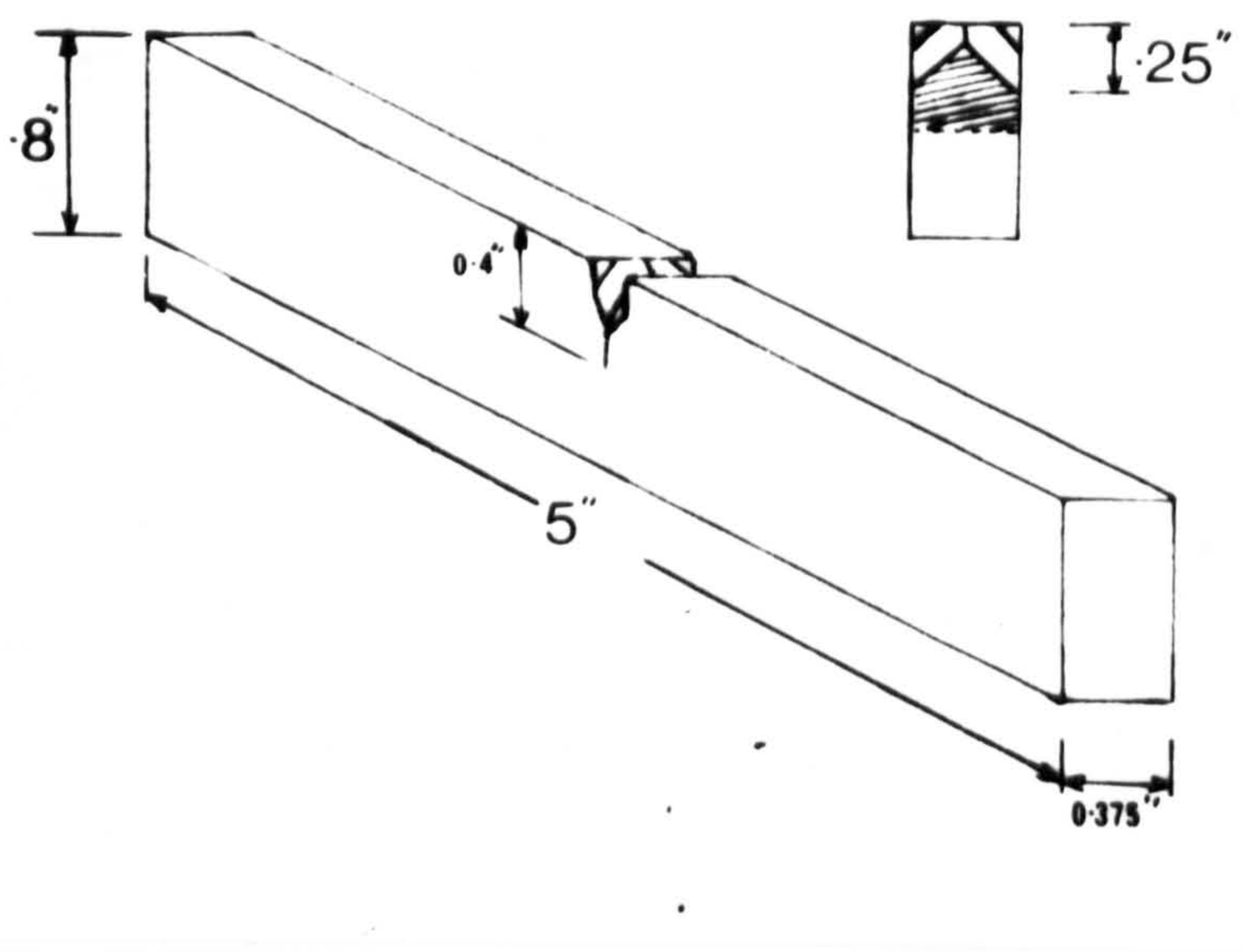

Fig. 2.2 Pre-cracked specimen.

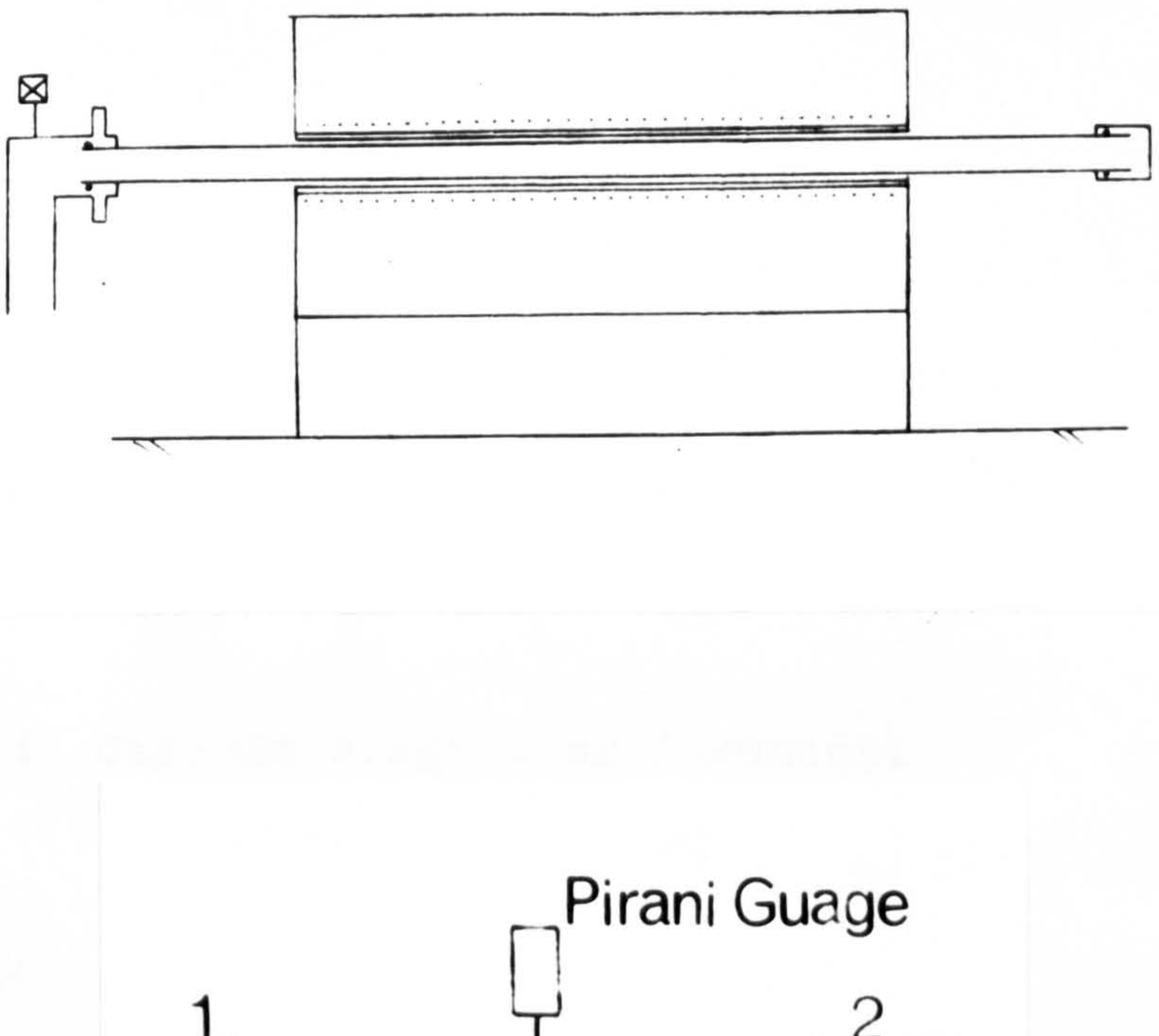

Fig. 2.3 Furnace and pump arrangement.

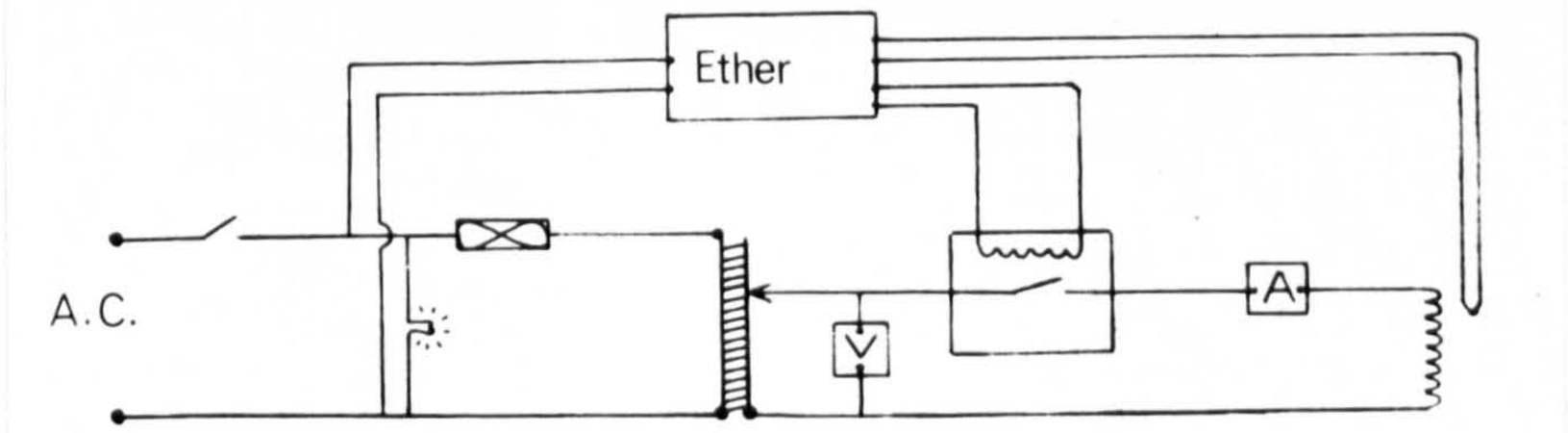

Fig. 2.4 Circuit diagram of furnaces.

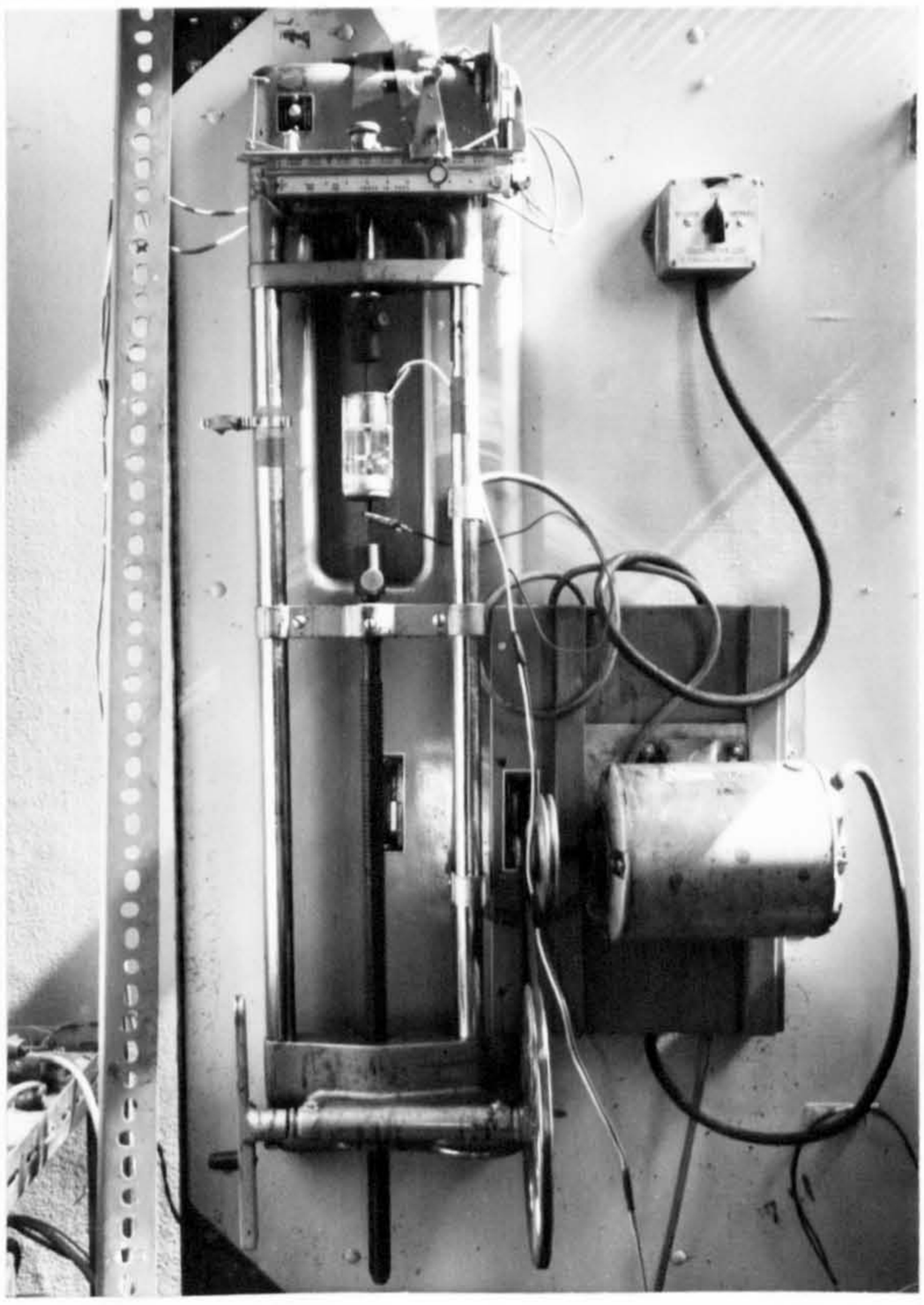

Fig. 2.5 Hounsfield tensometer.

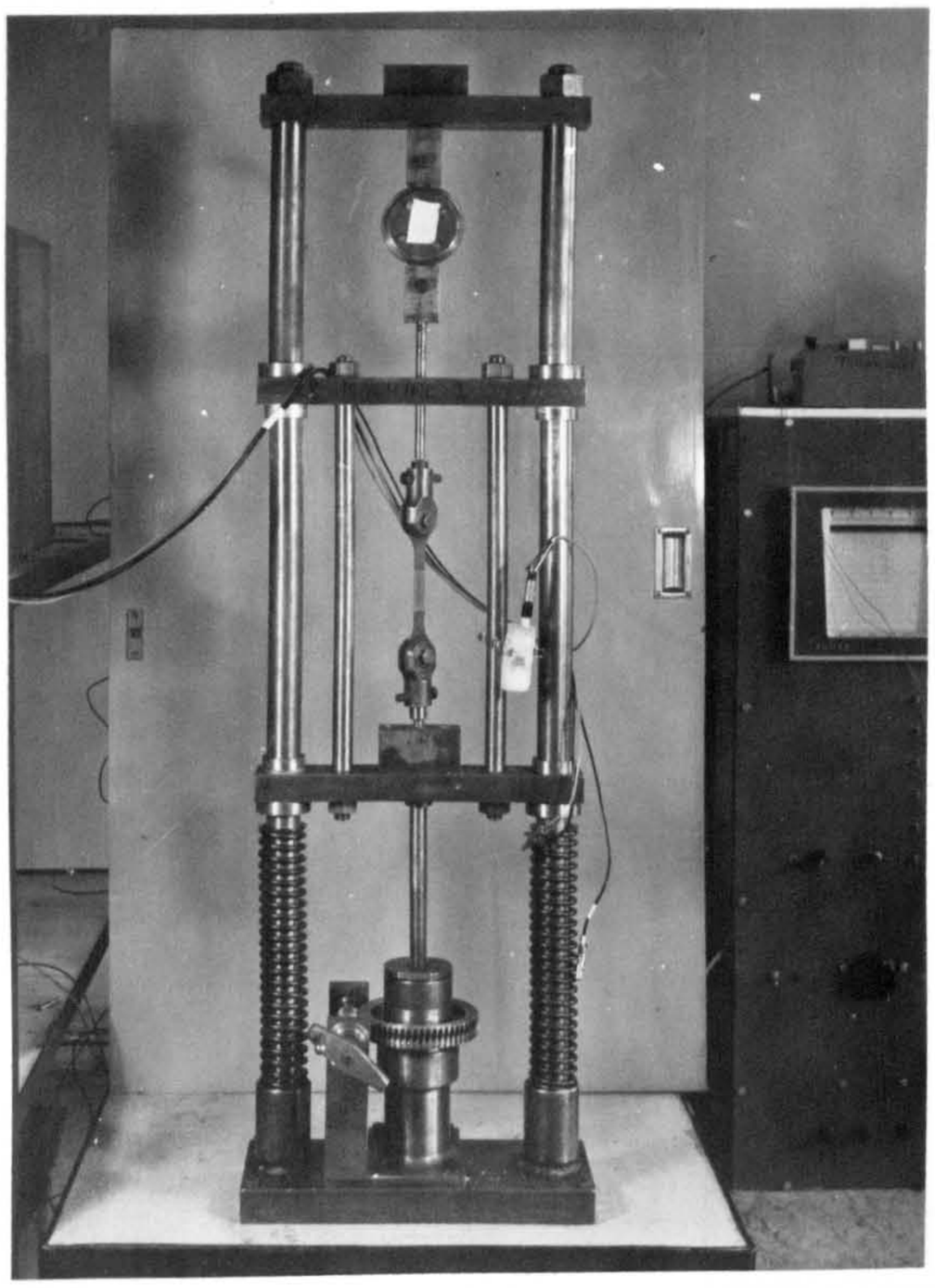

Fig. 2.6 Hardbeam tensometer.

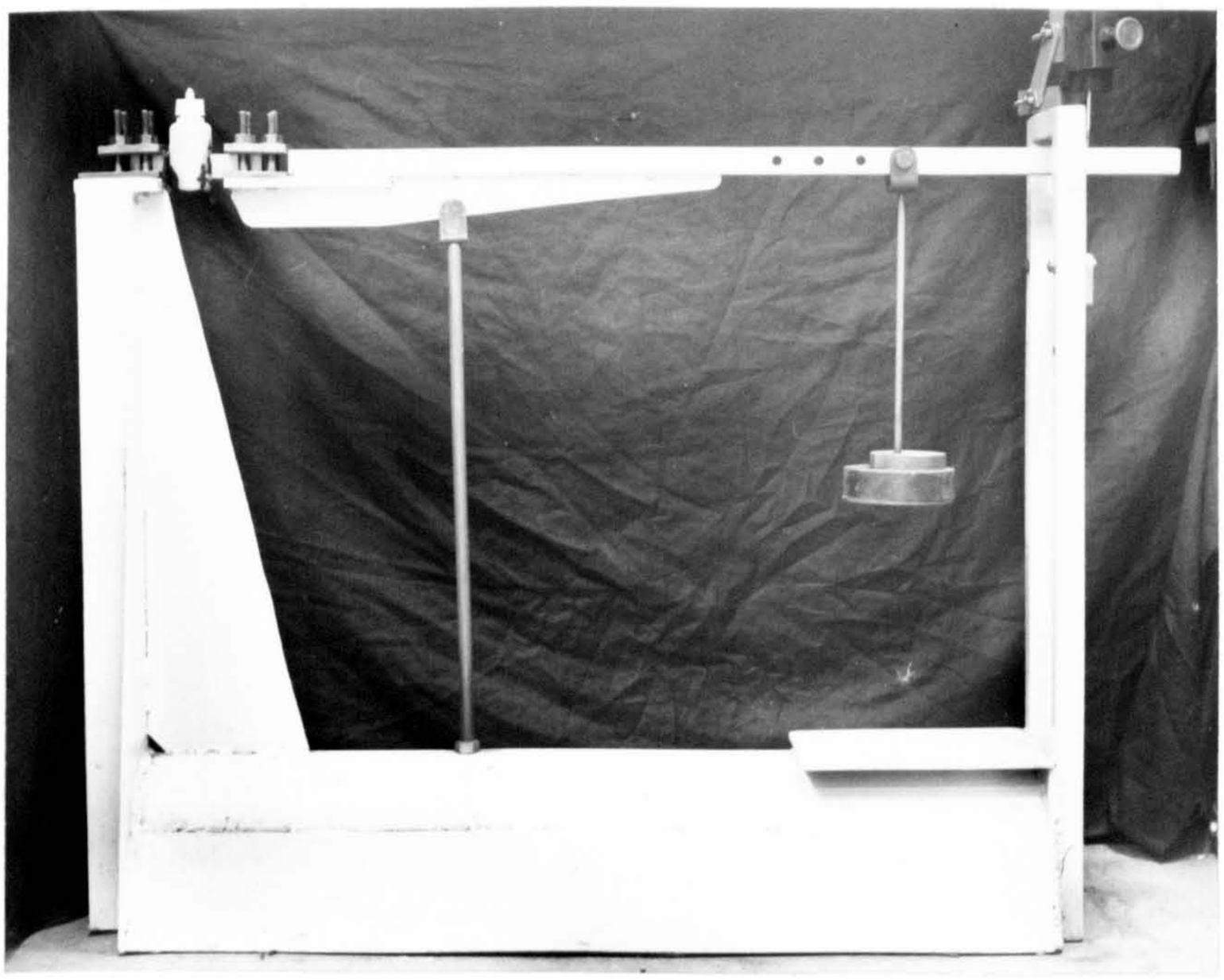

Fig. 2.7 Cantilever-beam arrangement.

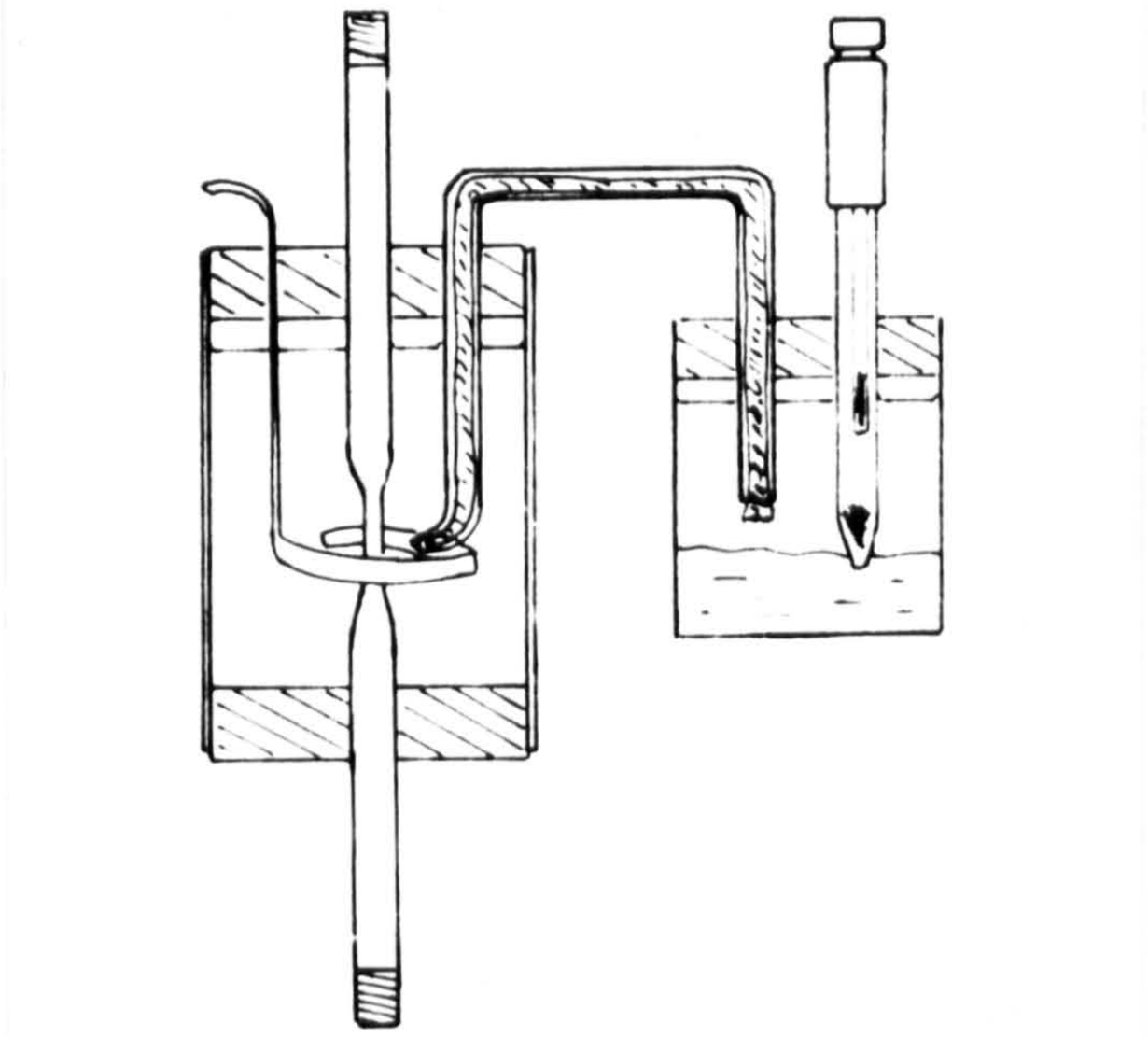

Fig. 2.8 Cell assembly showing positioning of Calomel and Auxiliary Electrodes.

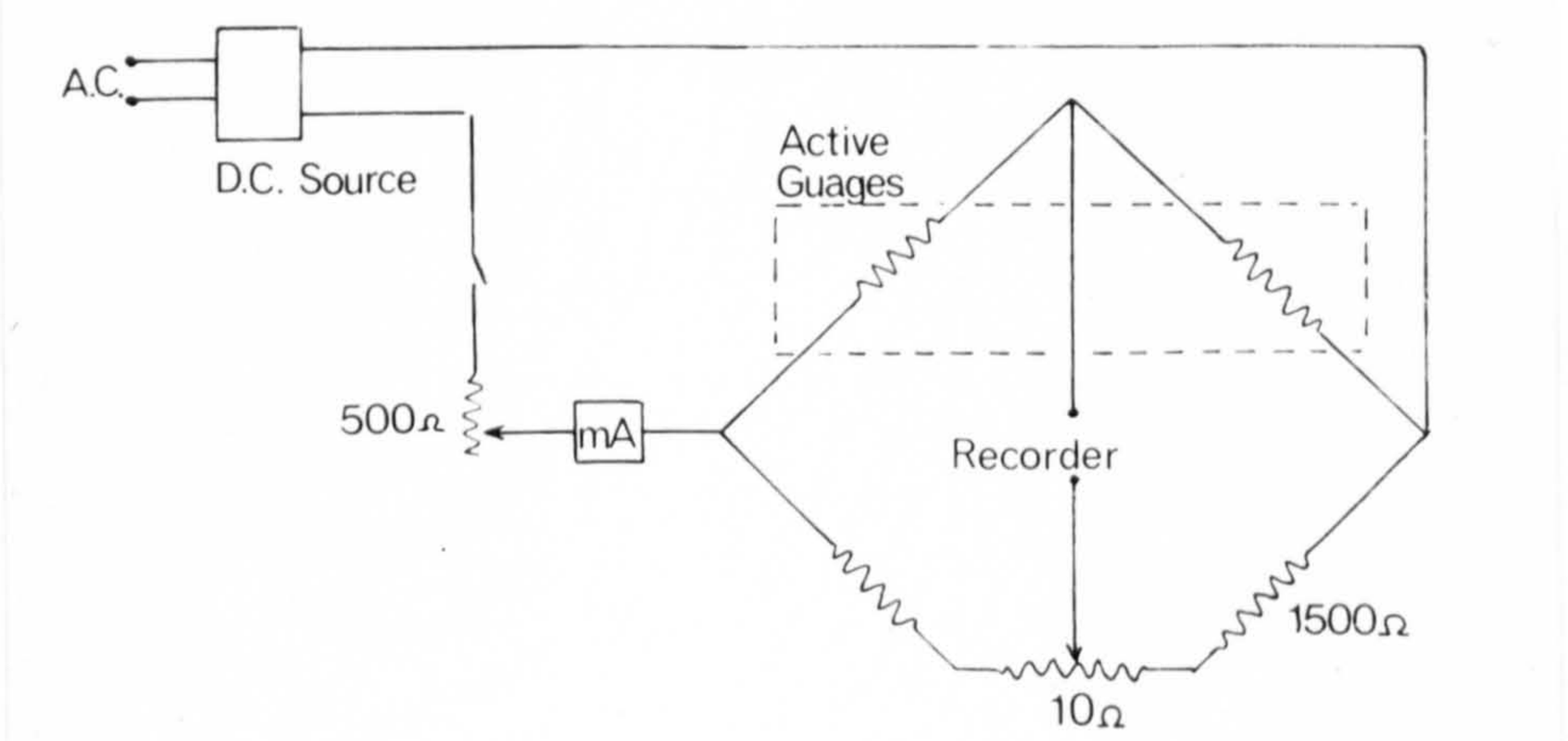

Fig. 2.9 Circuit diaram involving strain guages.

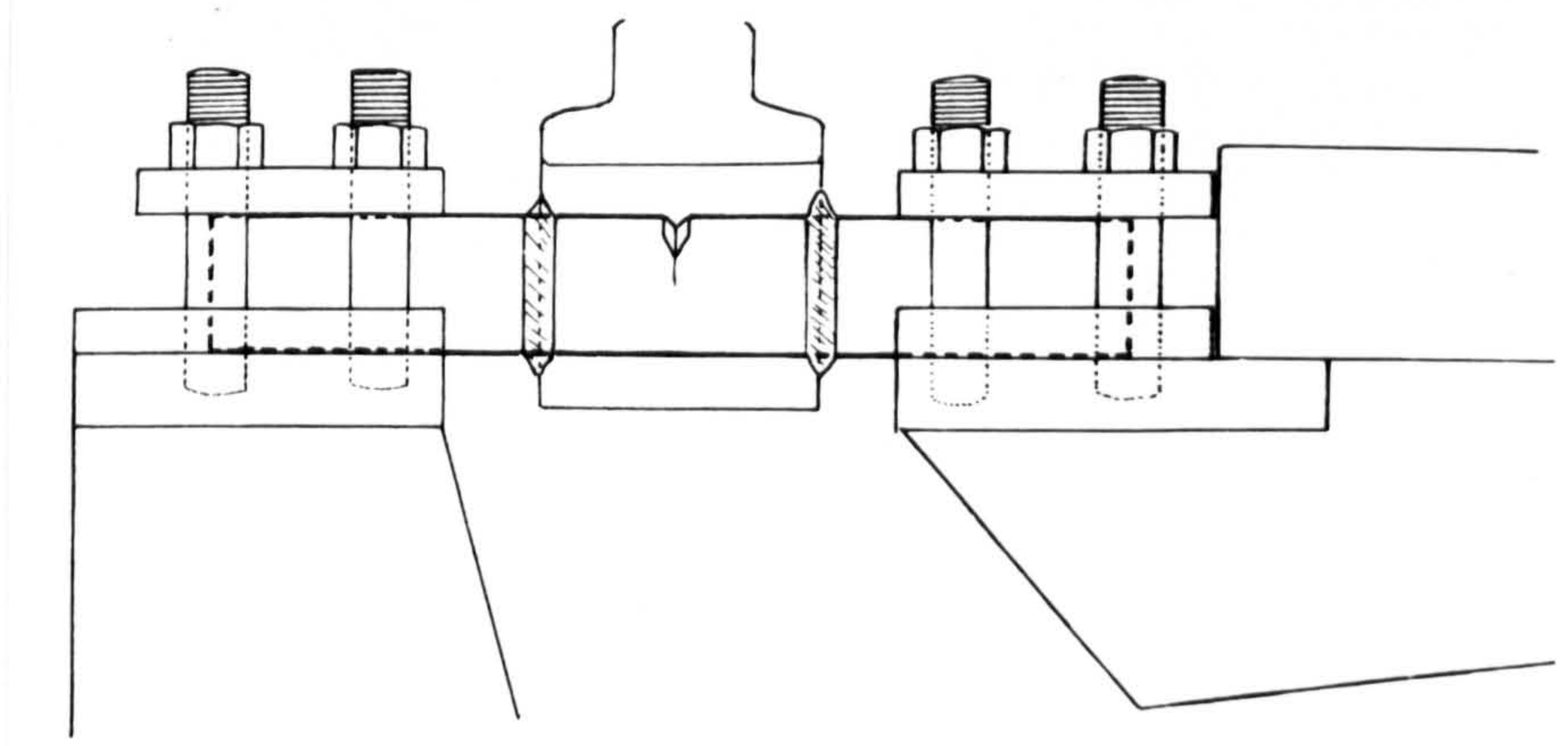

Fig. 2.10 Showing position of pre-cracked specimen and cell.

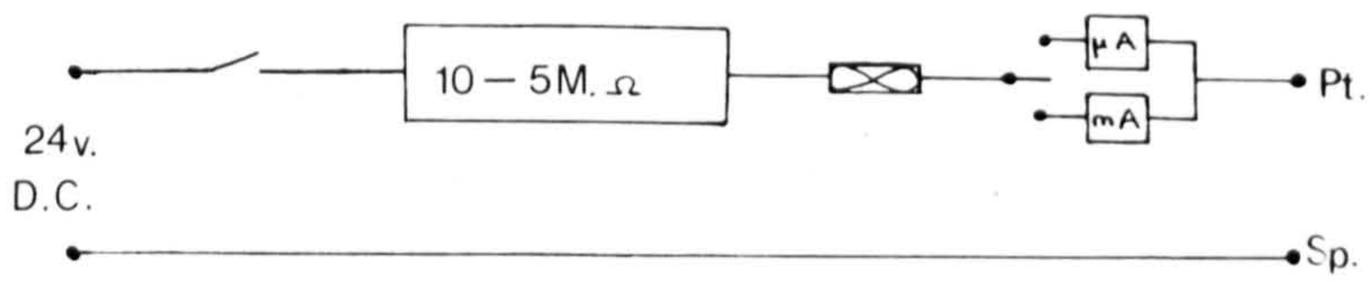

Fig. 2.11 Galvanostat Circuit.

Fig. 2.12 Quickfit cell, and Electrodes.

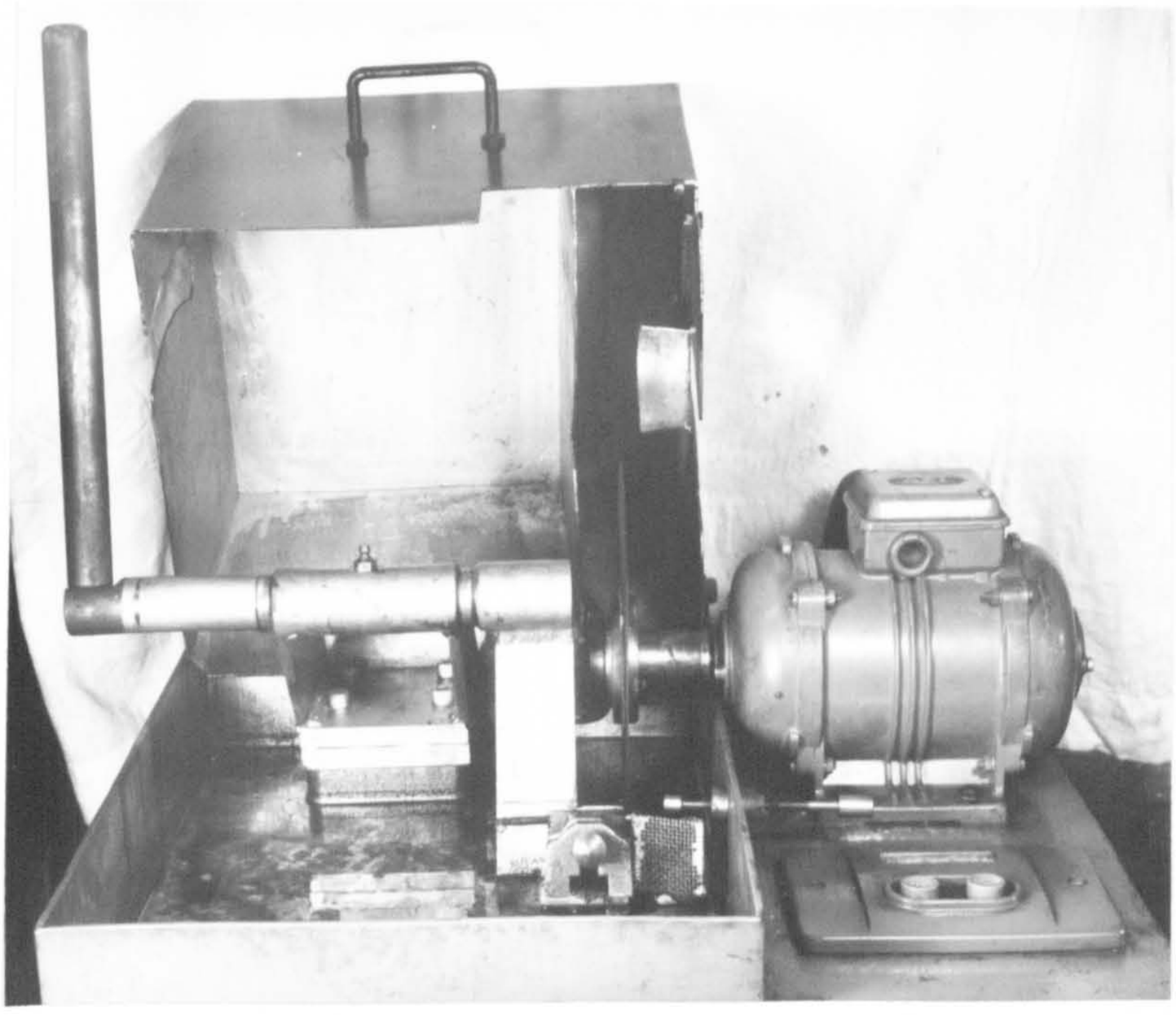

Fig. 2.13 Cut-off machine.

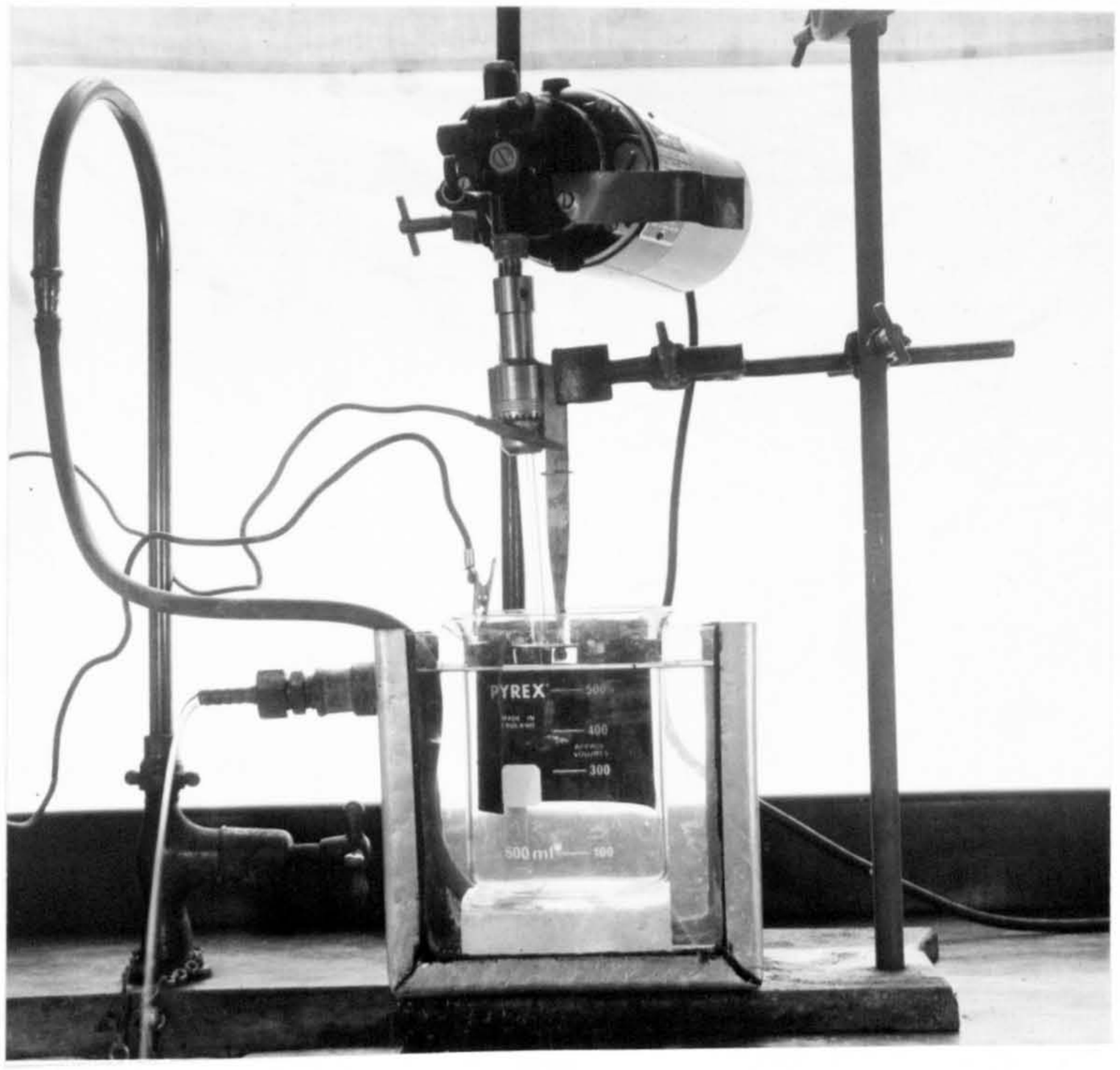

Fig. 2.14 Electropolishing Arrangement.

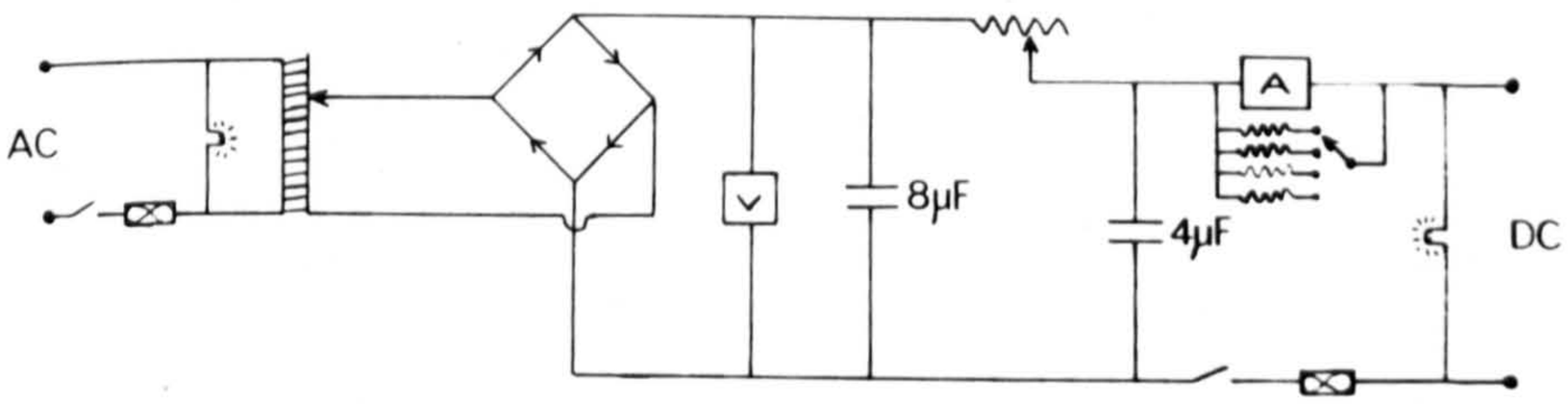

Fig. 2.15 Electropolisher circuit diagram.

3. RESULTS

3.1 Mode of Failure

Essentially two types of failure were encountered when specimens failed under naturally corroding conditions. Initiation occured by the development of surface pits (fissures) and when suitable active paths were present in the structure, crack propagation continued to produce an intergranular stress corrosion failure (Fig. 3.1). In cases where active paths were inoperative failure was achieved by propagation of the surface fissures across the specimen to produce a structure-independent type of cracking (Fig. 3.2). In both types final failure occured by mechanical rupture characterised by a dimple fracture surface to produce complete separation (Fig. 3.3).

3.2 Mechanical Testing

Data produced for the various conditions of heat treatment is shown associated with the appropriate stress corrosion results where necessary. The different steels

used produced similar strength levels and were typical of those quoted for a 125 t.s.i. grade maraging steel.

3.3 Variation in Stress Corrosion Susceptibility with Structure (solution pH 2)

3.3.1 Austenitising temperature

Figure 3.4 shows the stress-time to failure curves obtained for austenitising treatments at 760,800,900, and 1,000°C for 1 hour, all specimens being aged for 3 hours at 530°C. A distinct threshold stress was produced for each of the austenitising temperatures and tests indicated that below these stresses no apparent microscopic cracks were present in the structure. The austenitising treatments produced structures of various grain sizes, the values of which were obtained using the line intercept method and averaging the diameters for a count of 500 grains in each case. The results can be plotted using a Petch type analysis, where the stress required to form an open crack, σ scc, is related to the grain size of

the material l.

$$\sigma_{scc} = \sigma_o + K_{scc}\, l^{-\frac{1}{2}}$$

The threshold stress (σ scc) is found to be linearly related to the grain size (Fig. 3.5) but the latter does not affect the strength of the material in a similar manner. The results indicate that large grained structures are more susceptible to stress corrosion cracking than small grained as both the threshold stress and failure time at a given stress increase with decrease in grain size.

3.3.2 Austenitising Time

Treatments were carried out for up to 22 hours at 1,000°C (all subsequently aged for 3 hours at 480°C) the results of which show a decrease in time to failure with increase in austenitising time for material tested at a constant stress (Fig. 3.6). This effect was only apparent at high stresses, as the threshold stress was not affected by the time of

austenitising treatment (Fig. 3.7). Grain size measurements indicated little or no grain growth and the effect may be a result of a more complete solution or diffusion of elements occuring during the prolonged austenitising.

3.3.3 Aging Temperature

Seven aging temperatures were chosen in the range 300 to 600°C, and where possible stress - time to failure curves were obtained (Fig. 3.8). Material was found to be susceptible to intergranular stress corrosion cracking when aged at temperatures from 325 to 600°C and non-susceptible when treated at temperatures below 300°C or tested in the unaged condition. Tensile data indicate that the precipitation process produces strength increases above 300°C with overaging occuring above 530°C. On plotting tensile data and the times to failure at a constant stress against the aging temperatures, it can be seen (Fig. 3.9) that the effects appear to be related. Maximum susceptibility occurs slightly before maximum strength was attained, but otherwise the susceptibility

can be seen to reflect the precipitation reaction. To a certain extent this was also shown in the load-relaxation curves obtained for various aging temperatures (Fig. 3.10). These indicate that the maximum amount of load relaxation occured with material in the most susceptible condition and was a result of the presence of a large number of cracks.

Tests on material not susceptible to intergranular cracking (i.e. unaged or aged below 300°C) produced transgranular-type failures after long exposure times. Metallographic examination revealed that failure was due to the propagation of surface fissures across the specimen diameter and measurements of crack depth with time on unaged material austenitised at 900°C for 1 hour are shown in Fig. 3.11. Penetration rates were initially high but decreased to a constant value after about 100 hours, with final failure being produced after 1360 hours exposure.

The effect of aging temperature on the propagation stage of the cracking process was examined using specimens

which had been anodically polarised before testing (section 3.4.1) to introduce surface fissures and so eliminate or reduce the initiation period. The results using three times to indicate the susceptibility (section 3.4.2) were plotted (Fig. 3.12) against the aging temperatures employed. Susceptibility towards stress corrosion cracking was found to vary in a manner similar to that found using conventional tests (Fig. 3.9), and suggests a dependence of the cracking process on the aging temperature in both the initiation and propagation stages.

3.3.4 Aging Time

Variations in aging time from 2 minutes to 98 hours were found to have very little effect on the stress corrosion susceptibility except for very short aging times. In Figure 3.13 material aged for 48 hours is shown to exhibit similar times to failure and threshold stress as that aged for the standard time of 3 hours. Results of the variation in time to failure at a constant stress, and strength, with aging time show no change in

susceptibility between 1 and 40 hours (Fig. 3.14). In material aged for shorter times the precipitation reaction appeared incomplete and as a result the stress corrosion susceptibility was reduced. A slight strength increase occured after 40 hours aging, due to a change in precipitate type, but the susceptibility remained unaffected.

3.3.5 Amount of Cold Working

Austenitising was carried out for 1 hour at 800°C in an argon atmosphere, and 10,33,64 or 85% deformation was introduced by cold drawing. Material cold worked 10 or 33% failed by intergranular stress corrosion cracking (Fig. 3.15), which had a tendency to propagate at angles less than 90° to the tensile axis producing a fracture surface as shown in fig. 3.16. Stress-time to failure curves indicate (Fig. 3.17) that the times to failure and threshold stress increase with increasing amount of cold working until with 64 and 85% deformation no intergranular failure could be produced, even when loaded to stresses approaching their yield stress.

Failure could be achieved in the latter after long exposure times, by propagation of surface fissures across the specimen (Fig. 3.18) in a similar manner to cracking in unaged material, (section 3.3). The results thus tend to indicate that two possible cracking mechanisms occur at different rates, and the type of failure produced depends upon the structural condition of the material.

3.3.6 Ausaging

Specimens were tested after being subject to one of the following heat treatments:

(a) austenitised 1000°C, 1 hour air cool.

(b) austenitised 1000°C, 1 hour air cool, aged 480°C 3 hours, air cool.

(c) austenitised 1000°C, 1 hour cool 700°C and ausaged for up to 24 hours, and air cool.

(d) austenitised 1000°C 1 hour, cool 700°C and ausaged, air cool , aged 480°C 3 hours and air cool.

The ausaging treatments (or thermal embrittlement) were carried out in order to enhance any precipitation of

titanium carbide at the austenite grain boundaries in an attempt to induce unaged material to fail by intergranular cracking. Results of stress corrosion tests and UTS values produced by treatments (b) and (d) were similar and indicate that no effect is introduced by the additional ausaging treatment. Tests on treatments (a) and (c) also indicate that ausaging has no effect as no intergranular failure was produced in either case, and fissure depth-time measurements produced similar values.

3.5.7 Cooling Rates

Material was heat treated and cooled from temperature by (a) furnace cooling, (b) air cooling, (c) water quenching. Tests on the stress corrosion susceptibility showed the cooling rates to have no different effect on either times to failure or threshold stresses.

3.4 Variations of Stress Corrosion Cracking with Environment.

3.4.1 Initiation dependence of Stress Corrosion Cracking

Material was heat treated and tested in a solution of pH.11, in order to reproduce variations in susceptibility with austenitsing and aging effects similar to those found in solutions of pH-2. Stress corrosion failures could not be produced, however, unless the specimens were tested under potentiostatic conditions. A potential of -400 m.v. s.c.e. was chosen (approximating the free corrosion potential) and stress-time to failure curves were obtained for various austenitising temperatures. The results (Fig. 3.19), show no obvious trends and indicate the possible predominance of the impressed electrochemical conditions. Metallographic examination revealed the presence of surface fissures leading to intergranular cracking (Fig. 3.20), whereas material tested without potentiostatic control showed no surface attack. The importance of surface fissures in the

initiation process was thus inferred and a method was developed for introducing these fissures to a known depth in a specimen before stress corrosion testing. This technique involved anodic polarisation of the specimen in the unstressed condition for a known time and at a constant current density. Tests in solution pH-11 on material in which fissures had been introduced showed failure to occur readily in an intergranular manner. In pH-2 solutions, similar tests also produced rapid failure as a result of severe stress corrosion cracking (Fig. 3.21). This type of testing produced load relaxation plots which suggested that open crack propagation occured from the outset and this corresponded to the region just prior to fracture in conventional tests.

The development of surface fissures was examined using various polarising times at a given current density and the results are shown in fig. 3.22. Fissure penetration is initially rapid but decreases with increase in polarising time following a typical parabolic-

-type growth curve. Tests were carried out at a constant stress to determine the variation in time to failure with polarising time and similar results were produced for solutions of either pH 2 or 11. Failure times were reduced only slightly for polarising times greater than eight hours, and as a result the standard conditions of 18½ hours at a current density of 10 mA/in^2 were chosen.

3.4.2 The pH dependence of the Cracking Process

The dependence of the cracking process on solution pH was determined by testing specimens at a constant stress in solutions having pH values in the range 1 to 12. Surface fissures were introduced into the specimens before stress corrosion testing by anodic polarisation, in order to enable failures to be produced in solutions of pH - 11 under naturally corroding conditions. With this type of testing, times to failure of as little as several minutes could be produced, and using these only as a guide to the susceptibility could be unsatisfactory owing to the varying amounts of load relaxation encountered.

As a result three times were taken into consideration, (a) the overall time to failure, Tf, (b) the time elapsed before any load relaxation occurs, Ti, and (c) the ratio Ti/Tf expressed as a percentage. The results produced show (Fig. 3.23) a pH dependence with minima occuring at pH values of approximately 2 and 11.

3.4.3 Solution Condition

Stress corrosion testing was carried out under several environmental conditions and the results can be categorised in three sections:

(a) Tests in stirred solutions of pH-2 produced failures in shorter times than for unstirred conditions. Fig. 3.24 shows stress-time to failure curves for stirred and unstirred solutions, with the times to failure and the threshold stress being reduced by stirring, although the type and amount of cracking remained unchanged. Tests in stirred solutions ofpH-11 produced stress corrosion failure in bulk specimens under conditions which, in stagnant solutions, had not previously produced any failure.

The effects produced in solutions of both pH values may be due to the increased reaction rates as a result of depolarisation produced by the stirring action.

(b) Hydrogen peroxide was added to solutions in an amount approximating to 1% by volume. The effect in pH-2 solutions was to increase the time to failure by a factor of three, the specimen being covered by a rust-brown precipitate of ferric hydroxide. This was due to the oxidation by the hydrogen peroxide of the ferrous hydroxide "normally" present and the presence of this surface film reduced the susceptibility to stress corrosion cracking. In solutions of pH - 11, however, the effect was to produce stress corrosion failure after relatively short exposure times of as little as 100 mins., whereas tests without hydrogen peroxide in solutiondid not fail within the maximum time limit of 10,000 mins. Metallographic examination revealed a normal intergranular type of attack propagating from surface fissures, but of an intense nature producing a large number of cracks. These results to some extent indicate the importance of oxygen reduction

in the cracking process, and in the case of pH - 11 this may be the rate controlling factor.

(c) Stress corrosion tests carried out in solutions of 3N sodium chloride produced no differences in cracking type or failure times than those produced in 0.6.N solutions.

3.4.4 Crack Propagation Rates

Specimens examined metallographically after known exposure times revealed that the natural surface fissure propagation rate was independent of heat treatment and the value produced for a solution of pH - 2 was 0.001 mm/hr. Open crack propagation rates were observed using specimens in which surface fissures were generated to a fixed depth before testing. After stress corrosion testing the fracture surfaces revealed that cracks appear to propagate from many points on the circumference and produce an outer ring of stress corrosion cracking with a circular ductile area in the centre (Fig. 3.25). By viewing in both optical and scanning electron microscopes a value for the depth of the stress corrosion area could

be obtained. The results for solutions of pH 2 and 11 indicate that crack propagation in pH-2 (7 mm/hr.) was almost 10 times faster than a solution of pH-11 (0.8 mm/hr.)

3.5 Environmental Characteristics of Maraging Steels

3.5.1 Intergranular Penetration and Corrosion Rates

Specimens austenitised and aged over a range of temperatures were anodically polarised and, after sectioning and polishing, examined for the extent of intergranular penetration. In several cases grain boundaries appeared to have been attacked so that the grains dropped out, and a similar effect was seen to occur in certain stress corrosion fractures (Fig. 3.26). The amount of intergranular penetration was not excessive in any structure with the maximum penetration only occuring to a few grain diameters even in the largest grained material. Unaged structures were found not to be susceptible to intergranular attack, but suffered random penetration due to the growth of surface fissures and this suggests that

T A B L E I I I

CORROSION RATES

(a) Weight loss

Assuming the reaction:-

$$Fe - Fe^{2+} + 2e$$

Average corrosion current values:-

aerated pH - 2 ..... $4x10^{-5}$ A/cm.^{2}

deaerated pH - 2 ..... $Ix10^{-6}$ A/cm.^{2}

aerated pH - II ..... $1.5x10^{-6}$ A/cm.^{2}

deaerated pH - II ..... $4x10^{-7}$ A/cm.^{2}

(b) Pulsed Current Method.

Solution pH - 2

Tafel slopes anodic 36 mv per decade

cathodic 60 mv per decade

$\Delta E / \Delta I = 23.4$

$I_{corr.} = 1.2 \times 10^{-3}$ A / cm.^{2}

Solution pH - II

Tafel slopes anodic 24 mv per decade

cathodic 74 mv per decade

$\Delta E / \Delta I = 130$

$I_{corr.} = 6 \times 10^{-5}$ A / cm.^{2}

some difference in the nature of the grain boundaries may exist between aged and unaged material.

Corrosion rate measurements show all structures to be equally susceptible to general corrosion and the results obtained from wight loss and pulsed polarisation techniques are given in table 3. The trends follow a general sequence where the amount of corrosion depends on solution pH and oxygen content rather than structural condition.

3.5.2 Polarisation Curves

Potentiodynamic polarisation curves were determined under a variety of conditions to observe the effects of material conditions and solution on the polarisation characteristics. Curves produced for the various combinations of stirring rate, sweep rate, heat treatment and pH were found to follow no obvious trend, and conditions resembling those used in stress corrosion testing were chosen as standard i.e. unstirred at a slow sweep rate. The effect of stirring is shown in fig. 3.27, and in cases where the rate of film formation

could be important different sweep rates can produce different results (Fig. 3.28).

A) Comparison with Pure Elements

Polarisation curves were obtained for the major alloying elements present in the maraging steel and results in both pH - 2 and pH - 11 solutions are shown in figs. 3.29 and 3.30. In acidic solutions, maraging steel appeared to behave in a similar way to cobalt or iron under cathodic polarisation, and as a mixture of iron, cobalt, and nickel under anodic polarisation. The free corrosion potential was close to that obtained for pure cobalt and the curves produced similar values for limiting current densities. In solutions of pH - 11 the cathodic curve of maraging steel resembled those of Fe, Ni, and Co, but the anodic curve exhibited similar characteristics as those of nickel. Under these conditions pure nickel was relatively passive until potentials greater than +200 m.v. were applied and this could indicate that passive areas may exist at localised nickel rich anodic areas. In both solutions maraging steels developed a covering of black corrosion product at anodic potentials

greater than -200 m.v., and a similar effect was only produced for pure molybdenum. This film appeared to be non-protective as no passivating effects were produced as a result of it's presence.

Curves for titanium carbide were produced in pH-2 and pH-11 solutions (Fig. 3.31) and show the material to be relatively inactive over a large range of potentials. The free corrosion potentials obtained under naturally corroding conditions were approximately -100 m.v. in pH - 2 and -200 m.v. in pH - 11, both of which are noble to those of maraging steels.

B) Deoxygenated Solutions

Solutions of pH -2 and pH -11 were boiled under reflux for several hours to expel the oxygen and polarisation was carried out under an argon atmosphere. The results (Fig. 3.32) suggest that the main cathodic reaction is oxygen reduction under naturally corroding conditions. In pH - 2 solution a decrease in total cathodic current was produced for potentials greater than - 600 m.v., and below this value hydrogen ion

reduction was the probable major cathodic reaction. With pH - 11 solution a similar result was obtained, where a decrease in total cathodic current was produced for all potentials greater than -1000 m.v. in deaerated conditions.

C) Hydrogen Peroxide additions

Pure hydrogen peroxide was added to solutions to ensure a ready supply of oxygen for the cathodic reactions. The polarisation curves obtained (Fig. 3.33) indicate that an increase in the total cathodic current was obtained in the presence of the hydrogen peroxide for solutions of pH 2 and 11, and the free corrosion potentials were moved in the noble direction. These results also suggest that the main cathodic reaction is that of oxygen reduction for potentials greater than -650 m.v. in pH - 2 and -1000m.v. in pH 11 solutions.

D) Solution pH

Polarisation curves over a range of pH values are shown in fig. 3.34. In acid solutions the curves exhibit similar characteristics and very little change occurs even with pH values as low as 0.76. A careful

study was made in the range pH 0.76 to 2.2 to try and establish the pH value where hydrogen ion reduction replaced oxygen reduction as the main cathodic reaction. Results were obtained for values of pH 0.9, 1.12,1.42,1.7, & 2.0 for both aerated and deaerated conditions, but the effect was only to increase the free corrosion potential and no distinct change in characteristic was apparent.

Curves obtained for neutral solutions show similar features to that at pH 6.5 (Fig. 3.34). Cathodic currents produced were small, with hydrogen evolution only occuring in the region of -1000 m.v. The anodic curve indicates the possibility of some film formation, as the result obtained for the fast sweep rate produced a free corrosion potential at more negative potentials and initially higher anodic current values than that for a slow sweep rate. Results for pH - 11 solutions show a similar dependence on sweep rate and comparison with curves in pH - 12 could indicate the onset of some form of passivation.

E) Heat Treatment and Amount of Cold Work

Material in the unaged condition behaved in exactly the same way when subject to potentiodynamic polarisation at various sweep rates, both in the stirred and unstirred states. Specimens tested after varying amounts of cold work also produced a series of curves having similar characteristics, the only observable difference being an increasing reluctance for black film formation with increase in the amount of cold work. As this film is non-protective and conductive, no change in current value was produced as a result of its presence.

F) Variation in Chloride Ion concentration

A series of curves was produced for demineralised water at pH - 11 with, and without additions of chloride ions. The results (Fig. 3.35) show that, (a) in the absence of chloride ions reaction currents are small, and (b) with increasing amounts of chloride ions the curves tend to, (c) that obtained for a 0.6N solution at this pH. Tests in a 3N sodium chloride solution produced a similar curve, (d) only differing in the limiting current density values produced.

3.5.3 Free Corrosion Potential - Time Curves

Two types of curve were produced for the variation of free corrosion potential with time over the range of heat treatments investigated. Material aged at temperatures below 530°C produced a small negative potential drift during testing, with the largest change occuring at the onset of load relaxation and at fracture (Fig. 3.36). Aging at temperatures of 530°C and above generated conditions where a potential shift of up to 150 m.v. could be produced and fig. 3.37 shows a typical potential-time plot and the associated load relaxation curve. The greatest shift in this case also occured during load relaxation and fracture, but additionally the potential oscillated by up to 10 m.v. about the general trend throughout the test. This may be due to the presence of the thick black corrosion product on the surface which was readily produced on material aged under these conditions. With material aged below 530°C the specimens were only covered with a thin black film which did not cover the whole surface and the resulting potential plot was smooth.

In certain cases where tests resulted in long failure times the corrosive solution was changed periodically. The effect of renewing the solution on the free corrosion potential of the specimen could be explained by either concentration depolarisation or as a result of the pH change involved. Figure 3.38 shows typical variations obtained when the solution was changed during testing. Each change was accompanied by a large change in free corrosion potential and the results indicate this to be due to depolarisation.

Potential plots obtained for stirred tests were similar to those of figure 3.36, with small potential shifts occuring even where a thick corrosion product was formed.

3.5.4 Identification of Corrosion Products

The black corrosion product associated with stress corrosion fractures (Fig. 3.39) was examined using X-Ray Powder techniques, and the results (table 4) suggest the film to be a basic molybdenum oxide - $Mo_5\ O_5\ (OH)_{10}$, of very small crystallite size. No lines were produced characteristic of any iron or iron oxides and chemical

TABLE IV

Results for X-Ray Analysis

d-Spacing	Intensity	$Mo_5O_5(OH)_{10}$ 'd'	I/I_o
4.30	vvw		
3.41	vvw	3.36	40
3.31	vw		
2.46	vw	2.73	70
		2.50	40
2.34	vvw		
2.22	mw	2.26	80
2.02	mw	2.03	80
1.95	w	1.95	70
1.75	w	1.76	60
		1.72	60
1.62	vvw		
1.54	vw	1.58	50
1.47	vw	1.47	60
		1.45	40
1.38	w	1.36	70
1.18	vvw		

Strong reflections for Iron Oxides

I/I_o	100	60-80	50-60
FeO	2.14	1.51	2.47
Fe_3O_4	2.53	1.48	1.61
aFe_2O_3	2.69	2.51	1.84

tests on the oxide for molybdenum proved positive (molybdate test). Polarisation data also associated the film with molybdenum and showed it to be of a non-protective nature.

Chemical analysis on solutions after stress corrosion testing indicate the presence of ferrous ions, and in many cases these were precipitated in the cell as a green-black ferrous hydroxide. The latter was oxidised to brown ferric hydroxide when near the solution/atmosphere interface and this tends to reflect the neutral conditions which solutions attain during prolonged stagnant testing.

3.6 Structural Examination of Maraging Steels

3.6.1 Optical Microscopy

All structures showed similar features when examined optically and no difference could be distinguished between unaged and aged material. The prior austenite grain boundaries could be indentified in most cases and the matrix showed evidence of martensite platelets occuring in three principal directions.

3.6.2 Electron Microscopy

Thin films produced from material unaged or aged at various temperatures were examined and the structures were found to consist of a matrix of high dislocation density, with martensite laths a predominant feature (Fig. 3.40). In certain cases aged material revealed the presence of a grain boundary precipitate (Fig. 3.41) but this was not always visible and could not be indentified using select area diffraction.

Carbon replicas and extraction replicas on overaged material were produced in order to separate the grain

boundary precipitate and enable identification. Figure 3.42 shows a typical result, but indentification was not achieved owing to the small size of the precipitate.

Two forms of dipping tests on thin foils were carried out to determine any inherent difference in corrosion behaviour between the grain boundary and matrix areas. Foils were examined and then dipped into a stress corrosion solution whilst being stressed by bending. On re-examination the attack produced was found to be a random form of general attack, rather than selective on some specific feature. In some cases grain boundaries were left unattacked (Fig. 3.43), but this was probably a result of a thickness difference rather than selective attack. Thin foils were also examined before and after dipping in a solution containing chloroplatinic acid, used to produce platinum decoration of the anodic sites. The results obtained, however, did not indicate any specific anodic or cathodic sites, as platinum was found to deposit at random, particularly around the thinner areas of the foil. (Fig. 3.44).

3.6.3 Geoscan

To investigate the possible presence of segregate

in grain boundary regions, line and dispersion scans were carried out over several grain boundaries in a fully aged material. No segregation was detected and scans for several other elements (Si, S, P, Mn) also proved negative. The area examined was approximately fifty microns square and with a minimum probe diameter of one micron, the grain boundary regions appeared too small for segregation to be detected.

3.6.4. Scanning Electron Microscopy

Stress corrosion fracture surfaces were examined to reveal clean intergranular cracking as shown in figure 3.45. All stress corrosion surfaces showed similar features with occasionally secondary transgranular cracking being observed in cases where long failure times were involved (Fig. 3.46). Several tests were carried out on material austenitised at 1100°C, producing a large grained structure, and examination of the stress corrosion fractures showed markings present on the grain surfaces (Fig. 3.47). These were only observed with this heat treatment and appear to be indications of an irregular propagation of the crack front across the grain surface.

Mechanical failure in all cases occurred by normal ductile rupture (Fig. 3.48) with occasional shear rupture when tests were carried out at high stresses (Fig. 3.49).

Crack initiation occured by the formation of surface fissures and these appeared as 'V' shaped trenches (Fig. 3.50) in specimens which had been anodically polarised before stress corrosion testing. Crack propagation could be shown to occur at the grain boundaries (Fig. 3.51) by examination of surfaces which had been immersed and stressed in solutions containing chloroplatinic acid. Crack initiation in this case also appeared to be a result of the formation of surface fissures (micro-pits) which formed a continuous groove along the grain boundary (Fig. 3.52).

Fracture surfaces of stress corroded, pre-cracked, specimens exhibited typical intergranular failures with final mechanical ductile rupture. The pre-crack/stress corrosion area followed an approximate straight line (Fig. 3.53) but in large grained material the areas of stress corrosion cracking and fatigue fracture could

overlap by up to two grain diameters (Fig. 3.54).

3.7 Environmental Characteristics of Stress Corrosion and Hydrogen Embrittlement Failures.

3.7.1 Effect of Applied Potential

Specimens were maintained at various potentials in solutions of pH 2 and 11 and the time to failure determined when loaded to an initial constant stress. Figures 3.55 and 3.56 show the results obtained and indicate that stress corrosion and hydrogen embrittlement cracking occur in distinct potential regions. For solutions of pH - 2, hydrogen embrittlement failure did not occur until potentials of less than -700 m.v. were impressed, whilst stress corrosion cracking occured above -600 m.v., and the region between offered a range where cathodic protection was possible. Solutions of pH - 11 exhibited similar characteristics with hydrogen embrittlement occuring below -1000 m.v., stress corrosion cracking above -600 m.v., and no failure in between these values. Plotting these results on a potential -pH diagram for iron (Fig. 3.57)

shows that the stress corrosion or hydrogen embrittlement regions correspond approximately to potentials which either lie above or below the hydrogen line. Specimens at potentials above the oxygen line failed by the combined action of stress corrosion cracking and general corrosion in solutions of pH 2 or 11. In neutral solutions no stress corrosion failures were produced and failure was only observed at anodic potentials by reduction of the cross-sectional area as a result of general corrosion. Hydrogen embrittlement failures, however, could be produced at potentials below -800 m.v.

3.7.2 Effect of Applied Currents.

Investigations were carried out under galvanostatic conditions with solutions of pH 2 and 11 containing additions of (a) chloroplatinic acid, (b) sodium arsenate and (c) anthraquinone. Each addition should produce effects that could possibly be related to the dependence of stress corrosion or hydrogen embrittlement upon the hydrogen available at the metal surface, such that:-

(a) chloroplatinic acid enables hydrogen to be more readily evolved from the platinum cathodes produced on the metal surface than to enter the metal as atomic hydrogen. Thus the susceptibility towards hydrogen embrittlement should be decreased, and the susceptibility towards stress corrosion cracking should not be affected as the latter appears to be associated with oxygen reduction.

(b) Sodium arsenate additions promote hydrogen entry into the metal at potentials below -420 m.v. and should increase the susceptibility towards hydrogen embrittlement.

(c) Anthraquinone derivatives can take up hydrogen into their structure and should decrease the susceptibility to hydrogen embrittlement whilst not affecting the susceptibility towards stress corrosion cracking.

The results obtained are shown in figs. 3.58 and 3.59, all specimens being tested at a constant initial stress value. In solutions of pH -2 and 11 additions of chloroplatinic acid and anthraquinone were found to reduce the susceptibility towards hydrogen embrittlement and to have very little effect on the stress corrosion

cracking process. The effect of sodium arsenate additions was to increase the susceptibility towards hydrogen embrittlement and failures in as little as a few minutes could be achieved. Its effect on the stress corrosion process could not be evaluated as the promoter is effective only below potentials at which AsH_3 is stable.

3.7.3 Structural Effects

Hydrogen embrittlement and stress corrosion cracking were both found to exhibit stress-time to failure curves showing the same characteristics. However, hydrogen embrittlement tests on material subjected to various amounts of cold working produced results (Fig. 3.60) slightly different from those obtained with stress corrosion testing.

Metallographic examination of fractures produced at various potentials showed little difference between the stress corrosion or hydrogen embrittlement failures obtained, the majority of cracking appeared to be inter-granular with the occasional occurence of transgranular cracking in some hydrogen embrittlement failures. (Fig. 3.61).

In certain cases, however, material tested under stress corrosion conditions in solutions containing chloroplatinic acid additions showed quite an extensive load relaxation before failure, and examination revealed the presence of a large amount of secondary transgranular cracking, and an increase in general attack towards the central cracked regions of the specimen (Fig. 3.62). Polarisation data suggest that chloroplatinic acid additions to solutions of pH 2 and 11 should have no effect on the cathodic reaction under naturally corroding conditions. Effects, however, could be produced in solutions of pH value 0.76, where the major cathodic reaction would be hydrogen ion reduction. Specimens broken in such a solution produced fractures which showed a large amount of secondary transgranular cracking of a nature similar to that produced in specimens broken in pH 2 solutions. The results suggest that some pH or potential drop may occur down the propagating cracks, which could produce a change in the cathodic reactant from oxygen to hydrogen ion reduction. The latter can occur more readily in the presence of chloroplatinic acid, which enables the anodic reaction to increase and produces a

greater amount of attack towards the central cracked region of the specimen.

Examination of fracture surfaces using the Scanning Electron Microscope showed that stress corrosion failures were characterised by intergranular cracking but that hydrogen embrittlement failures proved to be a mixture of both intergranular and transgranular cracking with the latter being predominant (Fig. 3.63). A range of hydrogen embrittlement failures was produced under conditions of high and low loads, various applied currents, and after anodically polarising before testing, the results being given in table 5. The fracture surfaces were examined and were mainly transgranular with occasionally intergranular areas present near the "surface edge" of the fracture (Fig. 3.64). Similar types of failure were produced in unaged and aged materials, with clevage also being observed in specimens which were hydrogen charged in the unstressed condition and then mechanically failed (Fig. 3.65). Clevage steps and planes were visible in all fractures (Fig. 3.66) and in certain cases chevron markings were observed (Fig. 3.67) in which small cracks were found to be associated with each mark,

TABLE - V

Heat Treatment Aust. / Aged.		Potential mv.	Load Ton	Time to Failure, Mins.	Type of Cracking
1100	-	-1400	0.5	985	Mainly T.G.
1100	-	-1600	0.3	n.f. 5,000	Some "
1100		-1400	0.5	185	" "
(with surface fissures)					
1100	480	-1400	0.7	5	I.G. & T.G.
1100	480	-1400	0.5	532	" "
1100	480	-1400	0.5	3	" "
(with surface fissures)					

(Fig. 3.68). When intergranular areas were present these appeared featureless and showed no markings characteristic of clevage (Fig. 3.69). The latter appeared to be of the continuous type, but on some steps evidence was found of what may be shear rupture (Fig. 3.70).

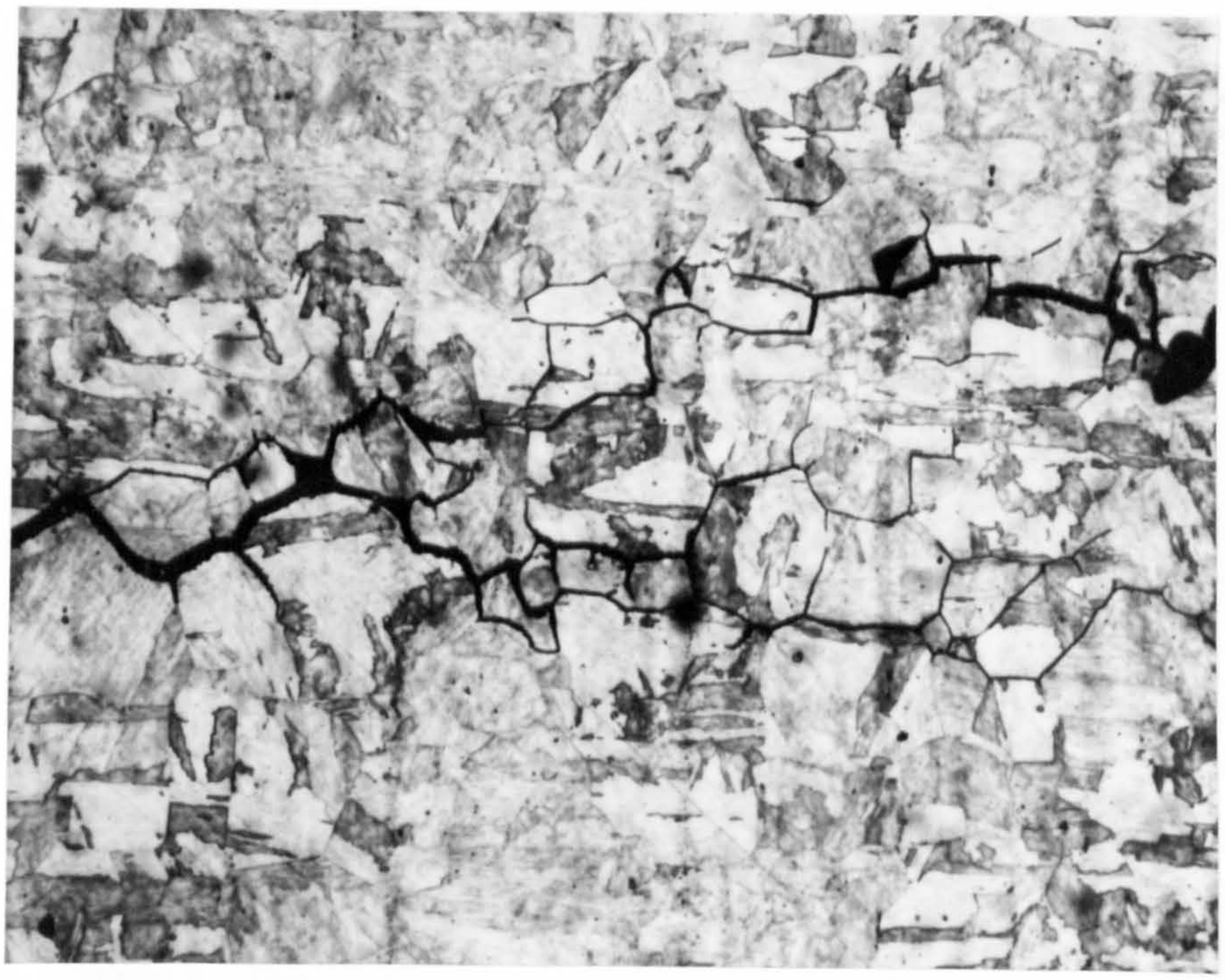

3.1 Typical Intergranular cracking (300x)

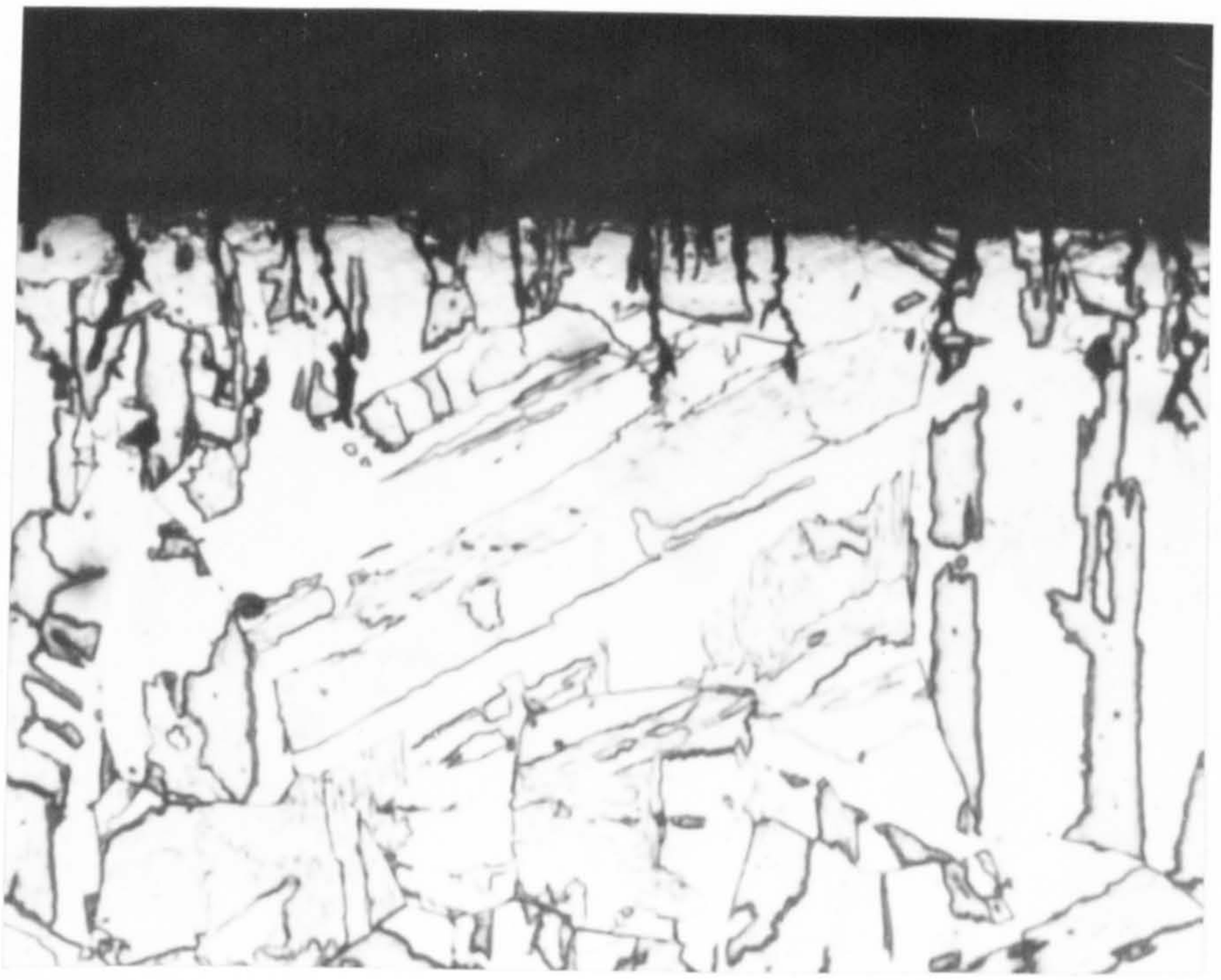

3.2 Surface fissures in an unaged material (600x)

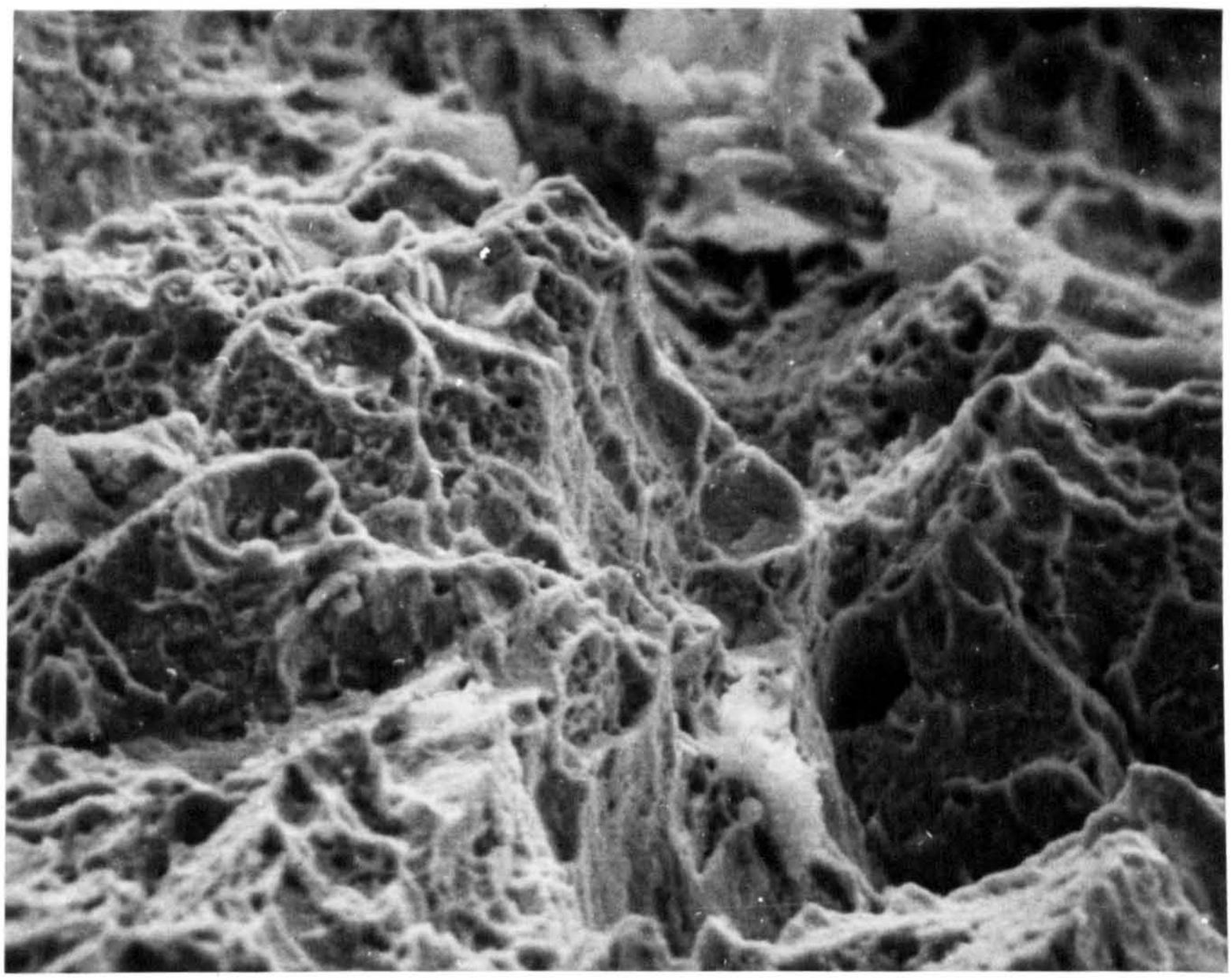

Fig. 3.3 Ductile rupture area (1000x)

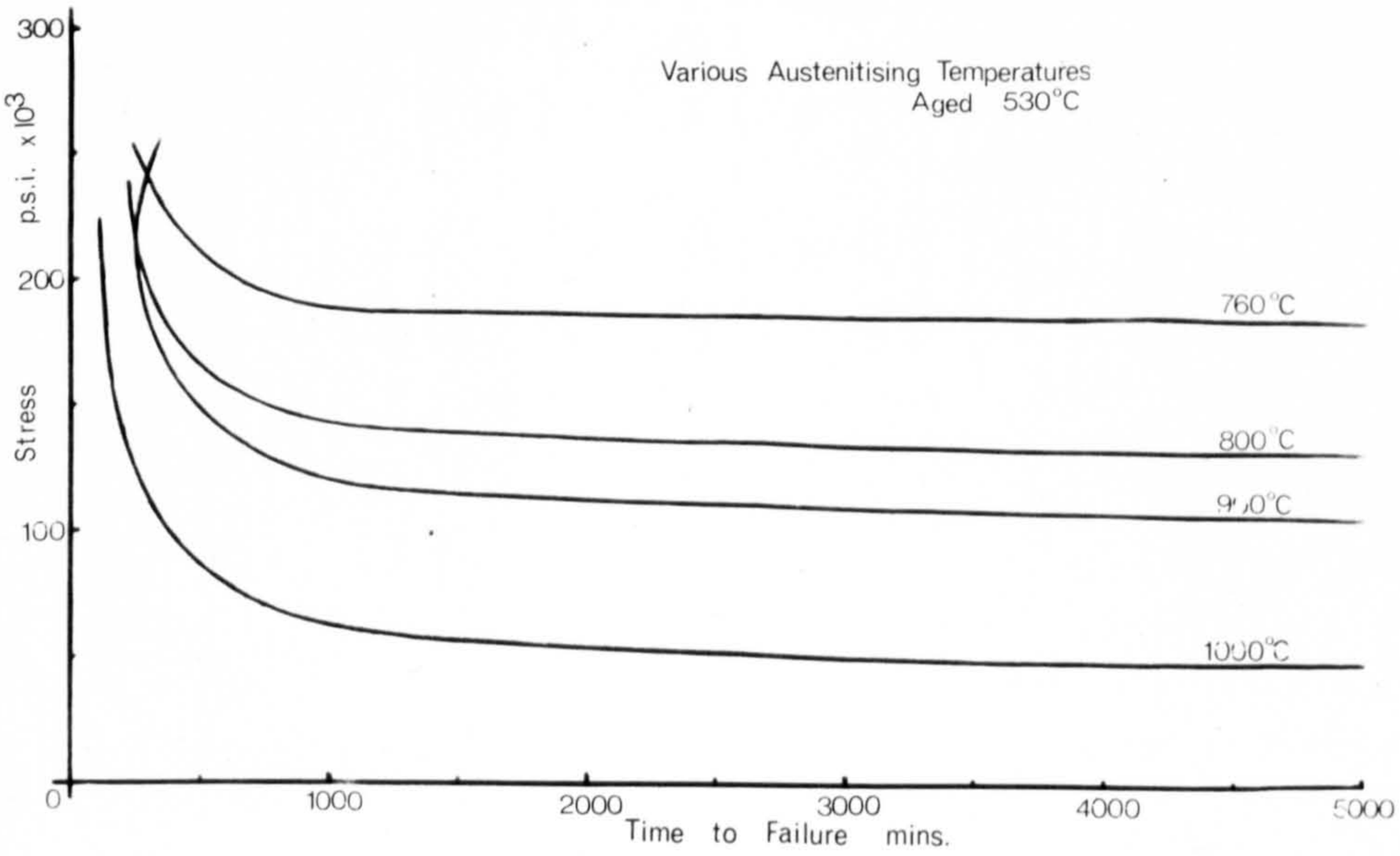

Fig. 3.4 Stress - time to failure curves in pH-2 soln.

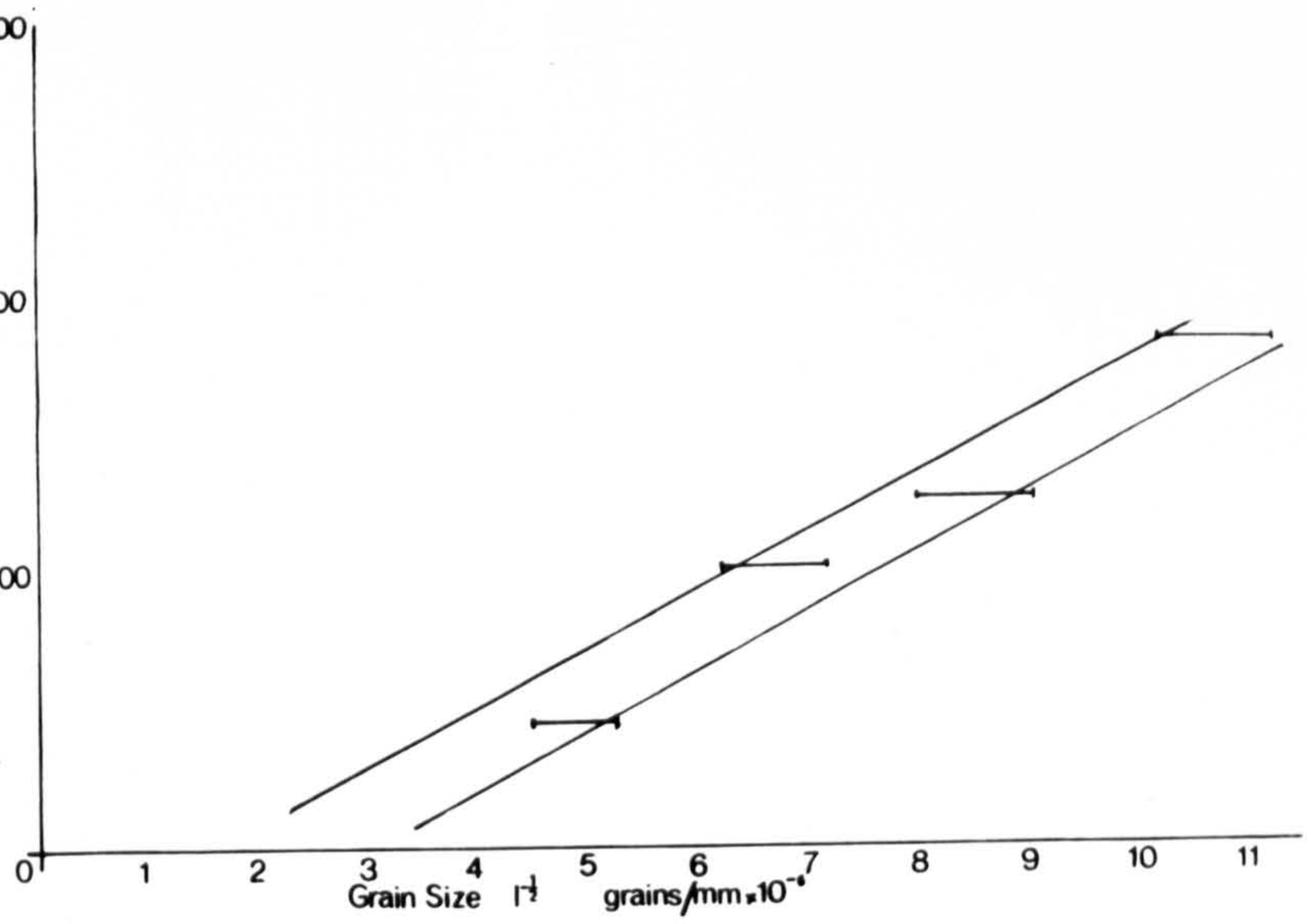

Fig. 3.5 Stress - grain size plot

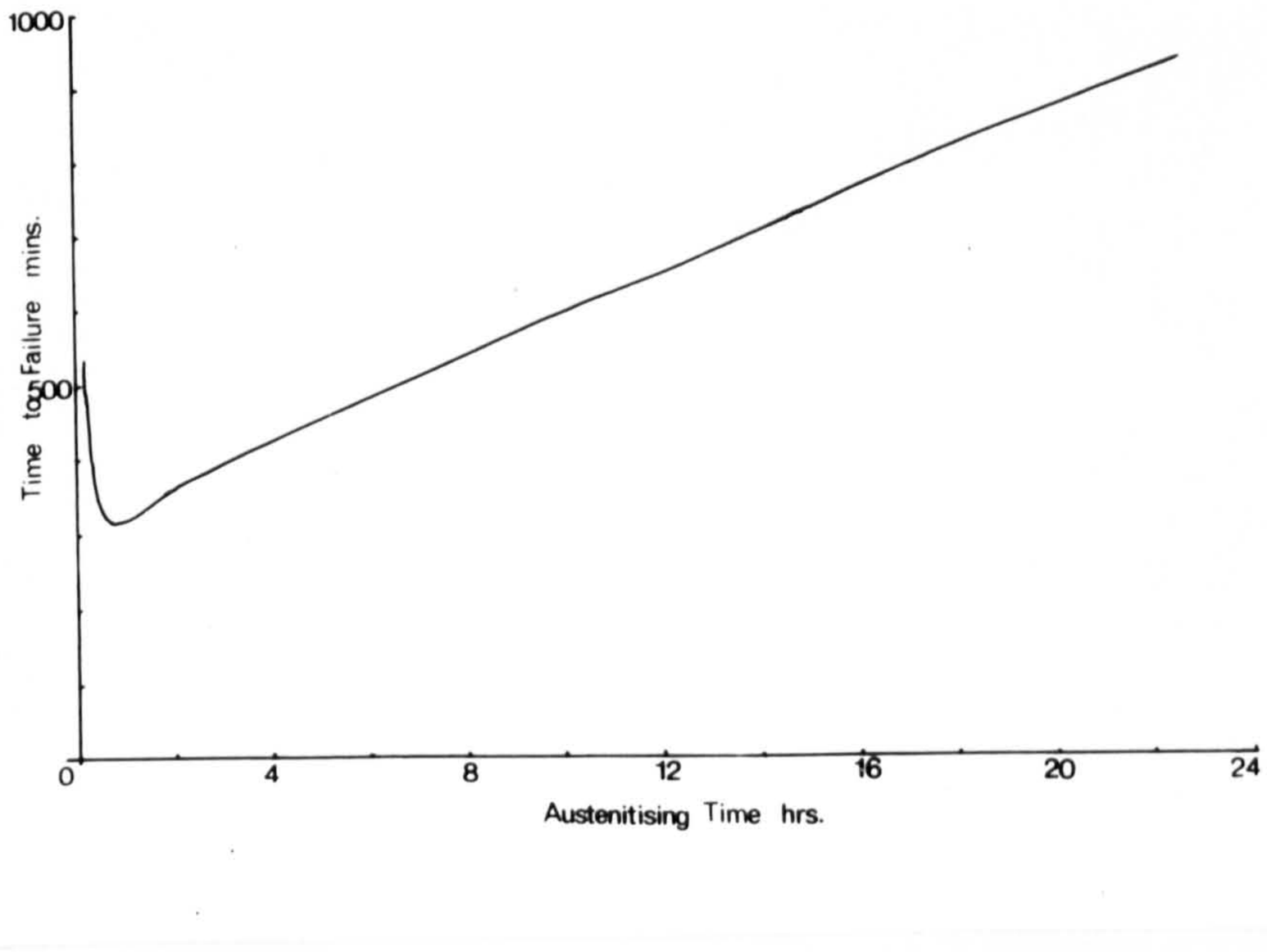

Fig. 3.6 Variation in failure time with austenitising time.

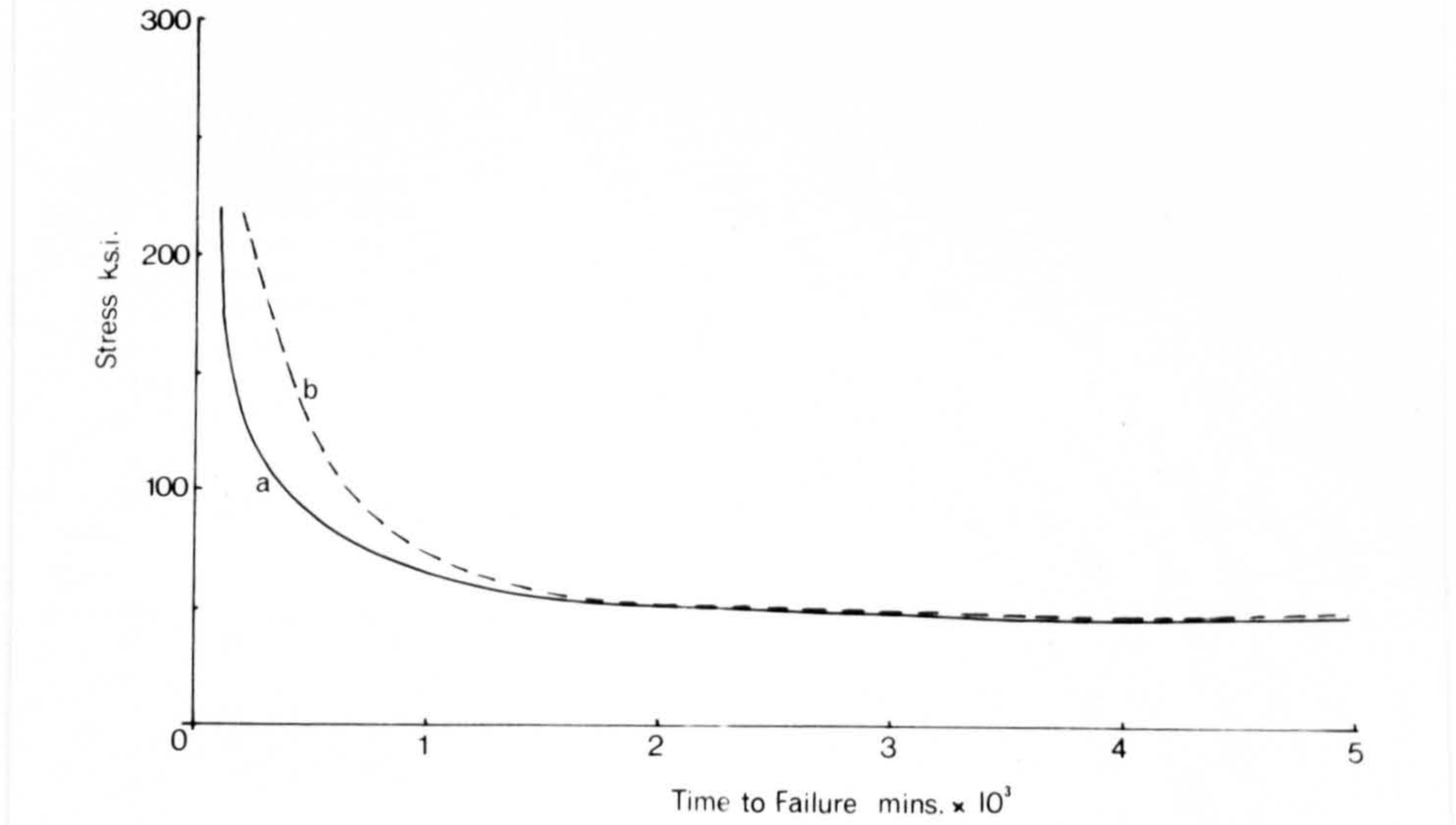

Fig. 3.7 Stress - time to failure curves for material (a) austenitised 1 hour, (b) austenitised for 20 hours.

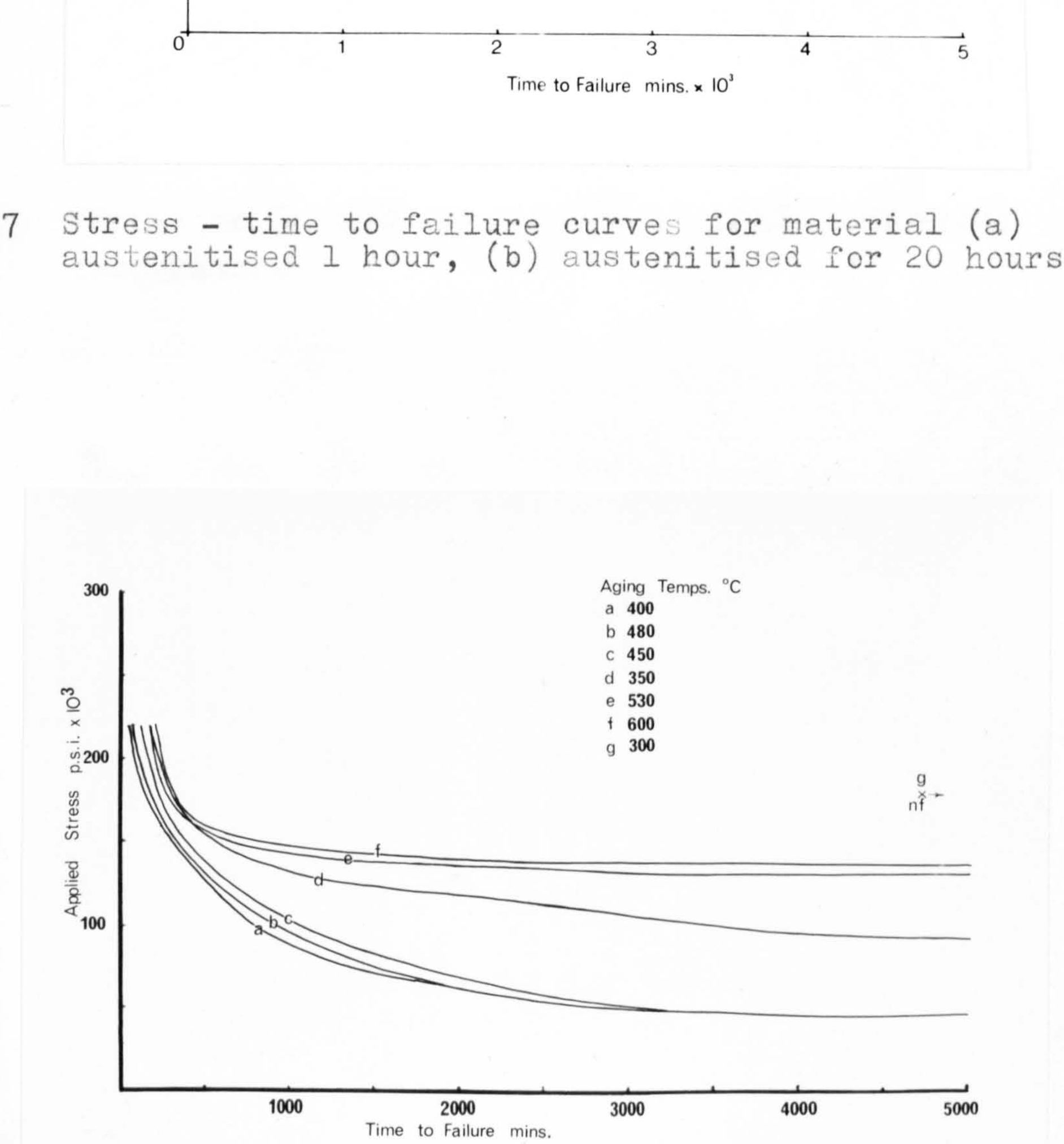

Fig. 3.8 Stress - time to failure curves for material austenitised 800°C 1 hr. and aged at various temperatures

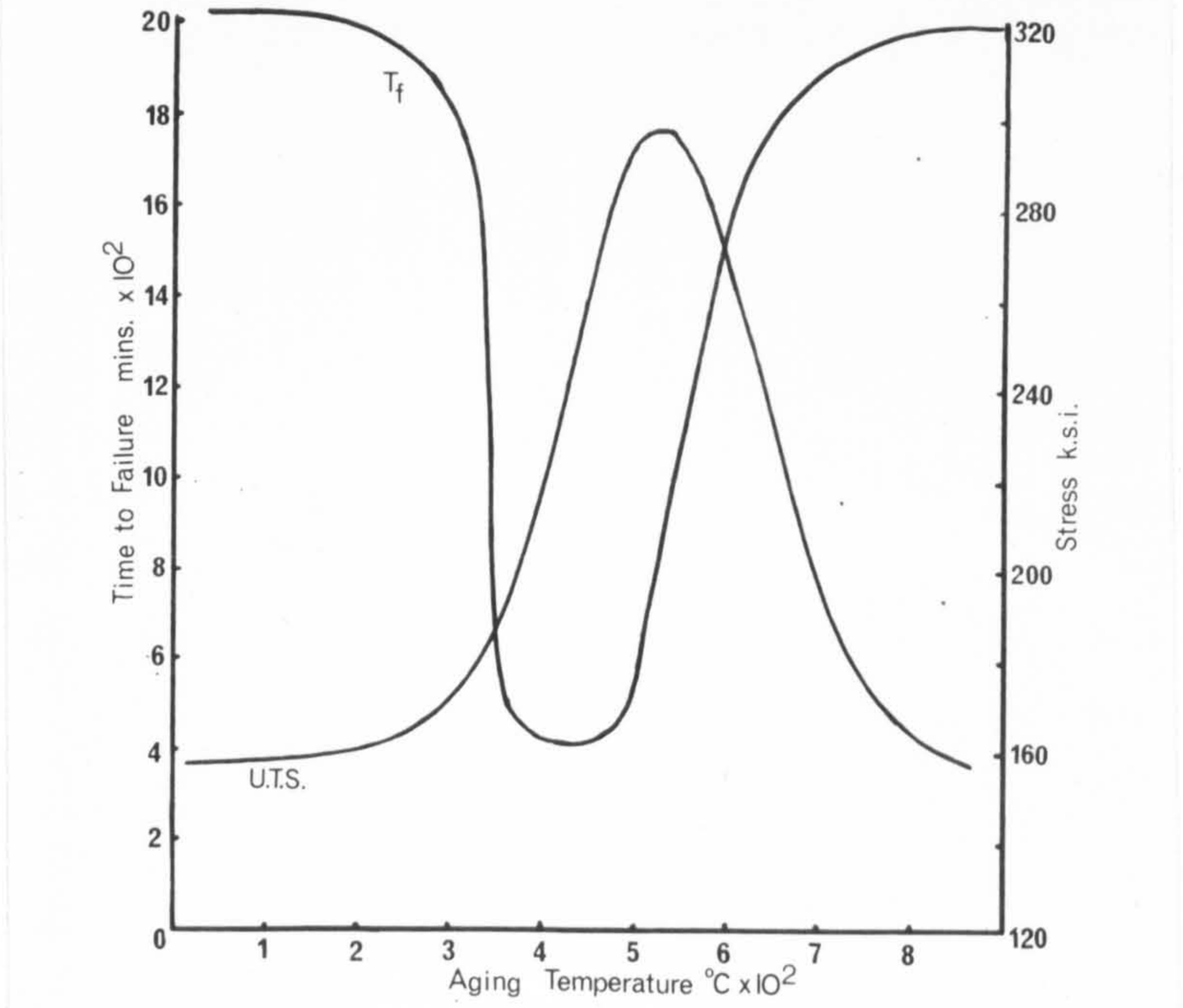

Fig. 3.9 Variation in time to failure and UTS with aging temperature.

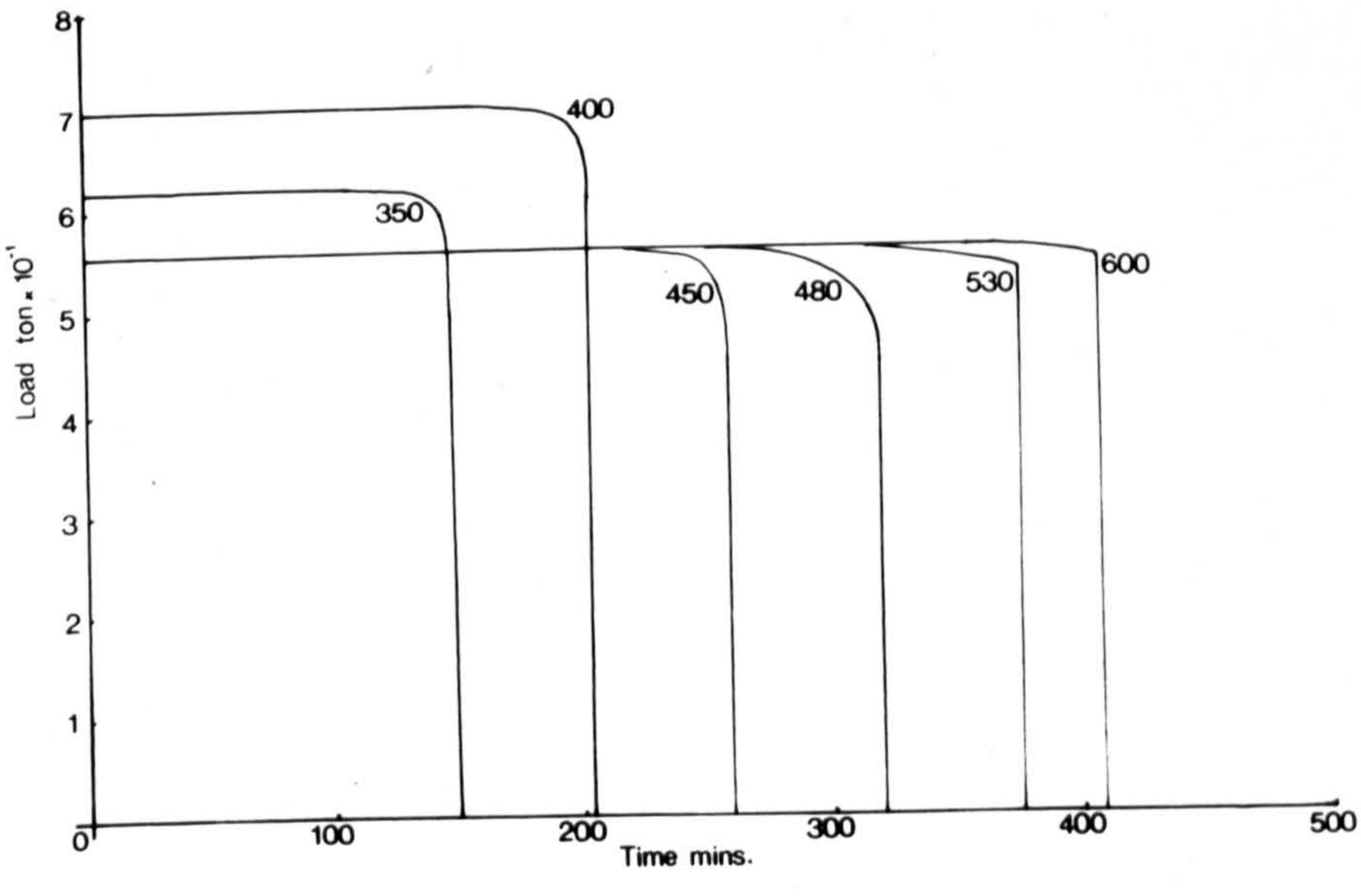

Fig. 3.10 Typical load relaxation curves obtained for several aging temperatures.

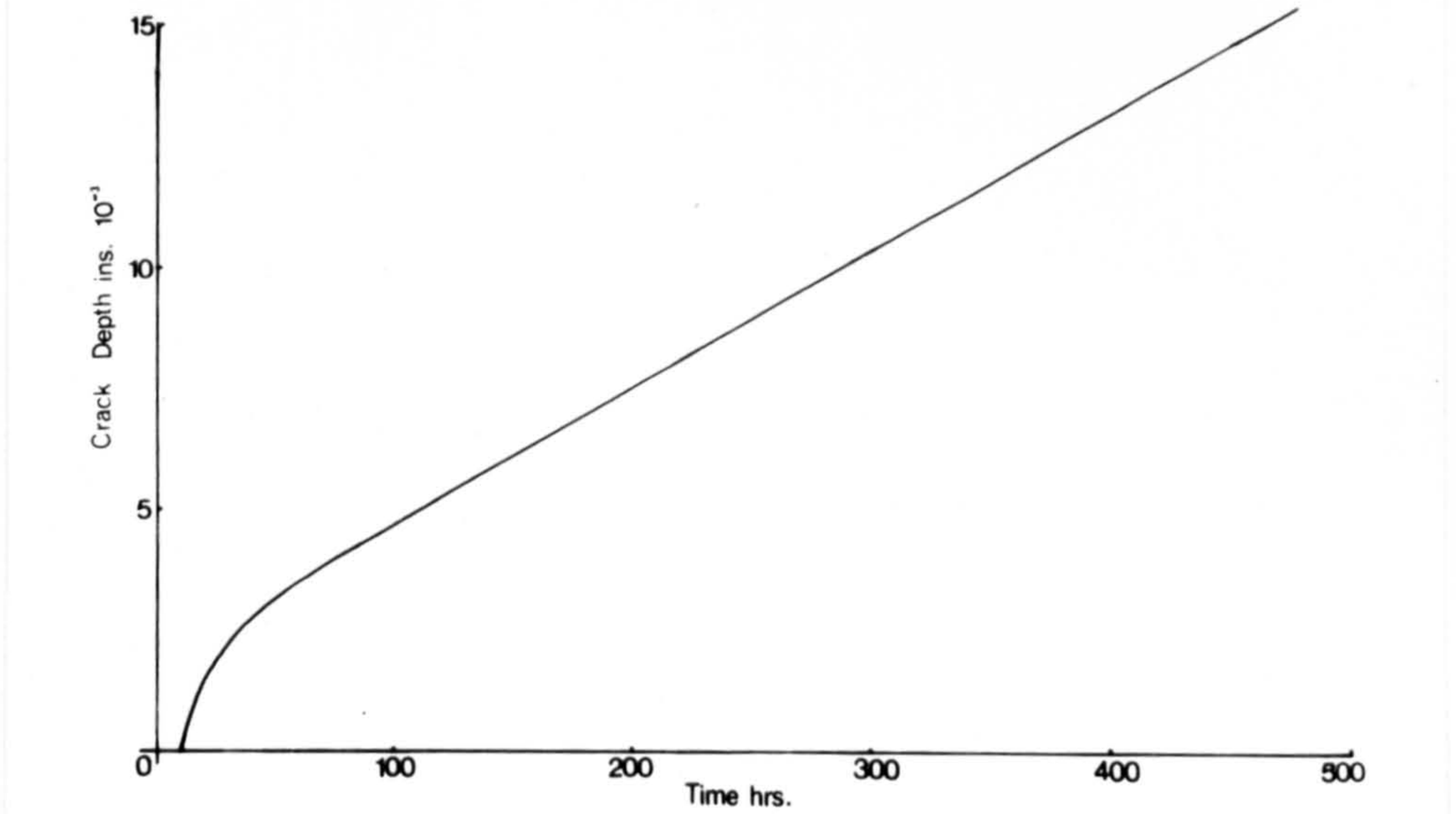

Fig. 3.11 Plot of crack depth after various exposure times.

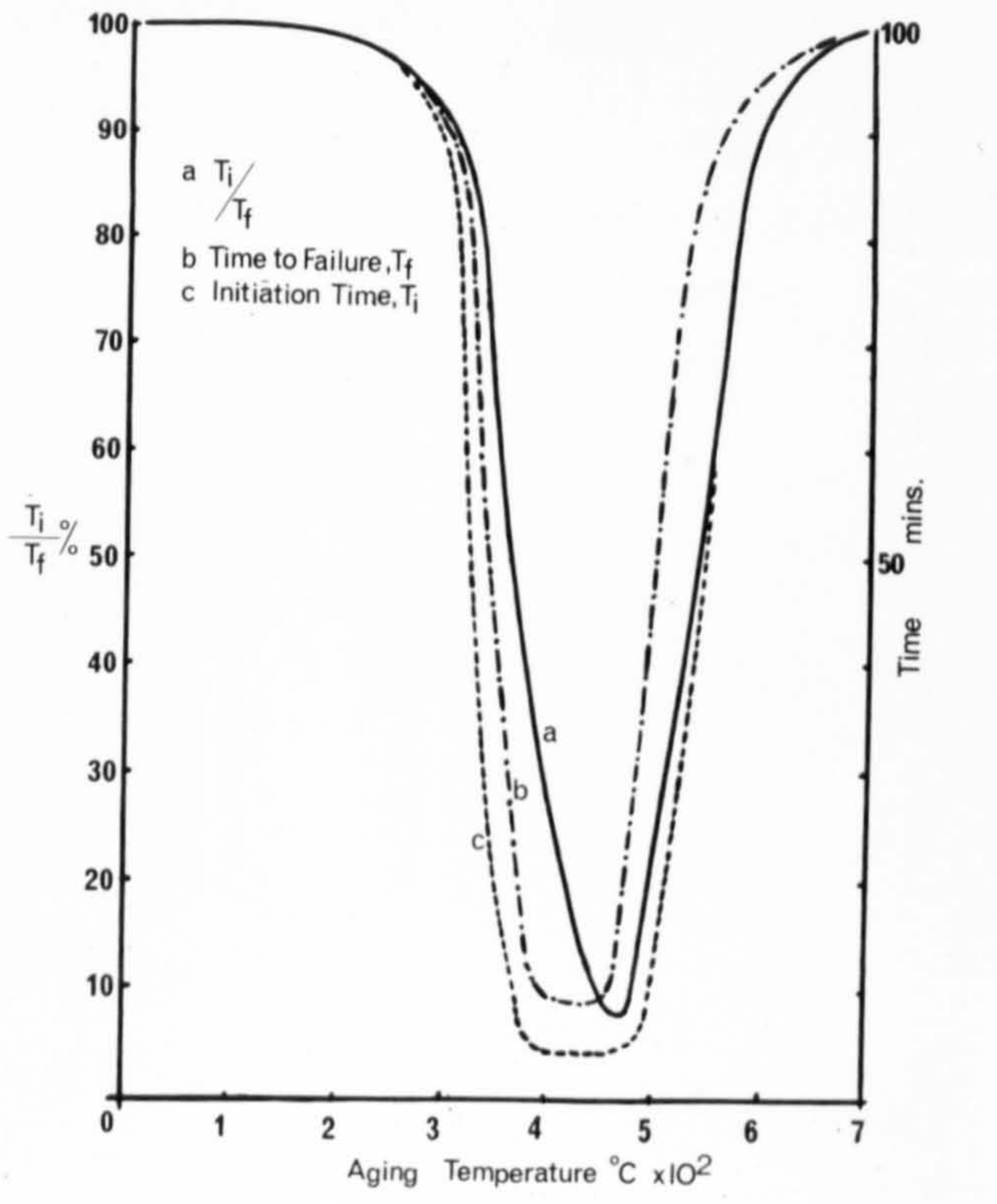

Fig. 3.12 Time to failure v.s. aging temperature for material after treatment to introduce surface fissures.

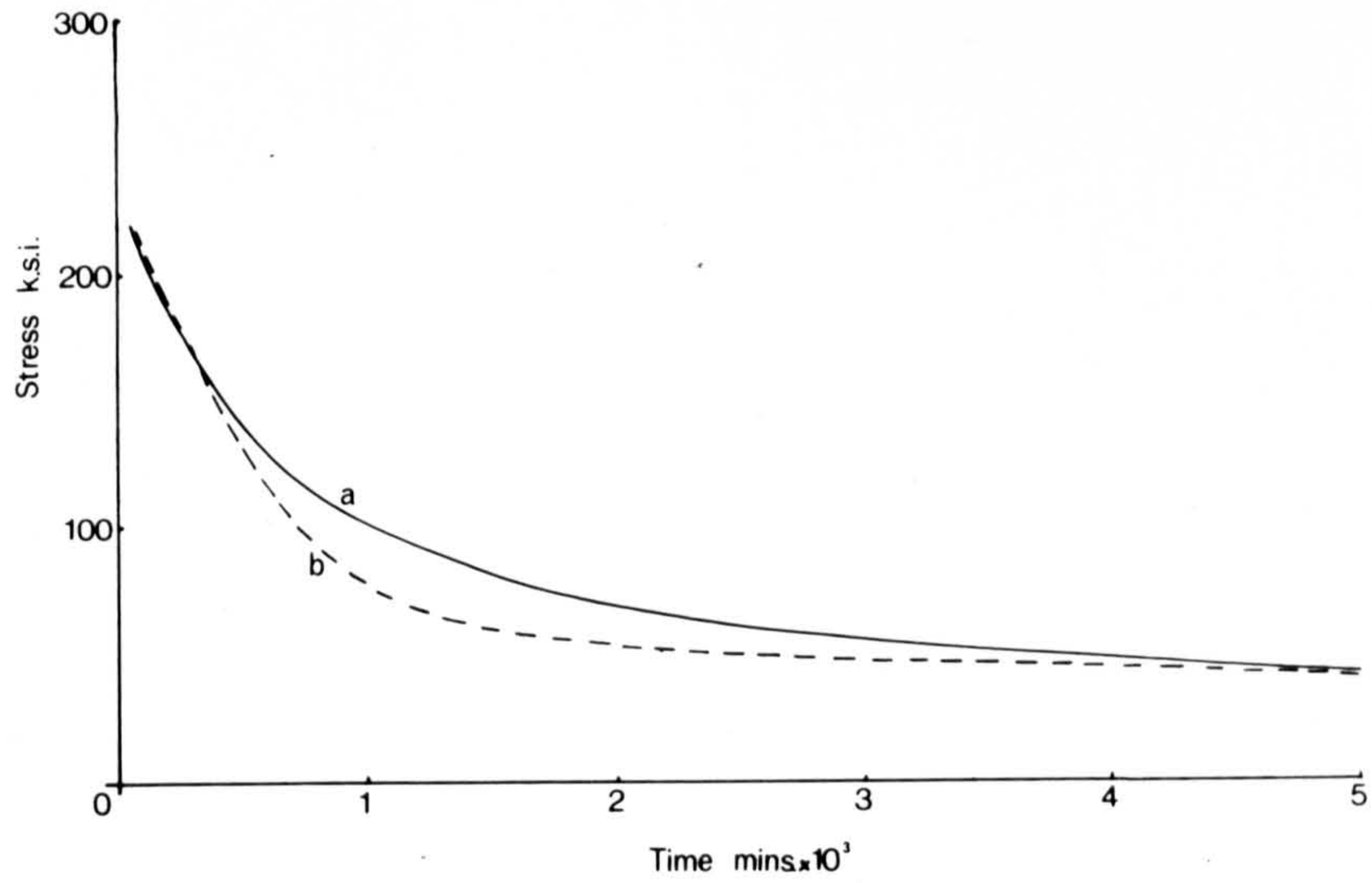

Fig. 3.13 Stress - time to failure curves for material (a) aged for 3 hrs., (b) aged for 48 hrs.

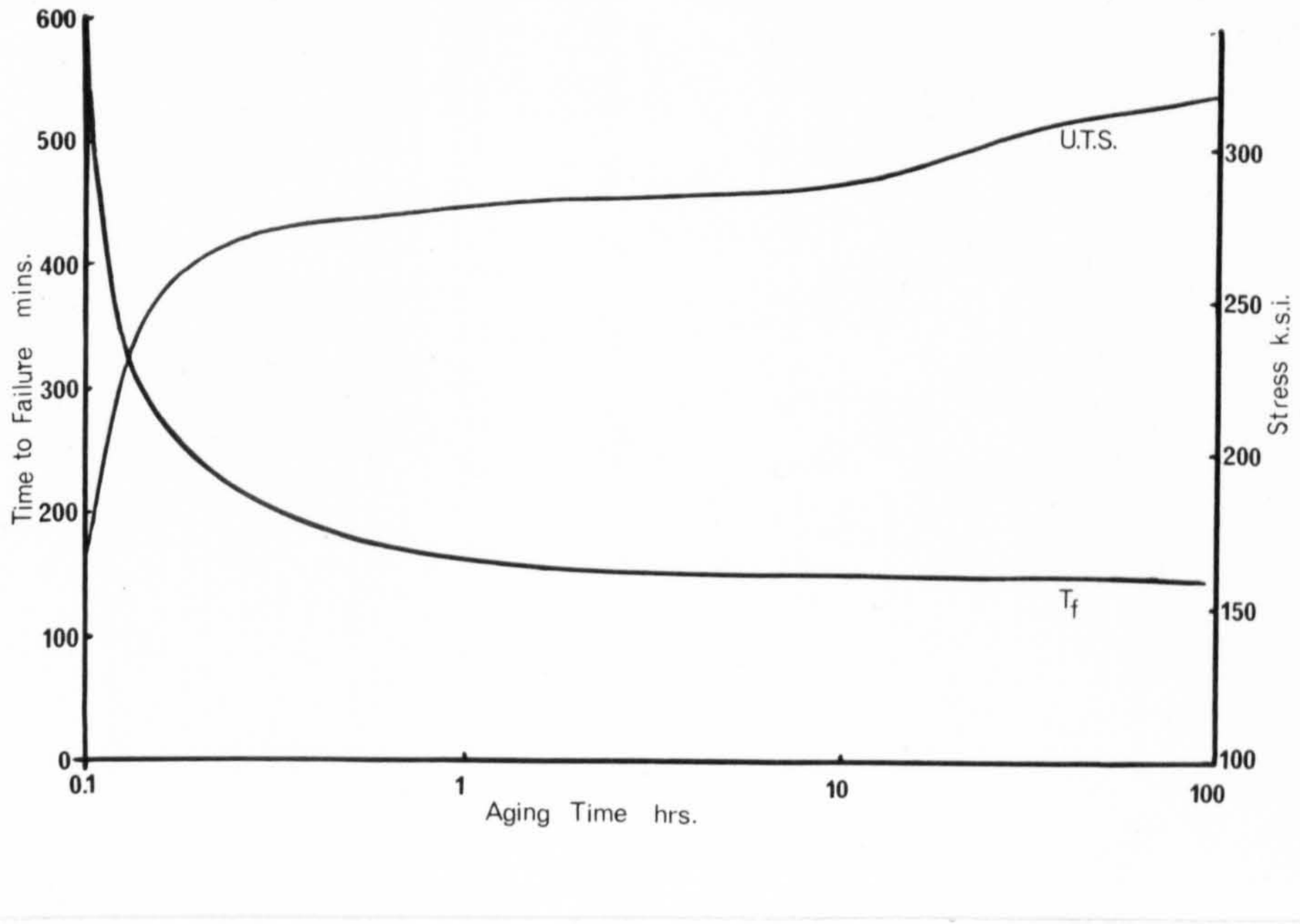

Fig. 3.14 Variation in failure time and UTS with aging temperature.

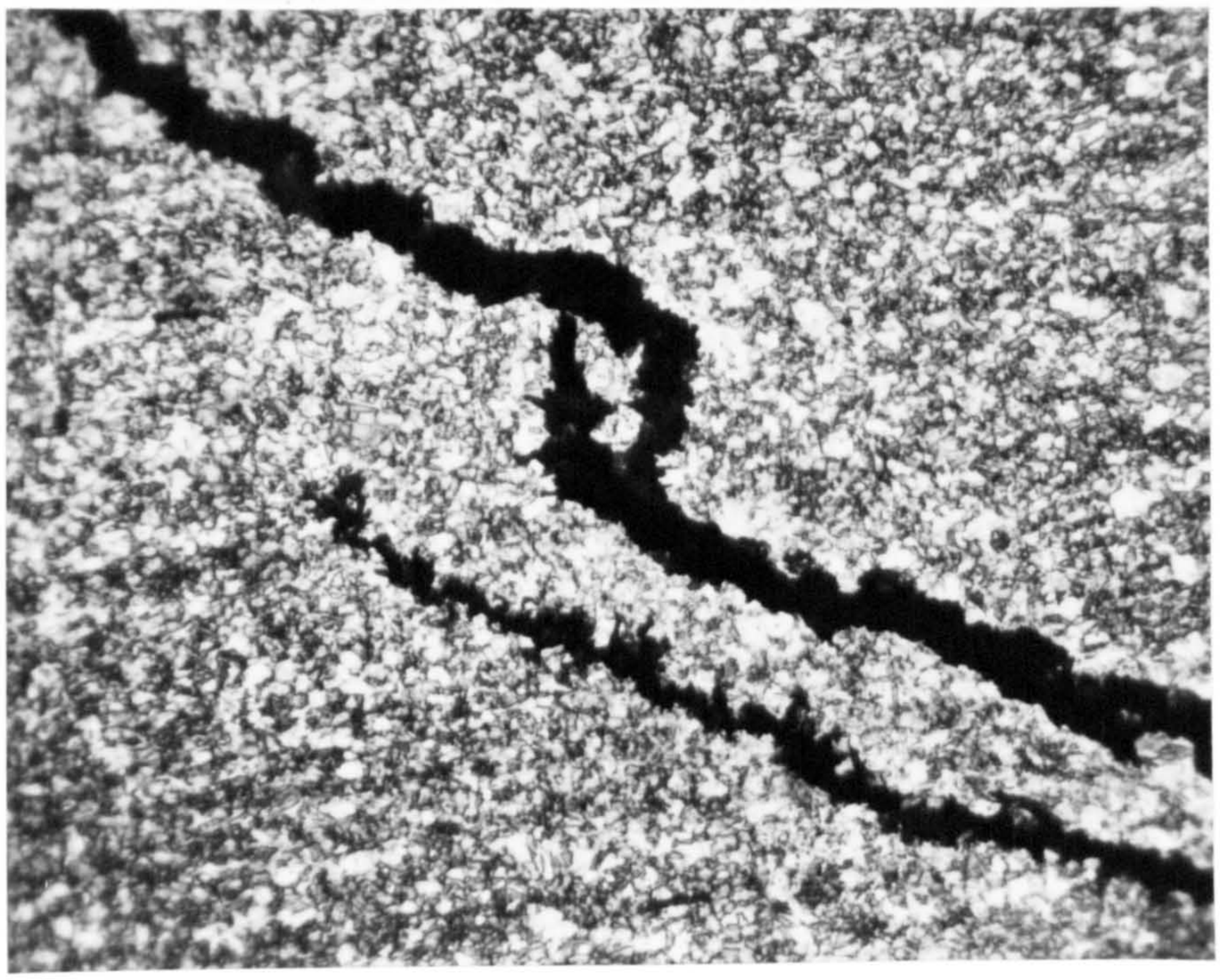

Fig. 3.15 Intergranular cracking in cold worked material as seen optically (300x)

Fig. 3.16 Intergranular cracking in cold worked material as viewed in the S.E.M. (300x)

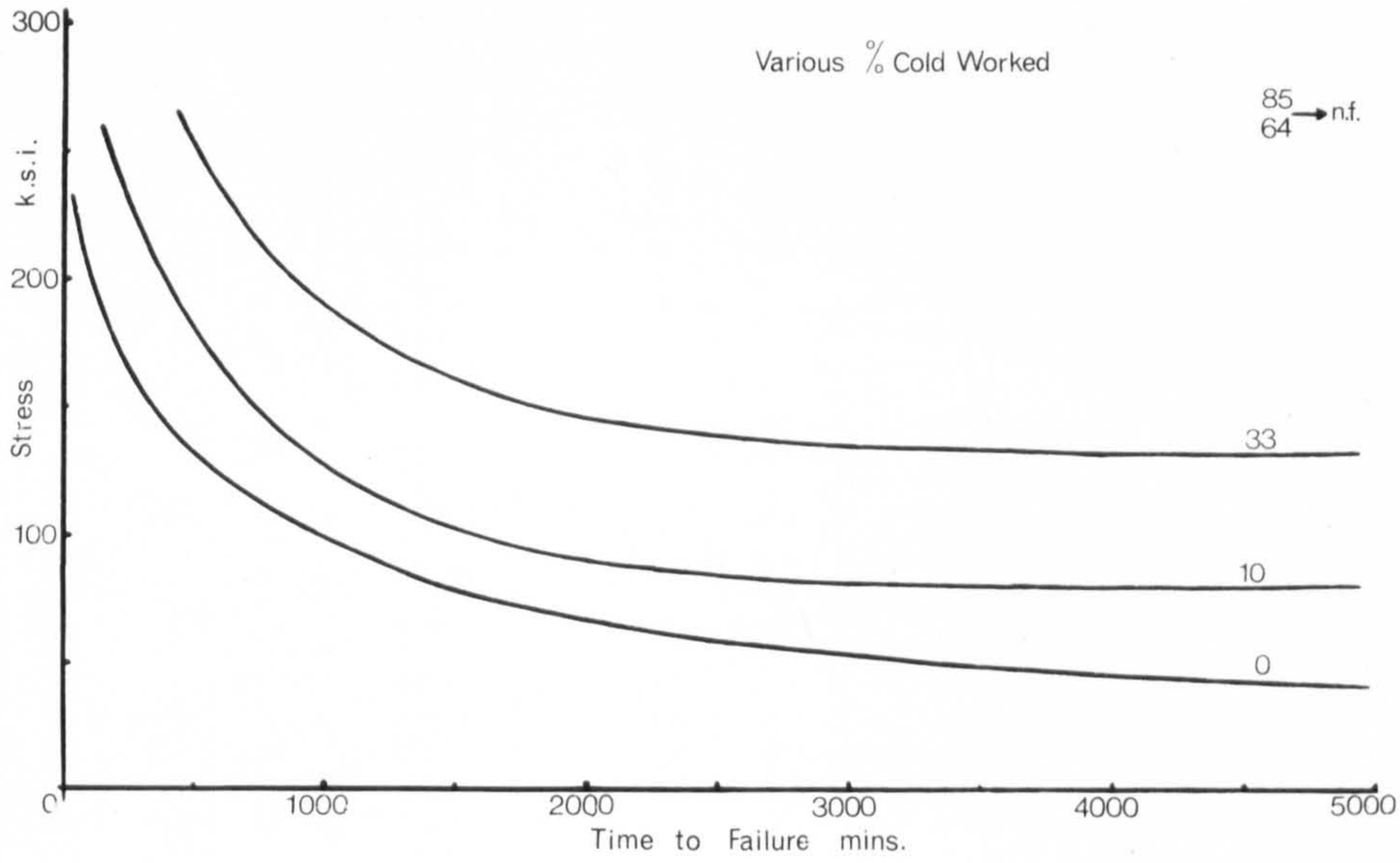

Fig. 3.17 Stress - time to failure curves for cold worked material.

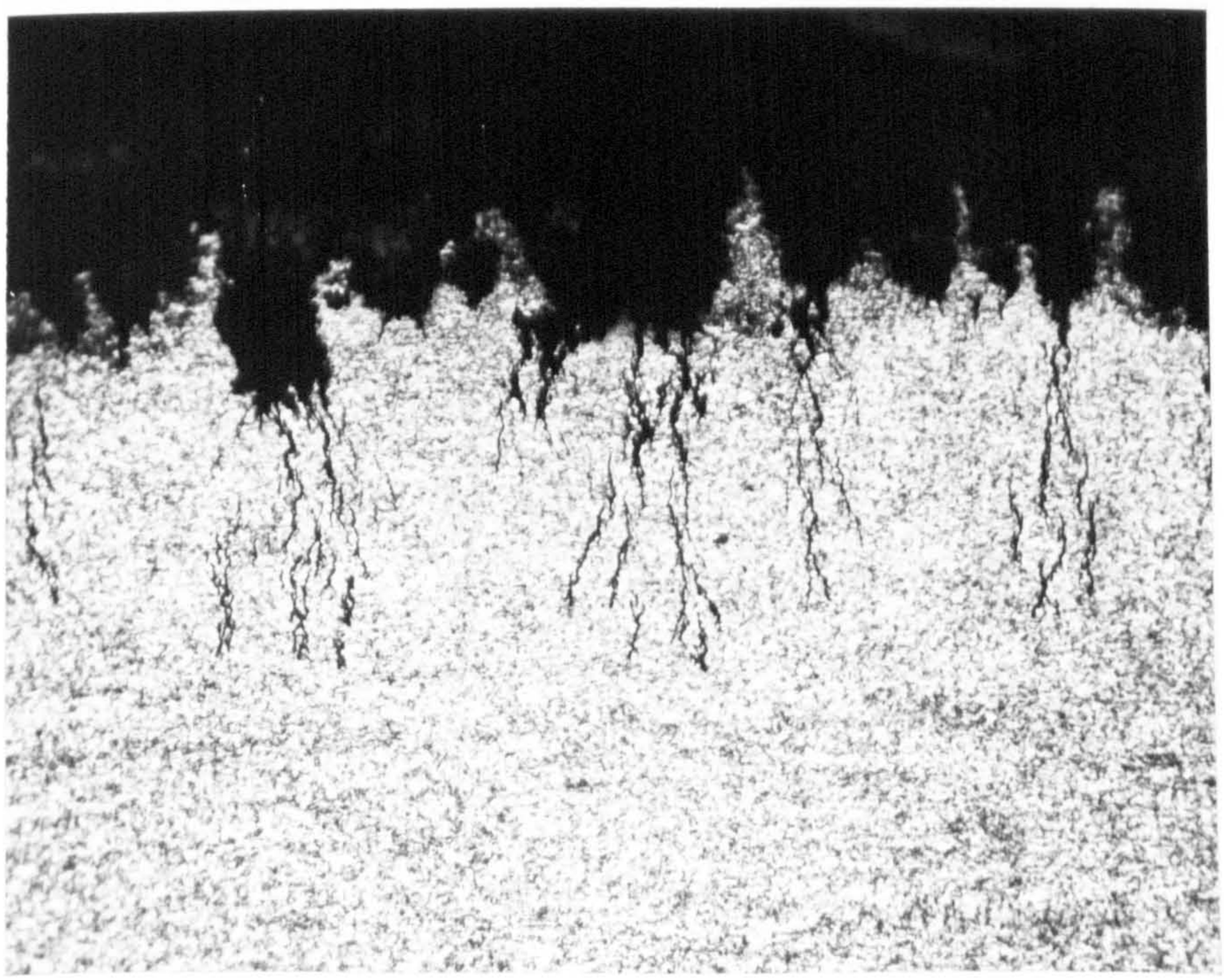

Fig. 3.18 Cracking in 85% cold worked material (300x)

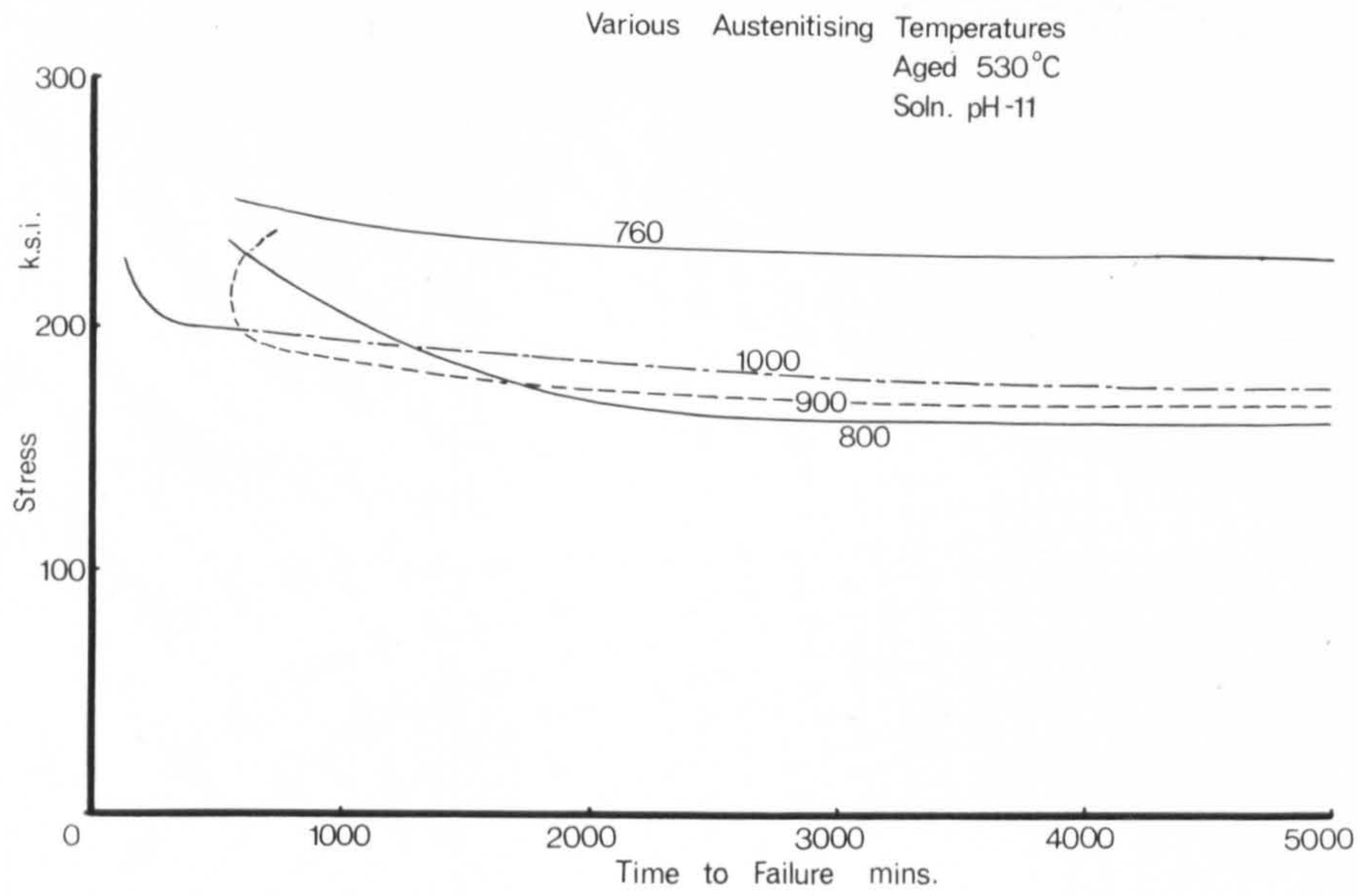

Fig. 3.19 Stress - time to failure curves in pH - 11 solution under potentiostatic control (-400 m.v.)

Fig. 3.20 Association of surface fissures and intergranular cracking (300x)

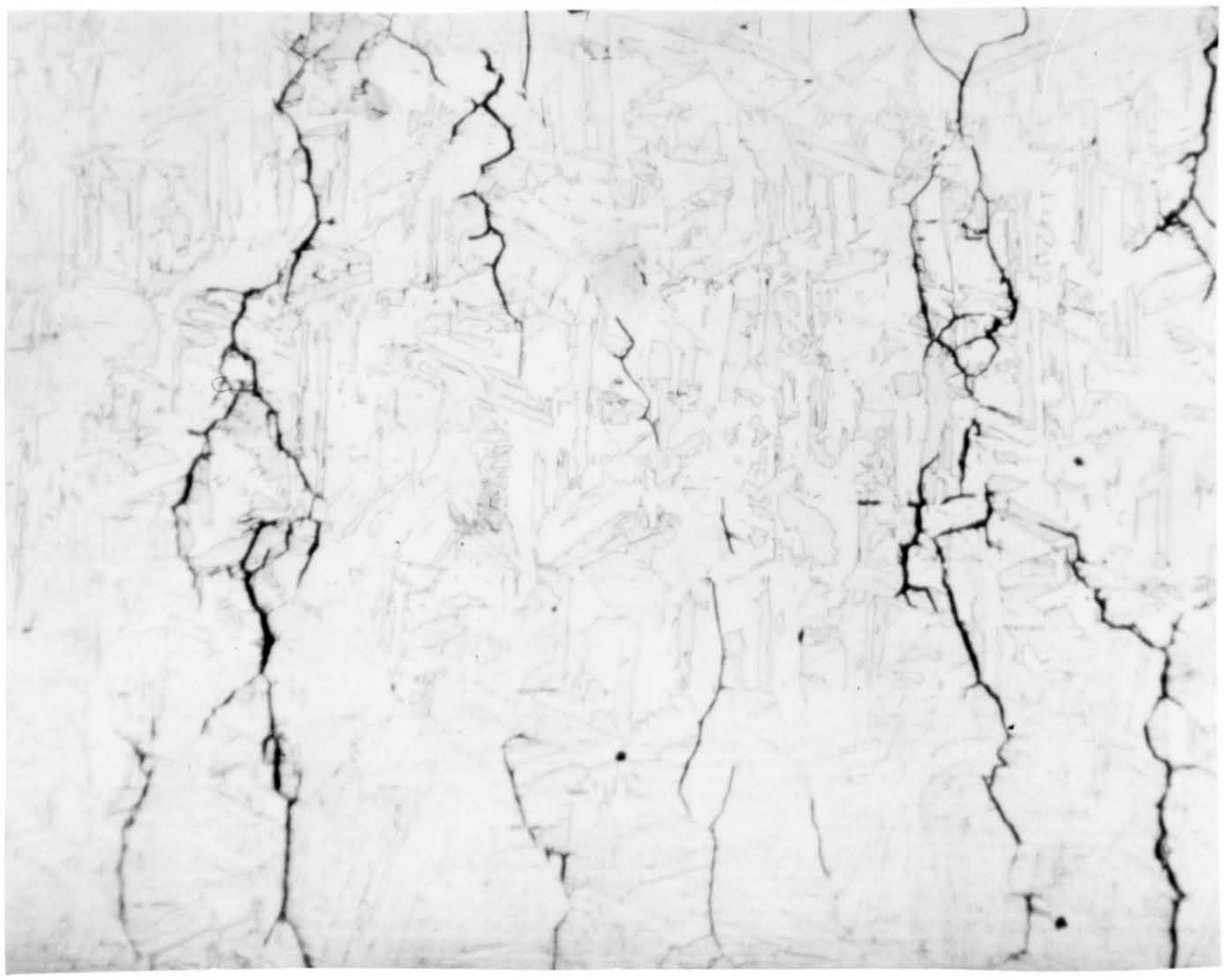

Fig. 3.21 Severe intergranular cracking in a pH - 2 solution.

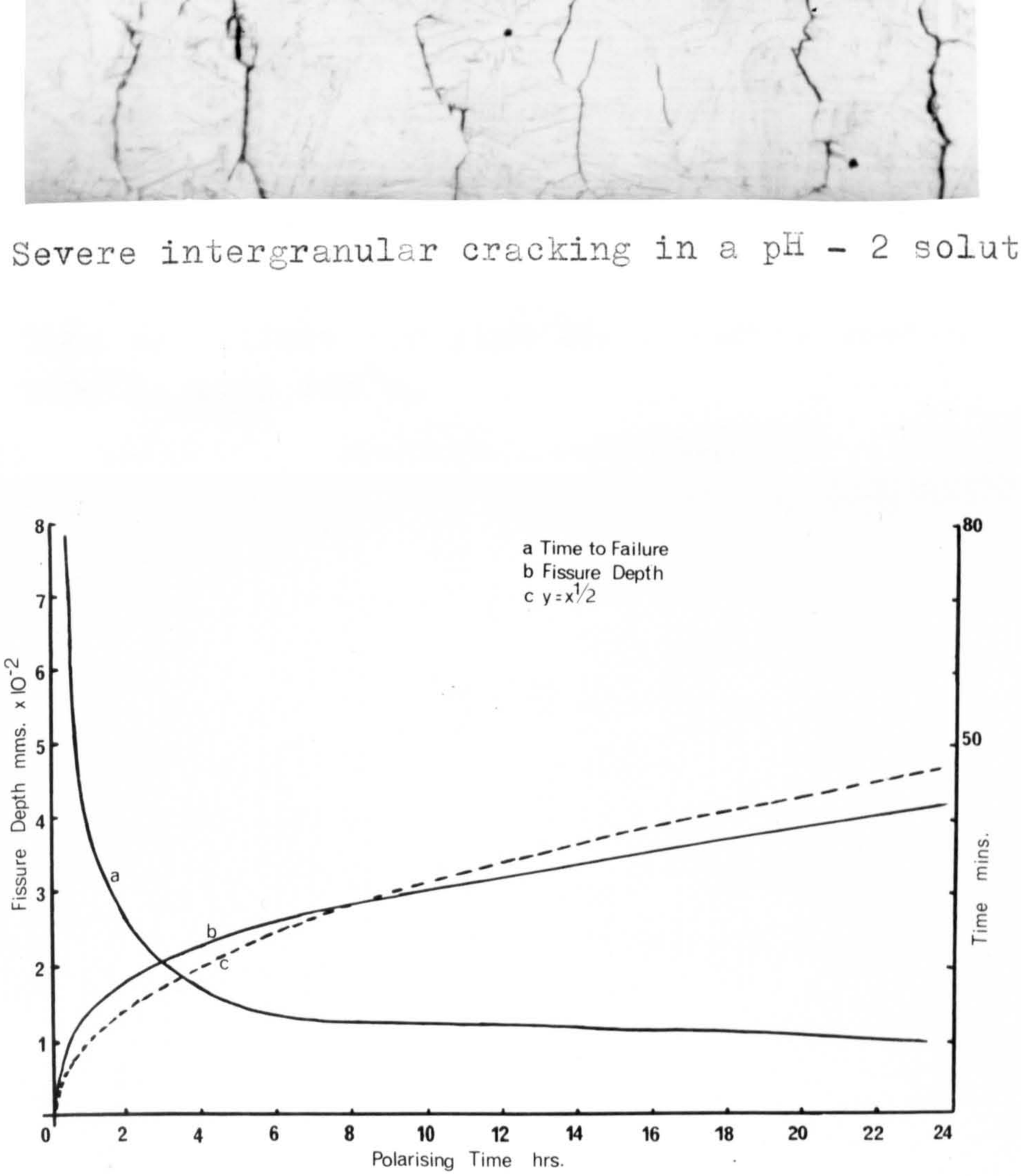

Fig. 3.22 Variation of fissure depth and failure time with polarising time.

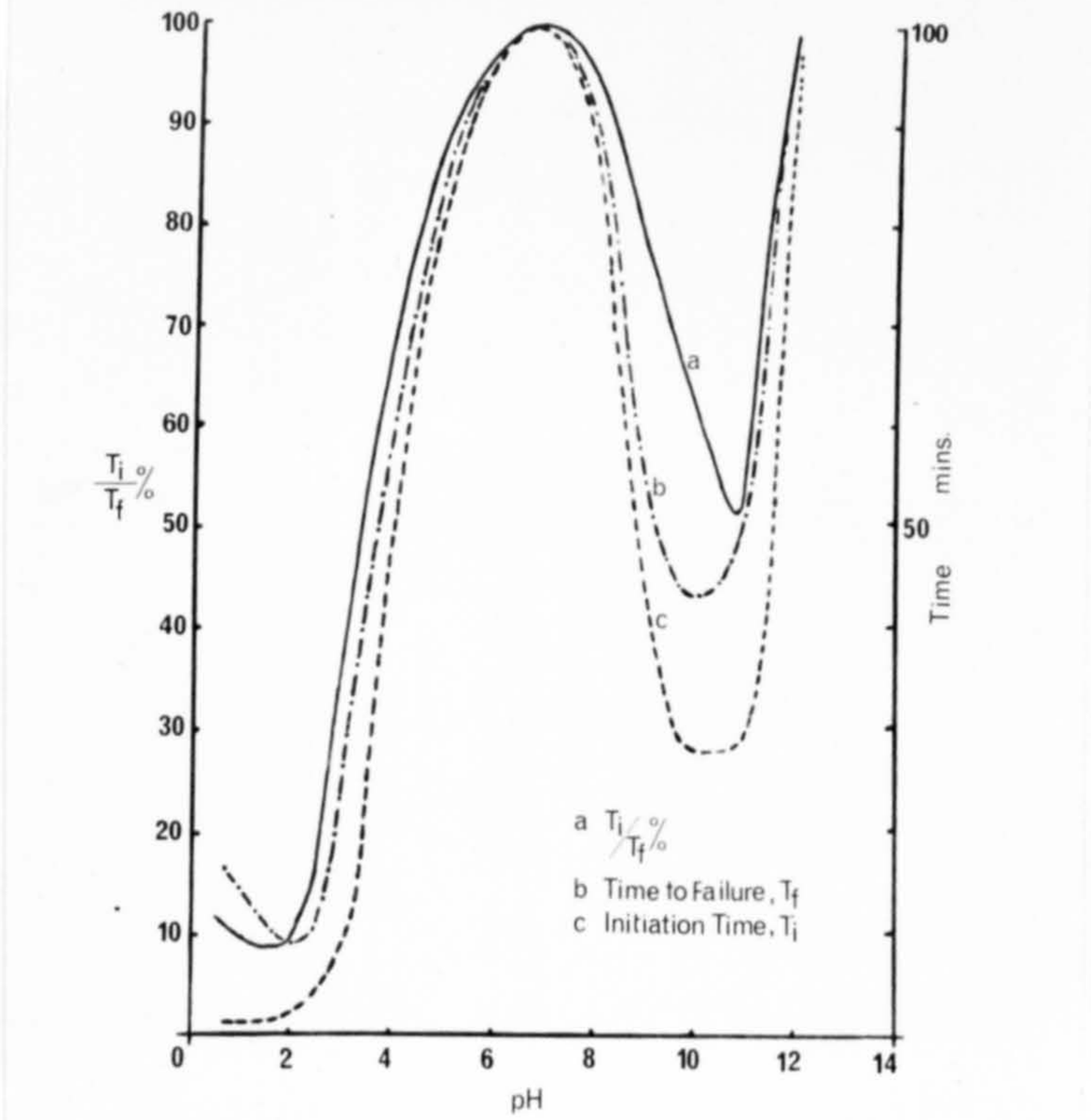

Fig. 3.23 Time to failure -pH plot for material austenitised 1000°C, aged 480°C.

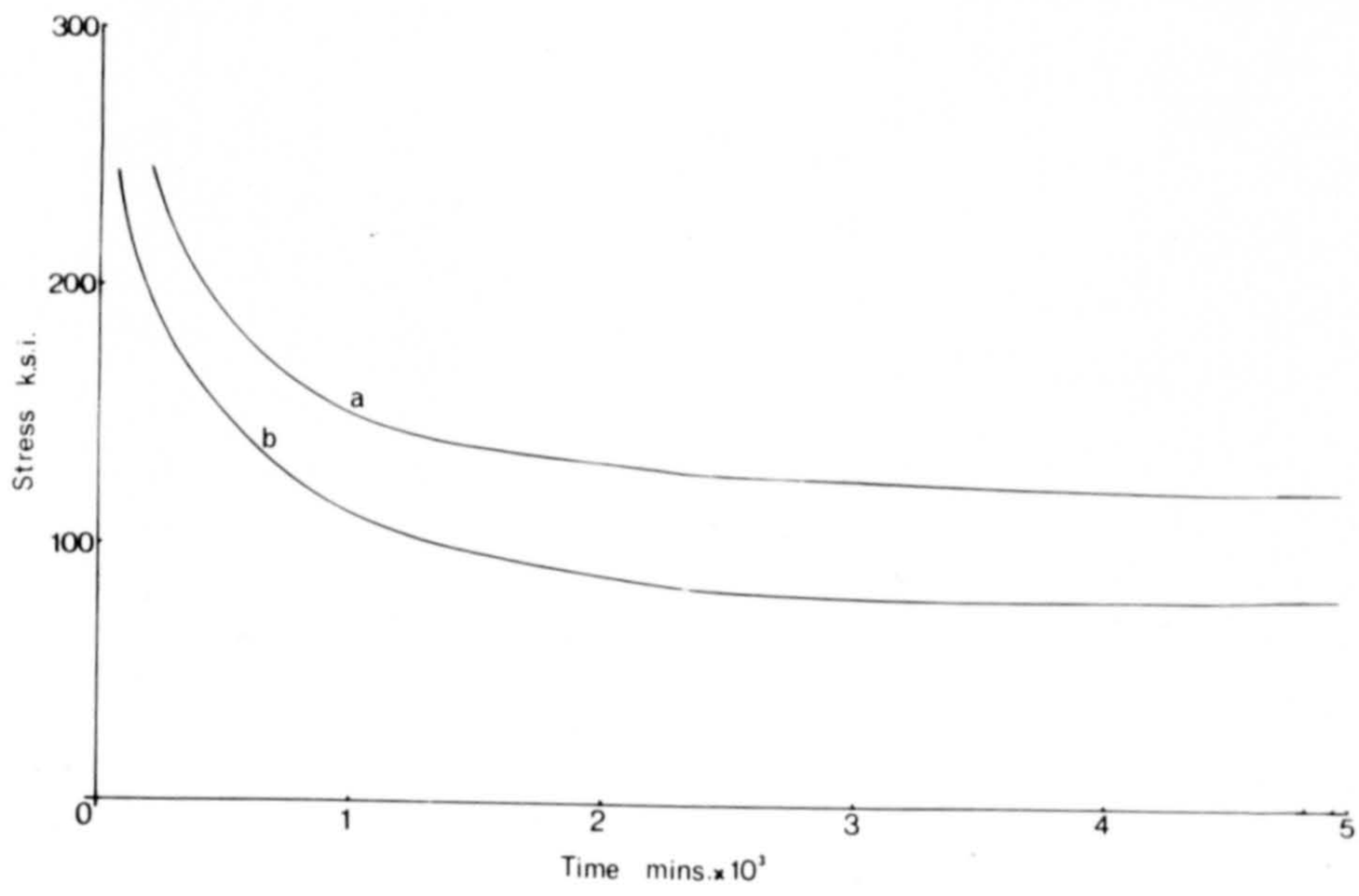

Fig. 3.24 Stress - time to failure curves for (a) unstirred and (b) stirred solutions of pH 2.

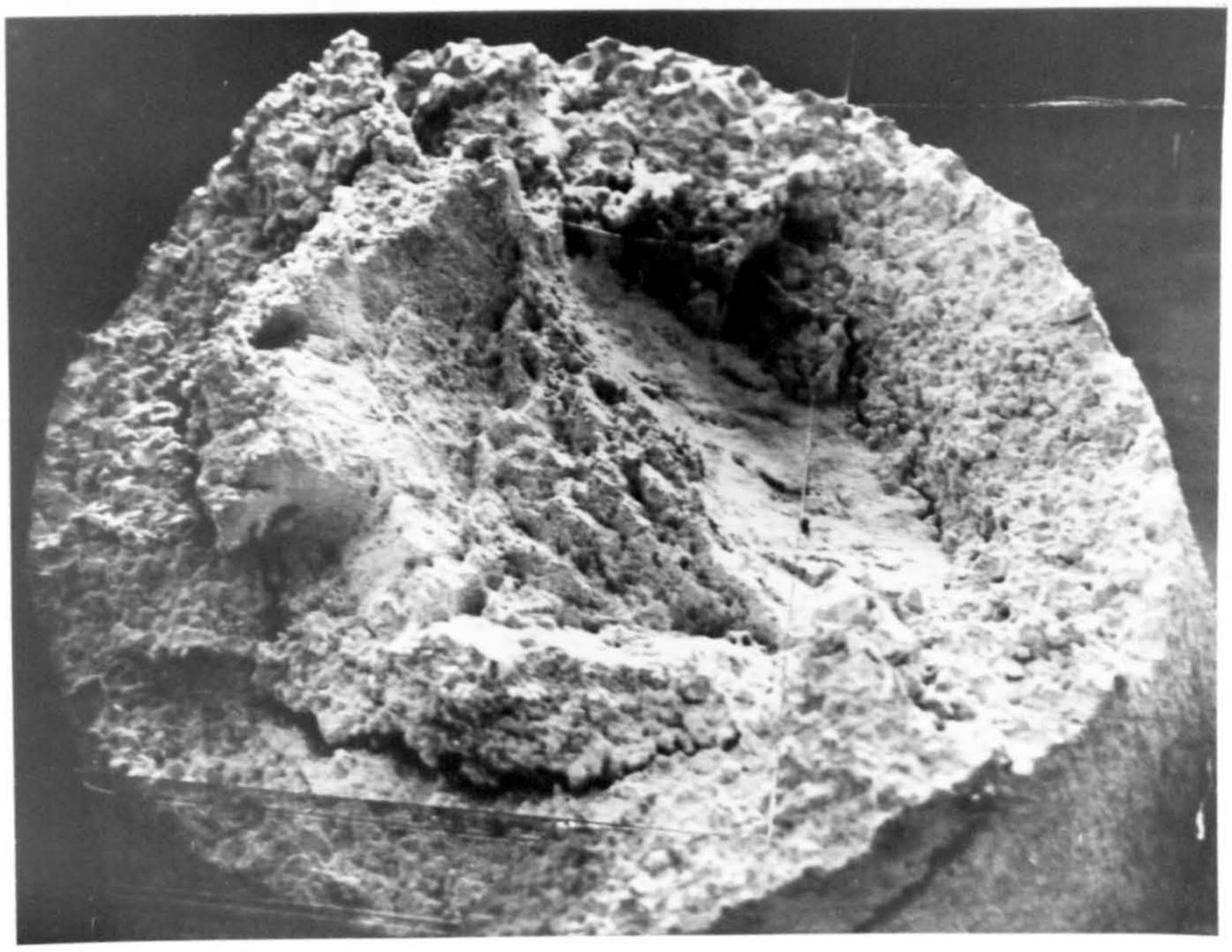

Fig. 3.25 Fracture surface showing stress corrosion and central ductile areas (50x)

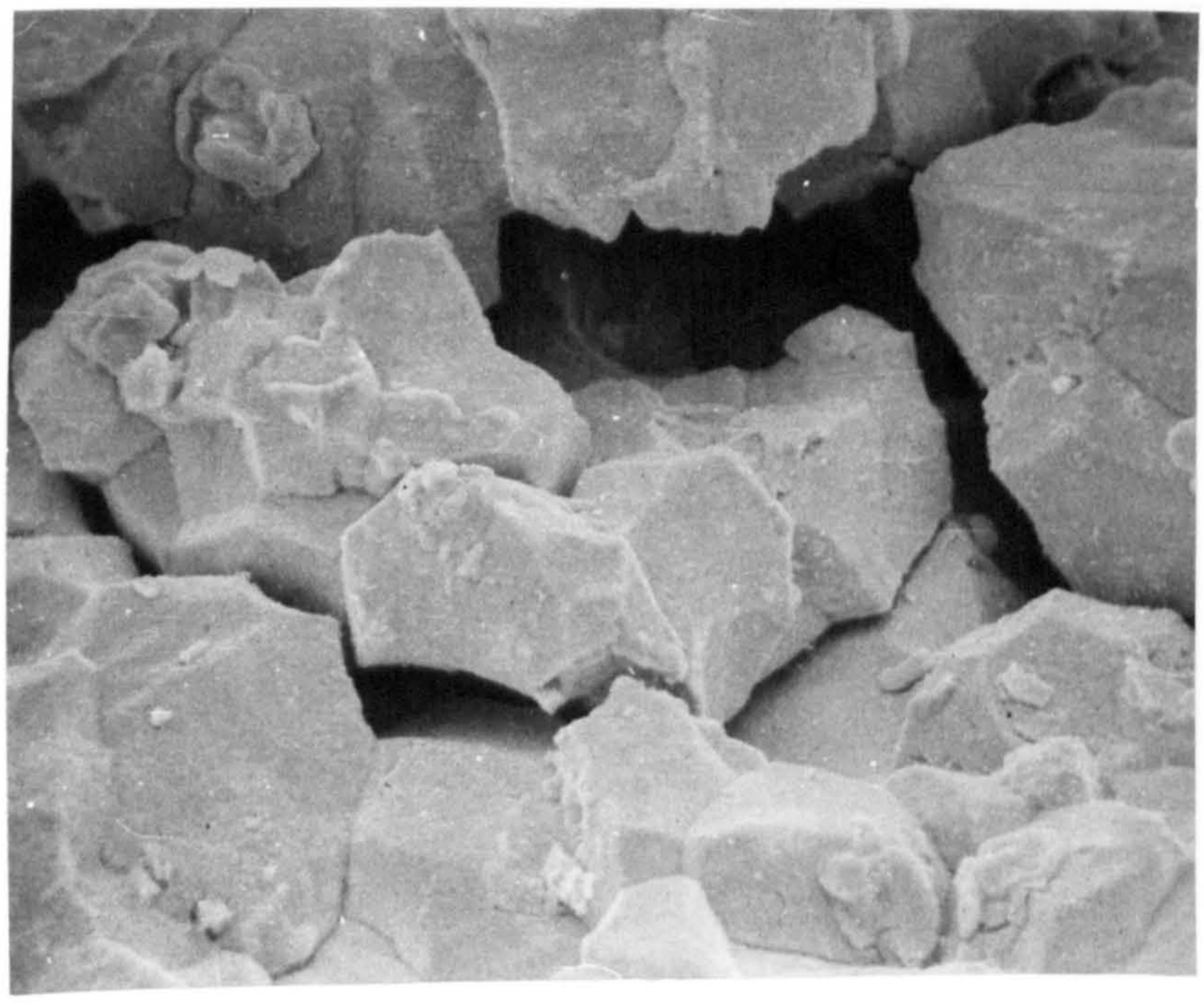

Fig. 3.26 Intergranular attack exposing individual grains (560x)

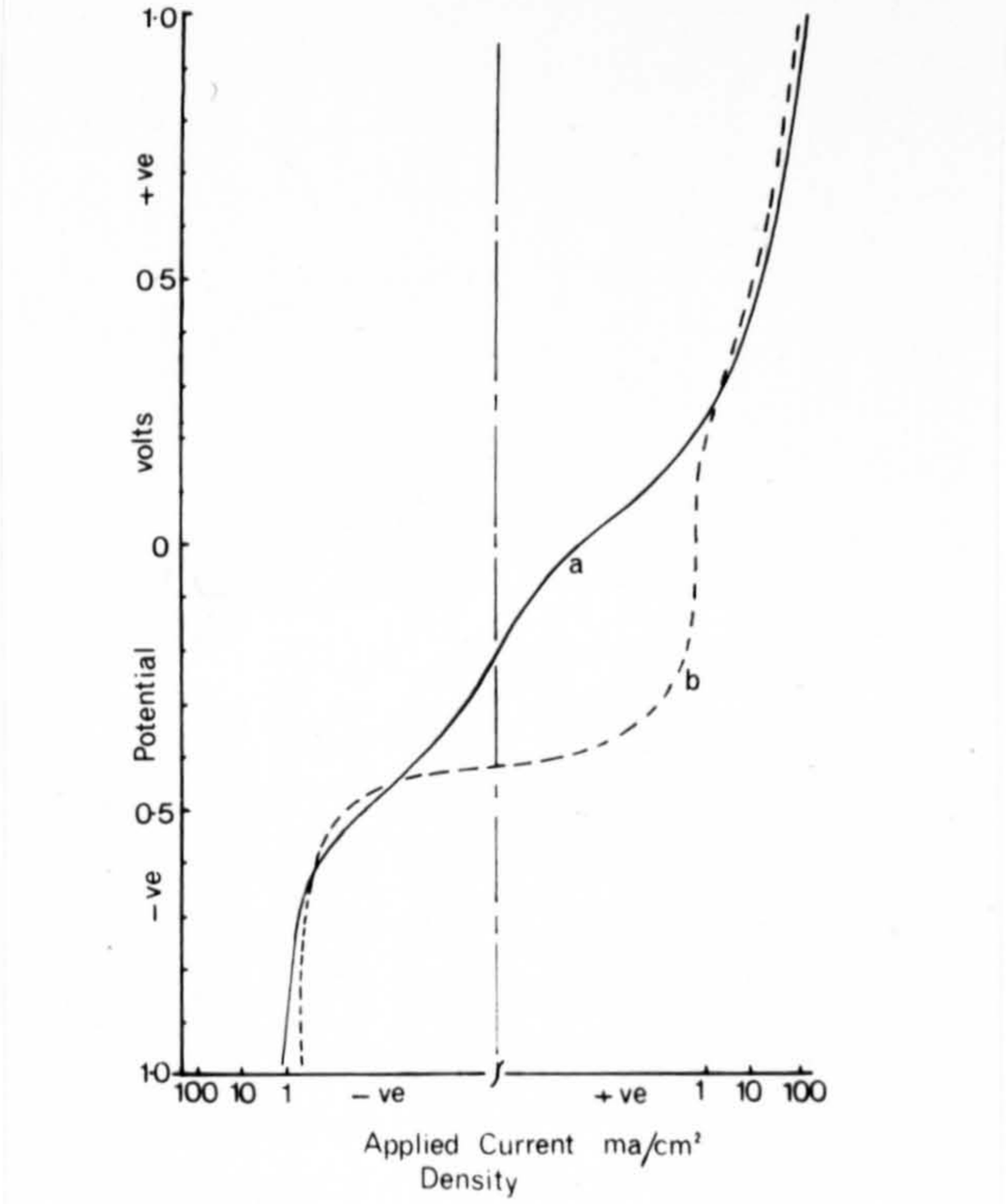

Fig. 3.27 Polarisation curves for pure Mo (a) unstirred and (b) stirred in pH 2 solns

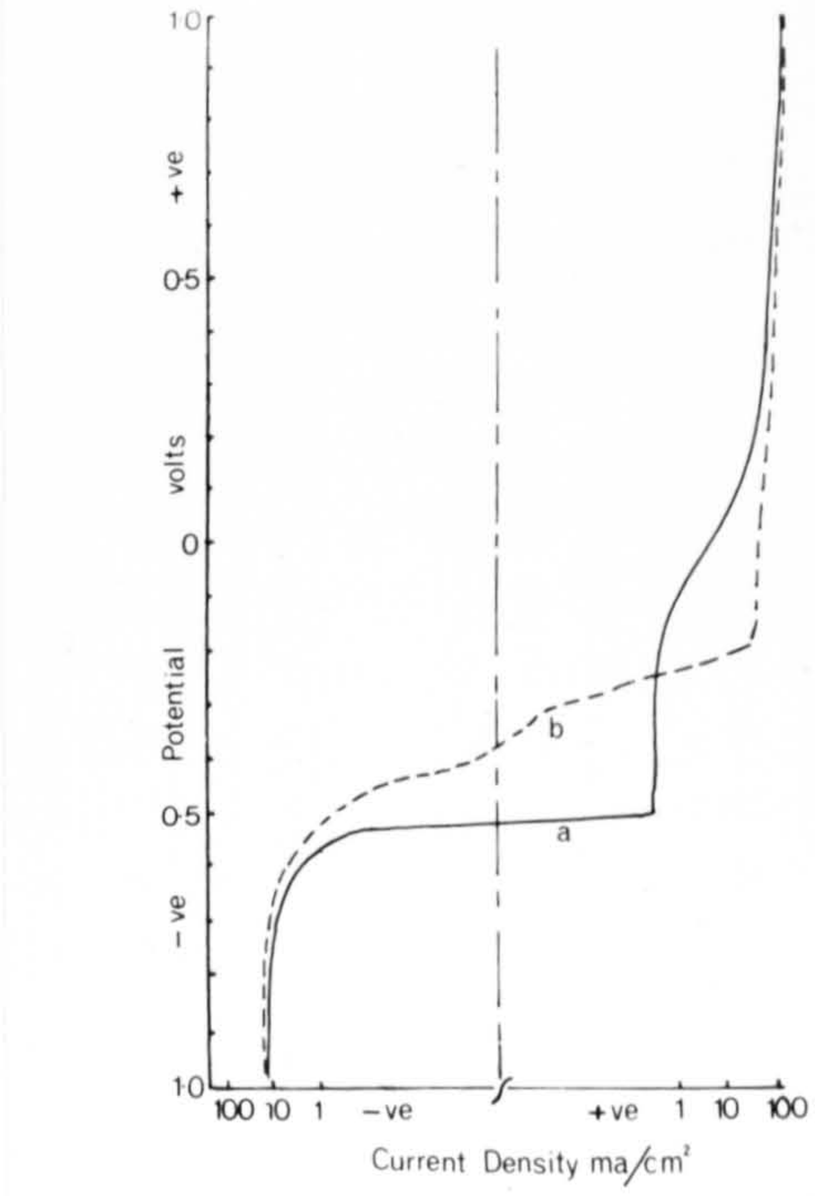

Fig. 3.28 Curves of (a) fast and (b) slow sweep rates for maraging steel in pH-11 solution.

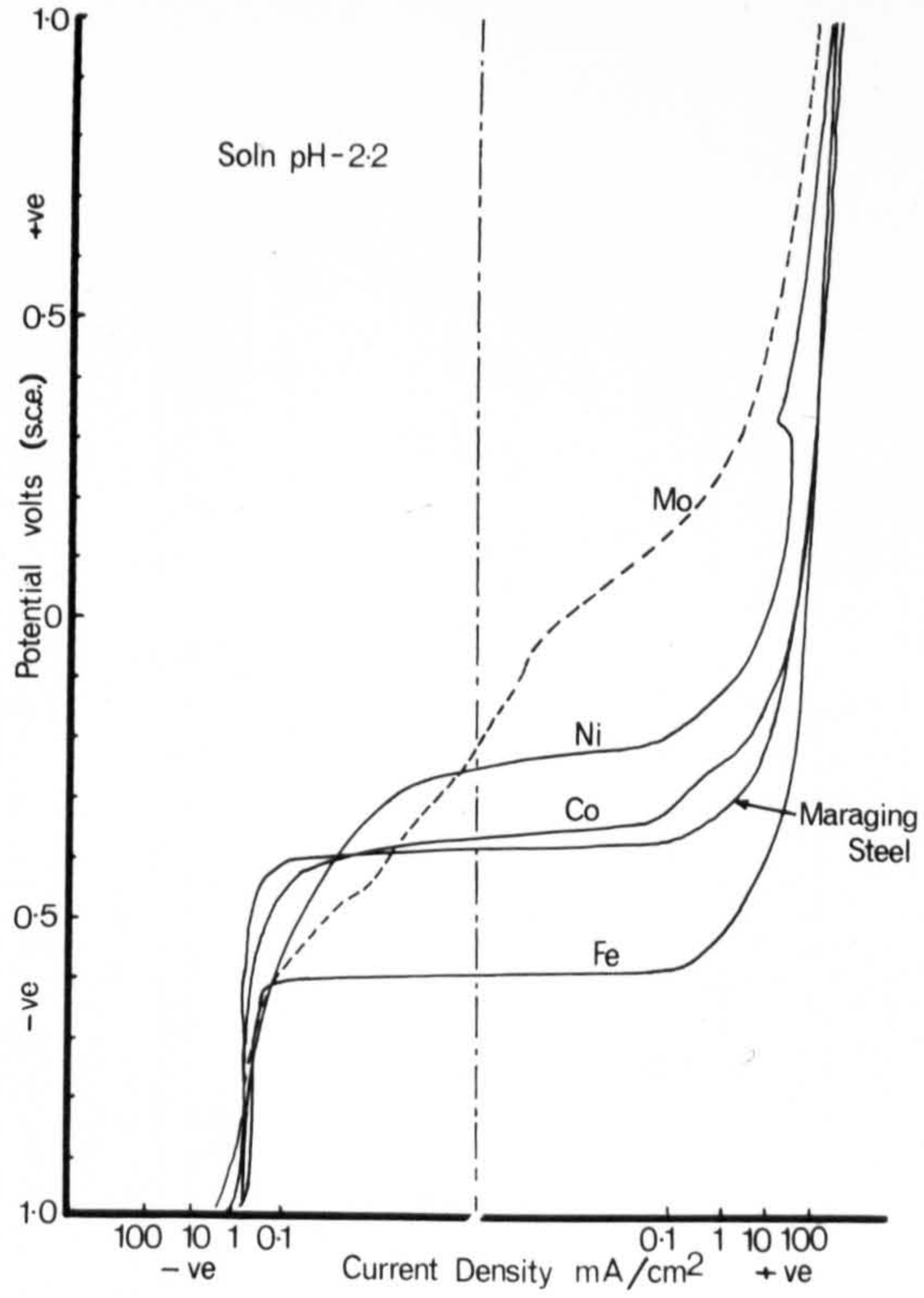

Fig. 3.29 Polarisation curves for maraging steel and pure elements in pH 2 solution

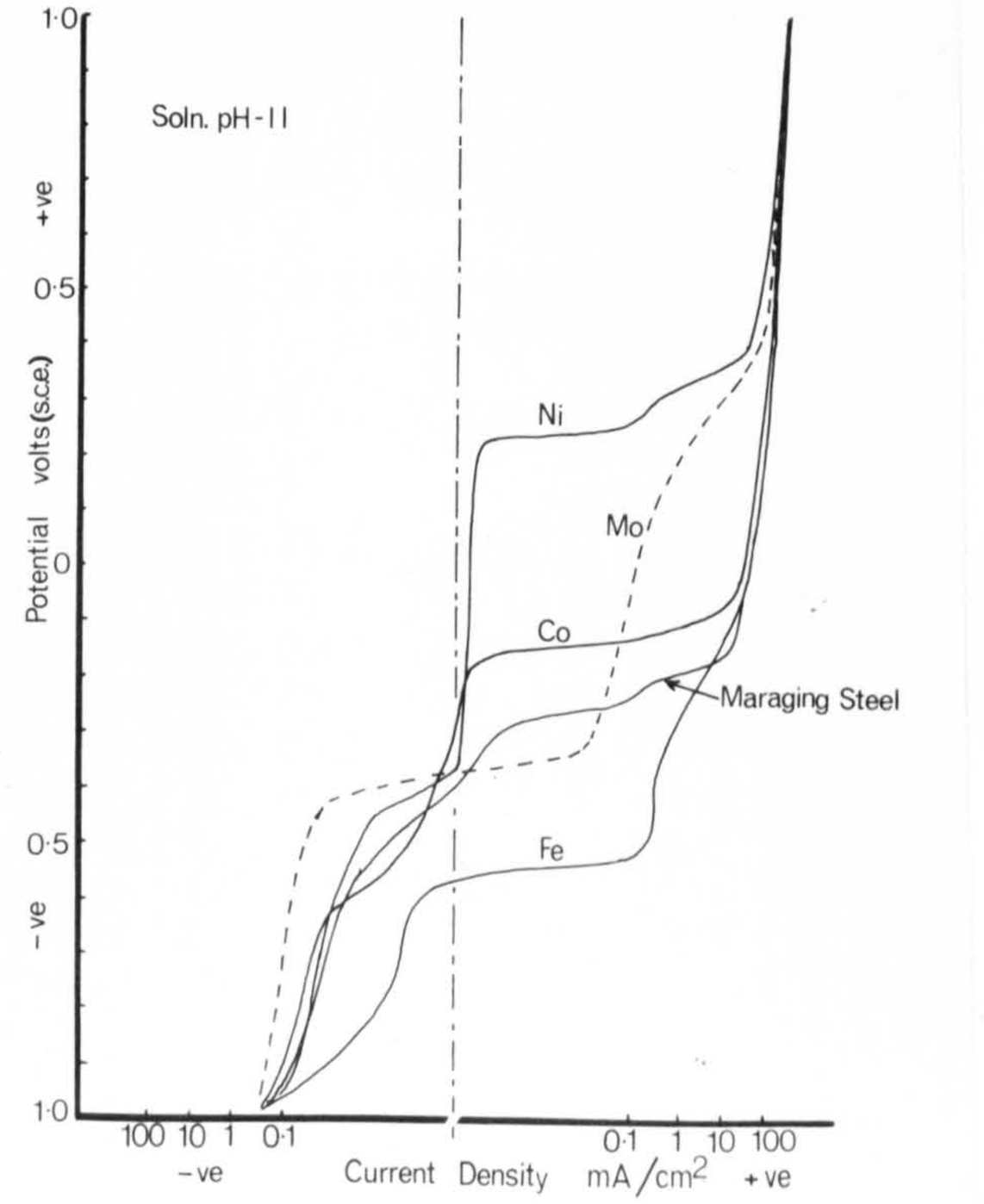

Fig. 3.30 Polarisation curves for maraging steel and pure elements in pH 11 solution.

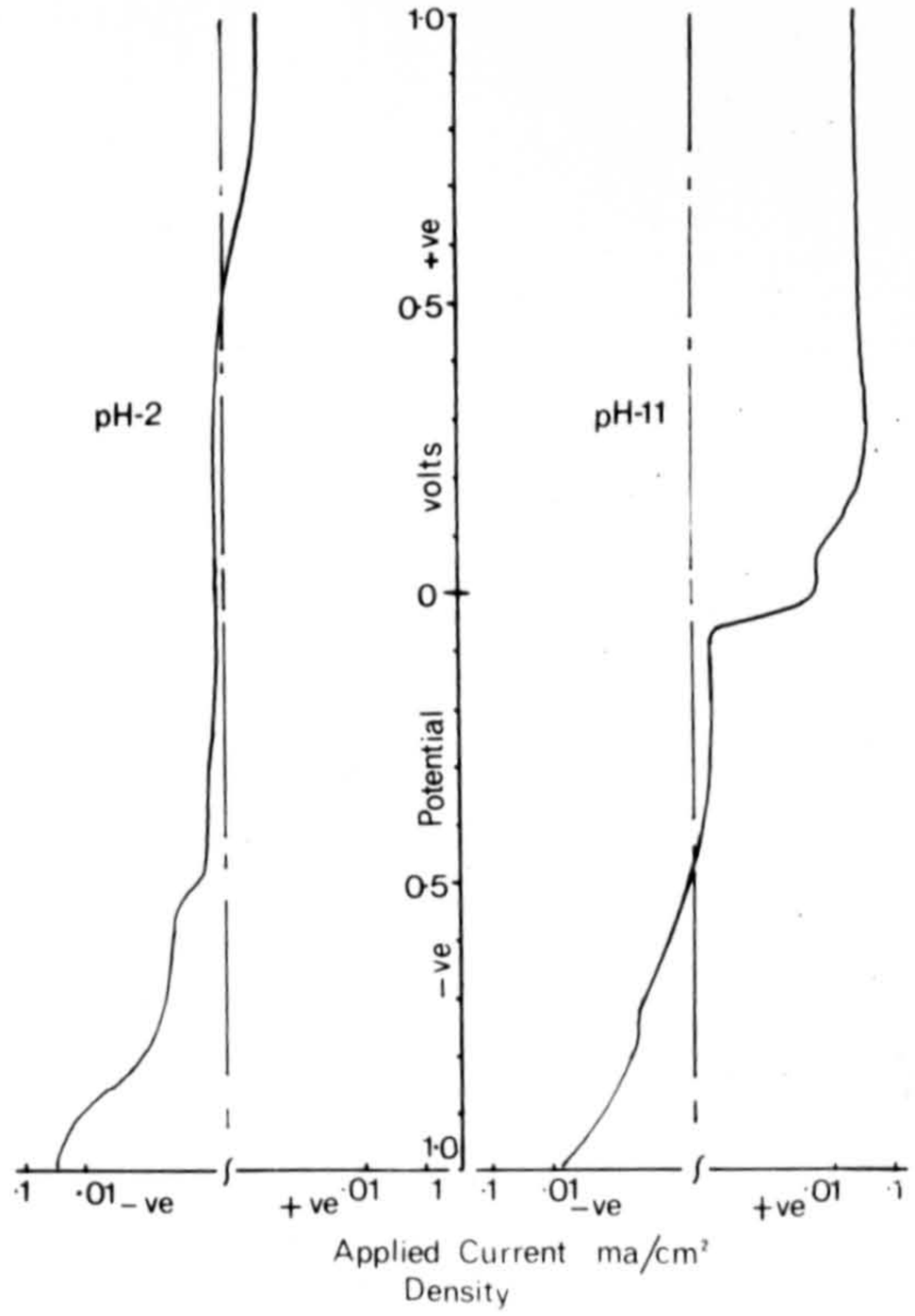

Fig. 3.31 Polarisation curves for pure titanium carbide

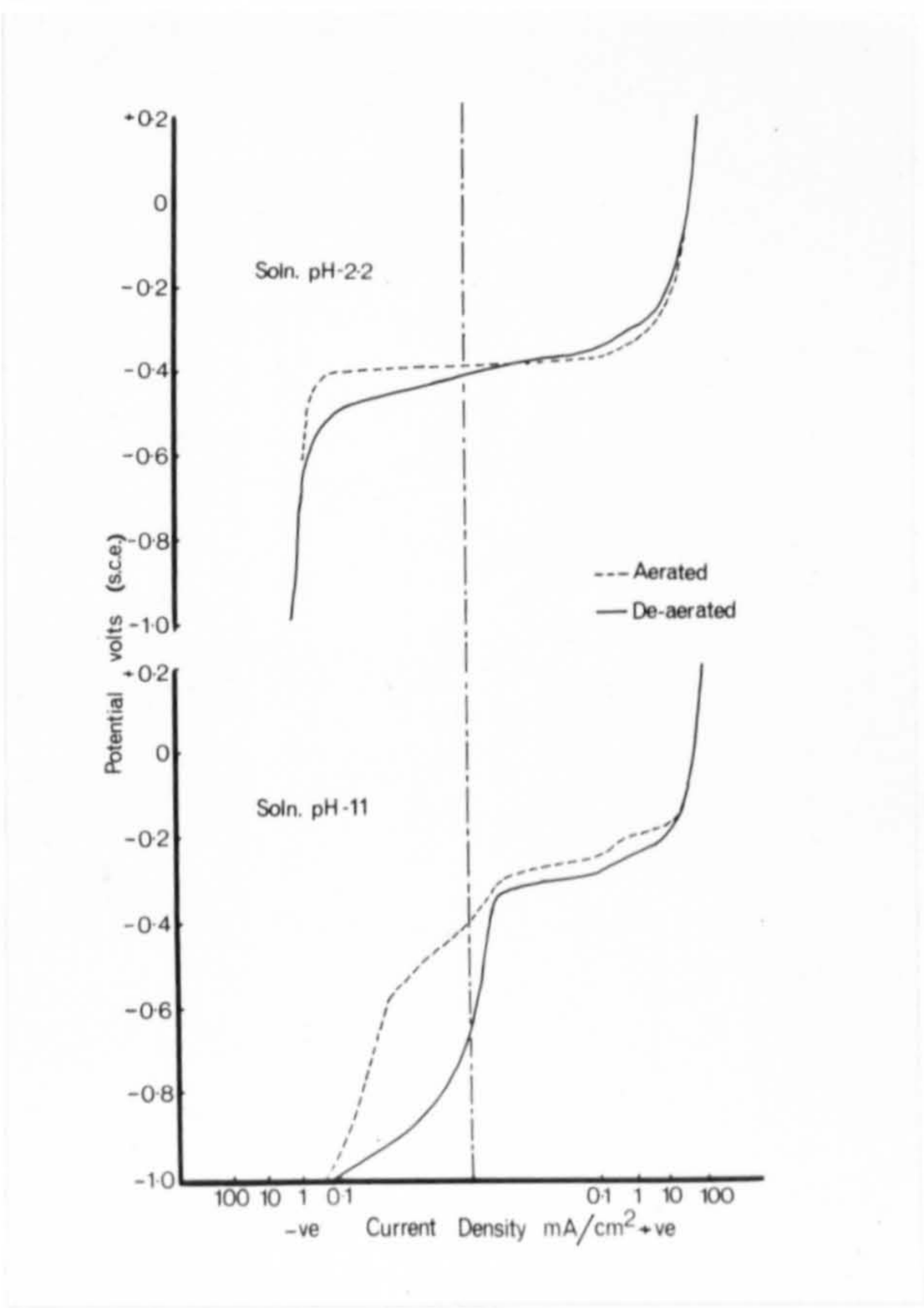

Fig. 3.32 Effect of deoxygenation on polarisation curves for maraging steels.

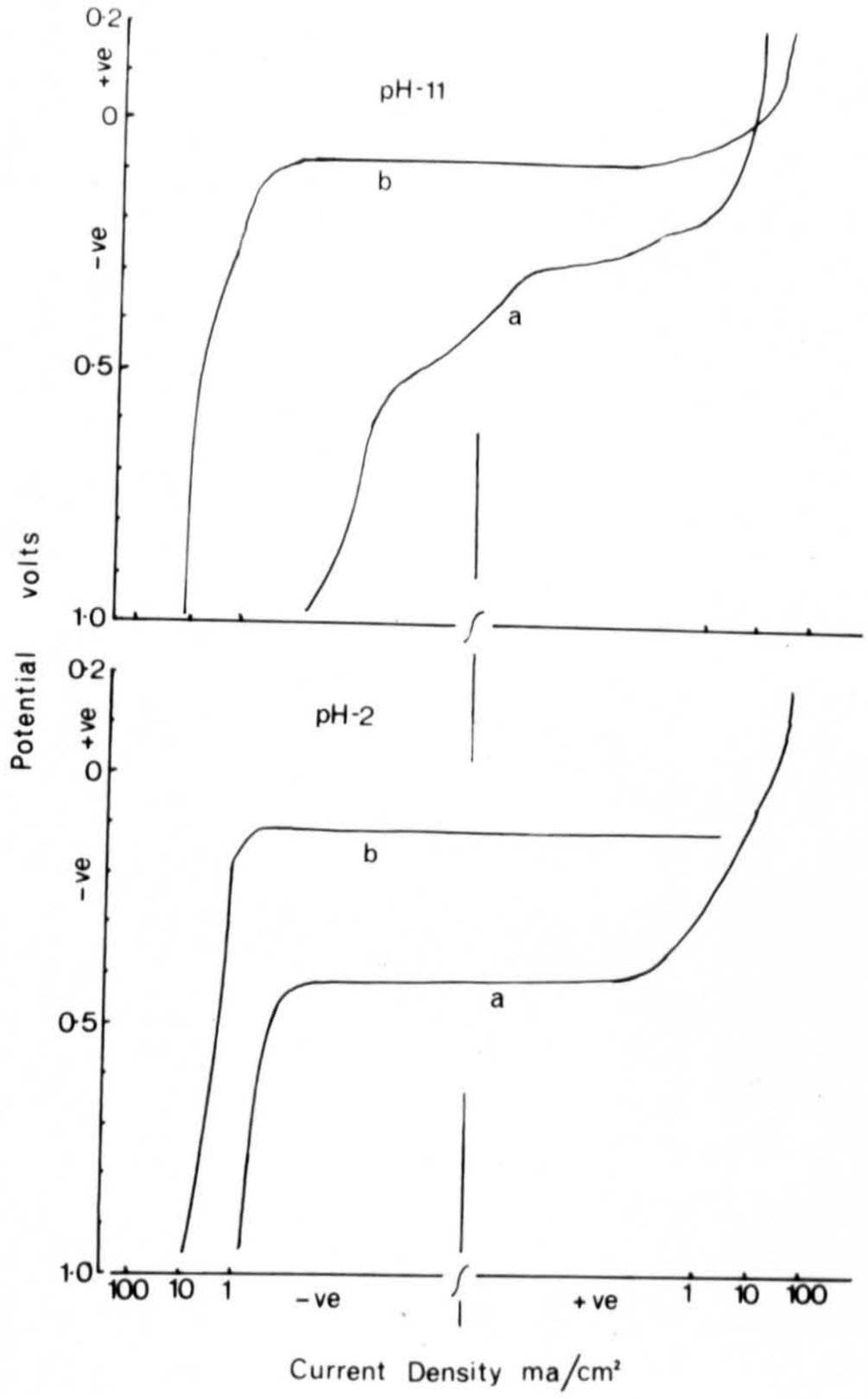

Fig. 3.33 Polarisation curves for maraging steel (a) without and (b) with addition of hydrogen peroxide.

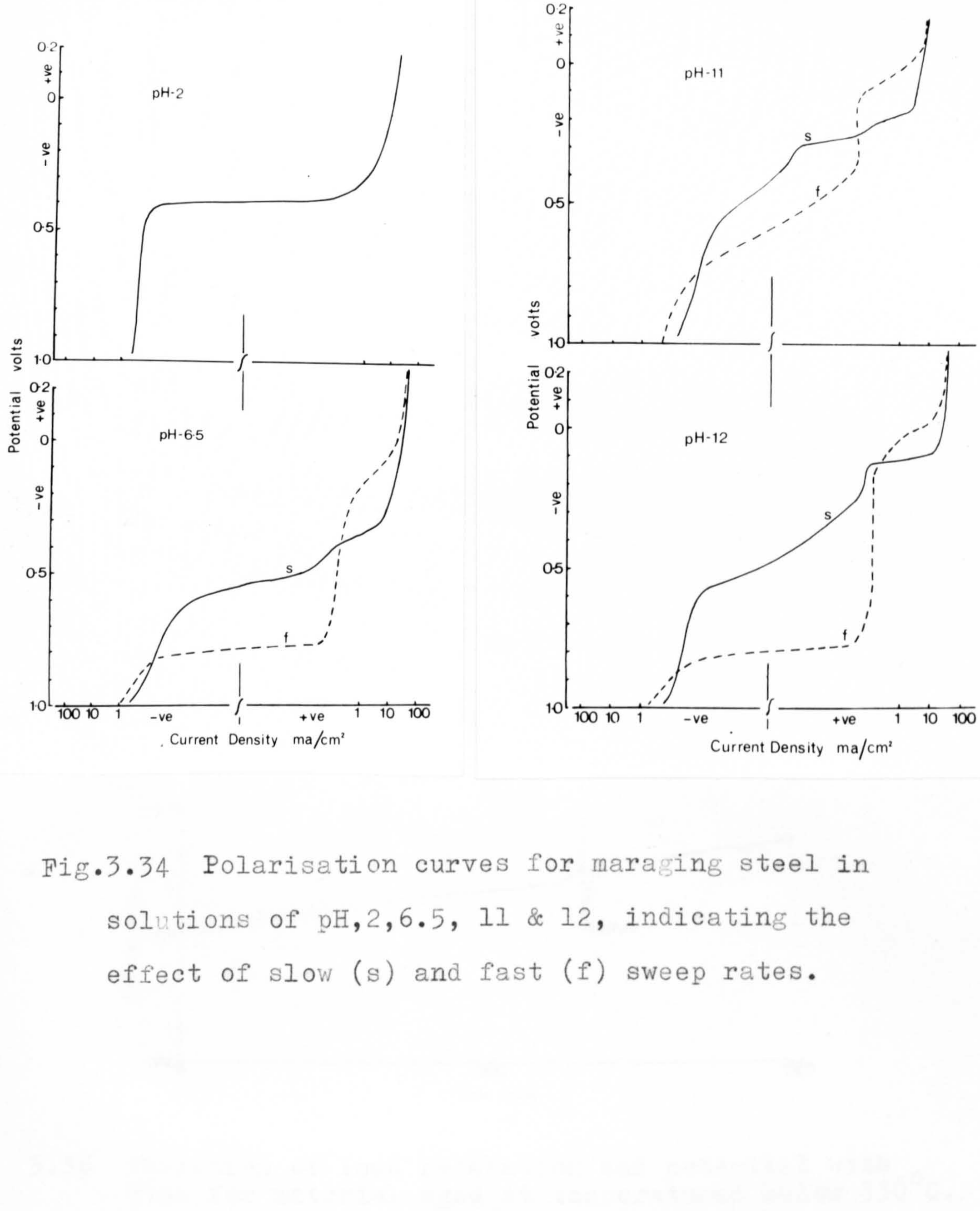

Fig.3.34 Polarisation curves for maraging steel in solutions of pH,2,6.5, 11 & 12, indicating the effect of slow (s) and fast (f) sweep rates.

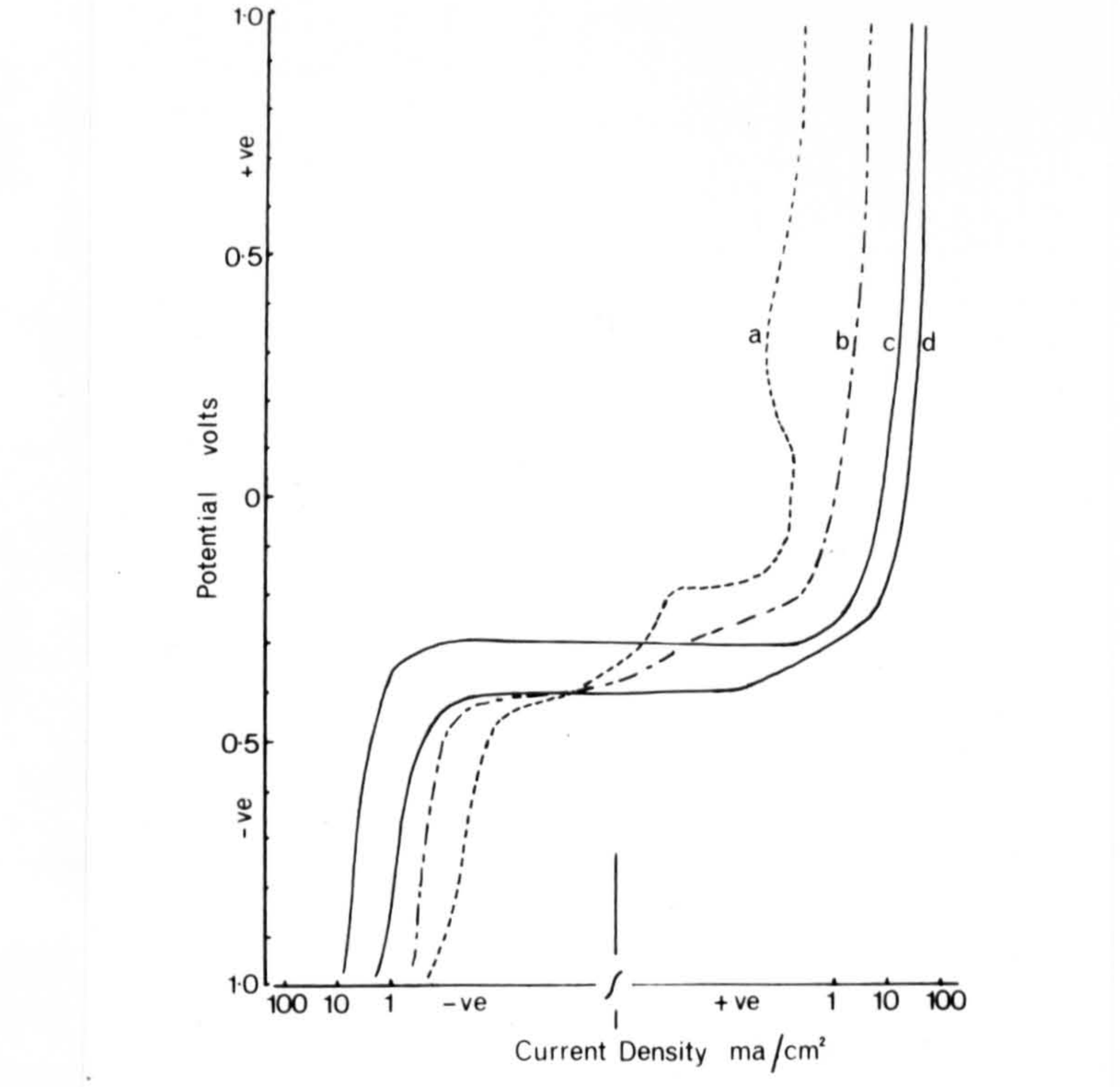

Fig. 3.35 Effect of chloride ion concentration on the polarisation characteristics of maraging steel in pH-11 solution.

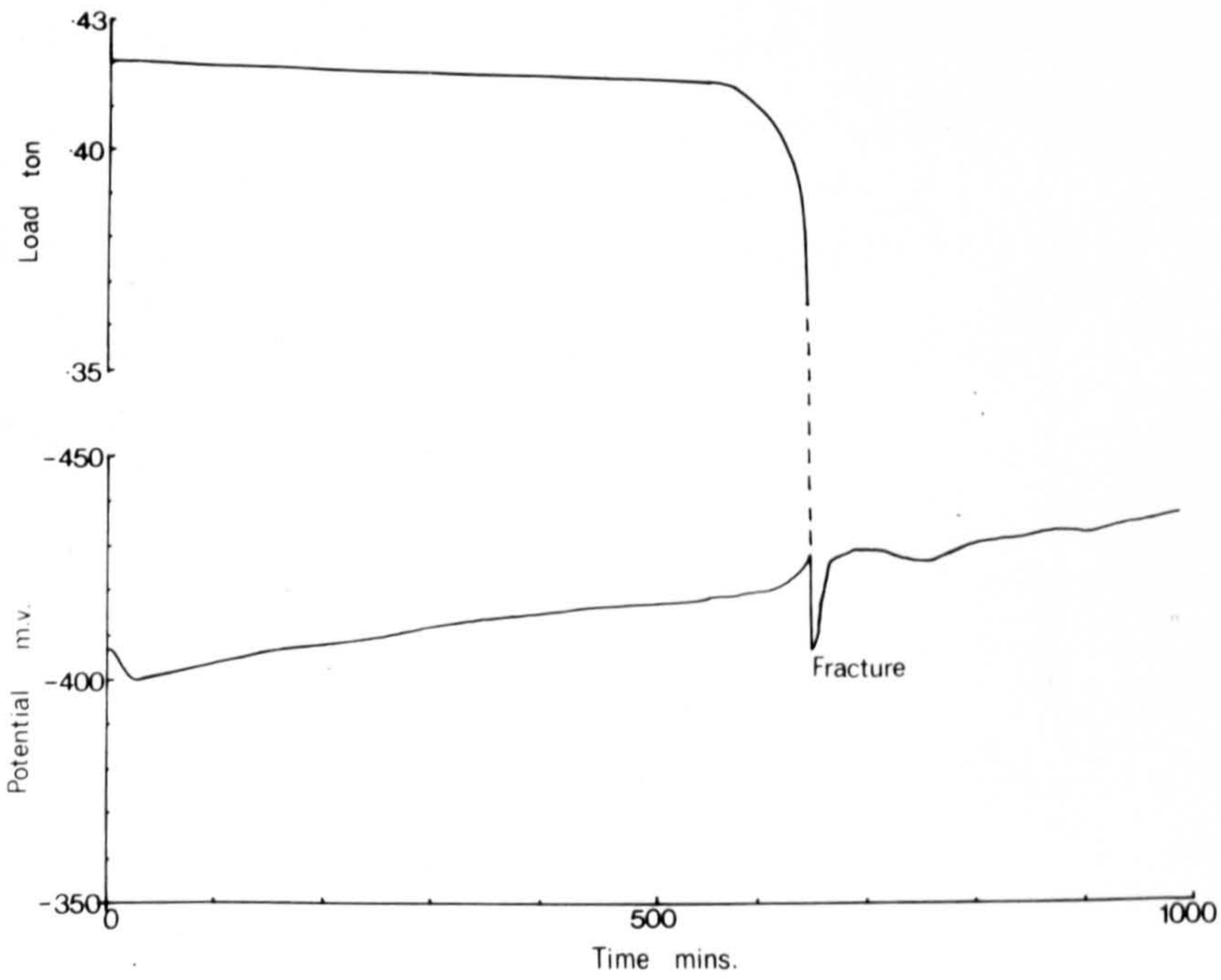

Fig. 3.36 Variation of load relaxation and potential with time for material aged at temperatures below 530°C.

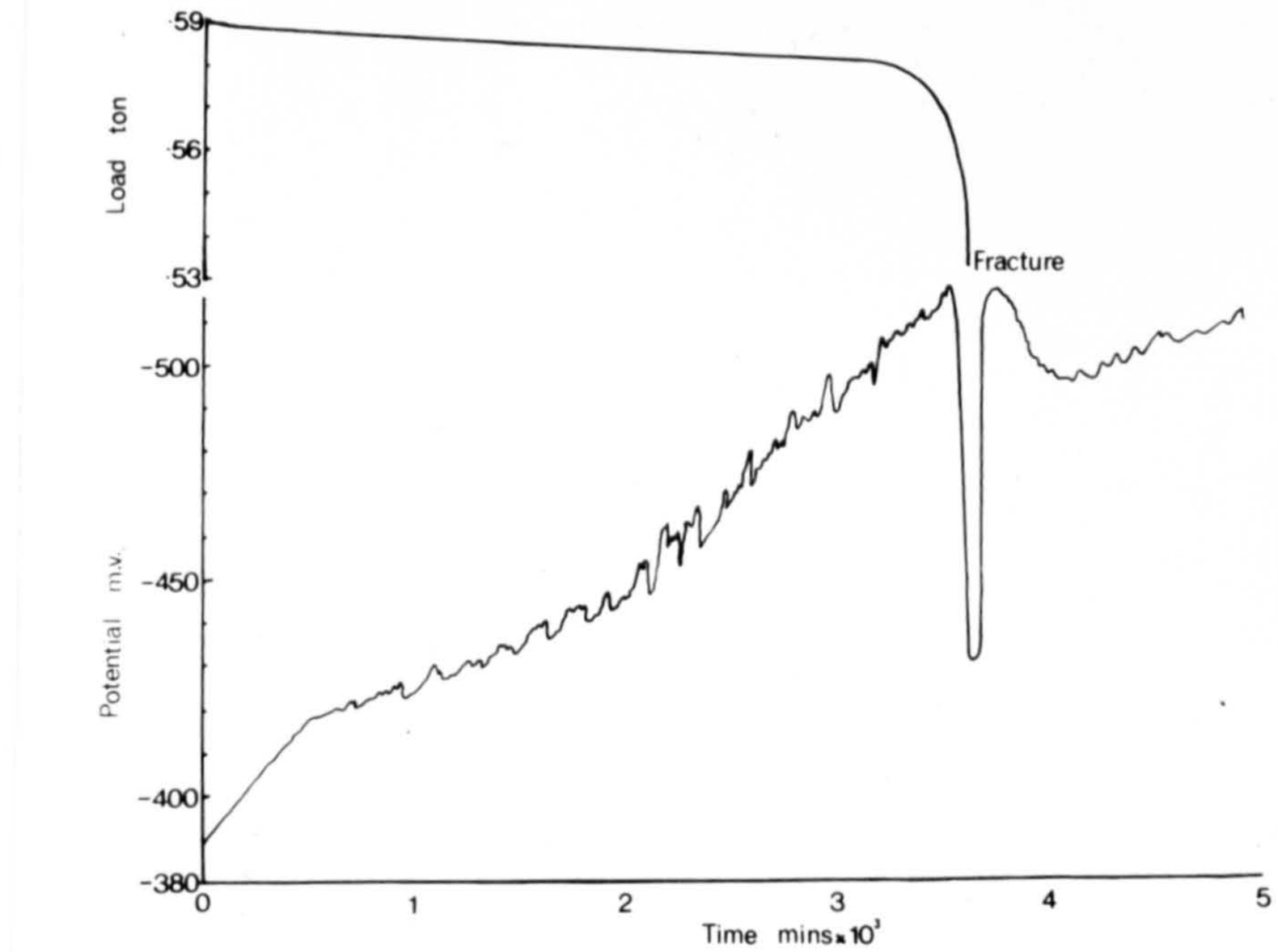

Fig. 3.37 Variation of load relaxation and potential with time for material aged at 530°C and above.

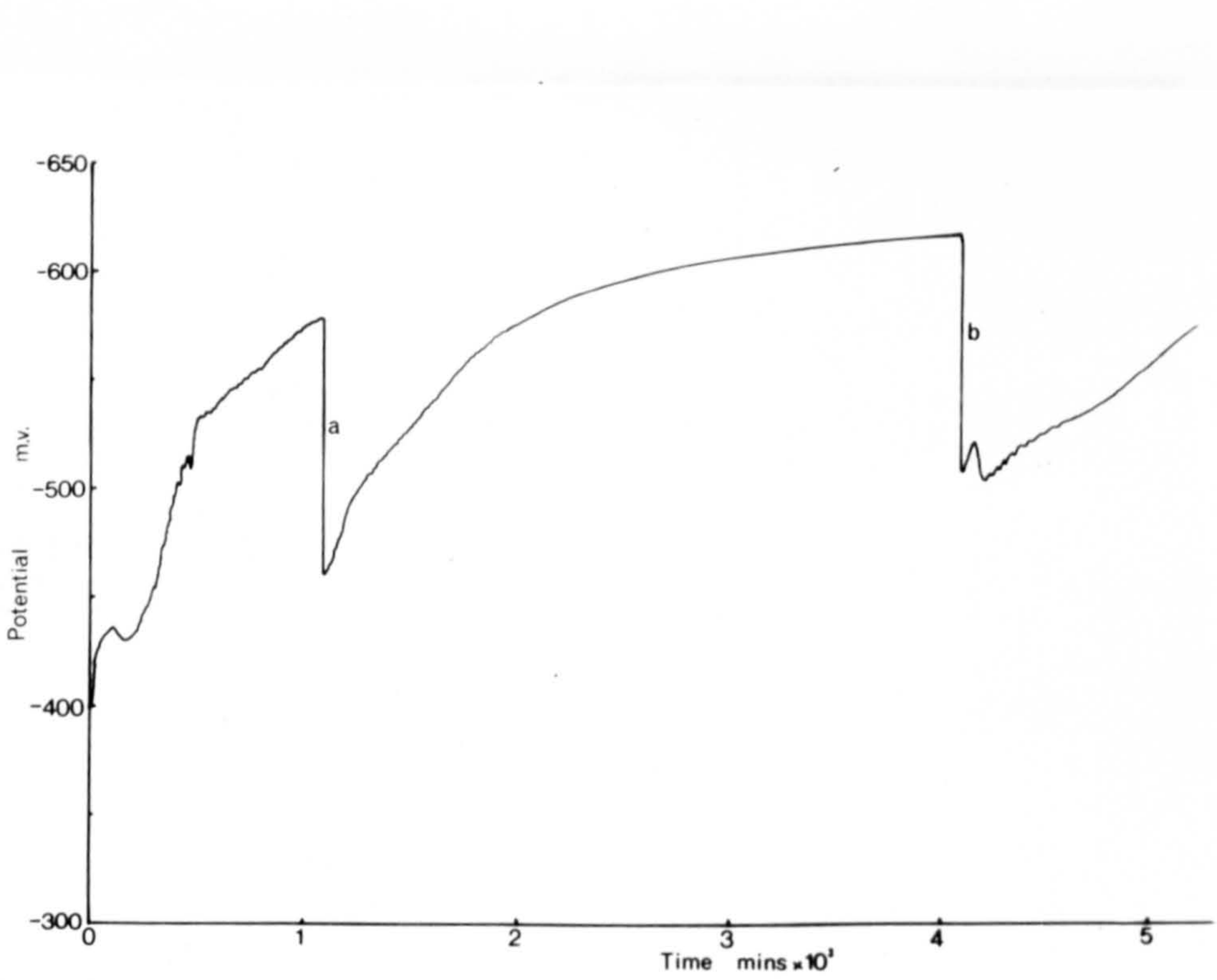

g. 3.38 Change in potential-time curve produced by renewing corrosive solution of pH 2. The associated pH change was (a) 0.4 unit and (b) 1.2 unit in the acid direction in each case.

Fig. 3.39 Showing appearance of surface corrosion product (120x)

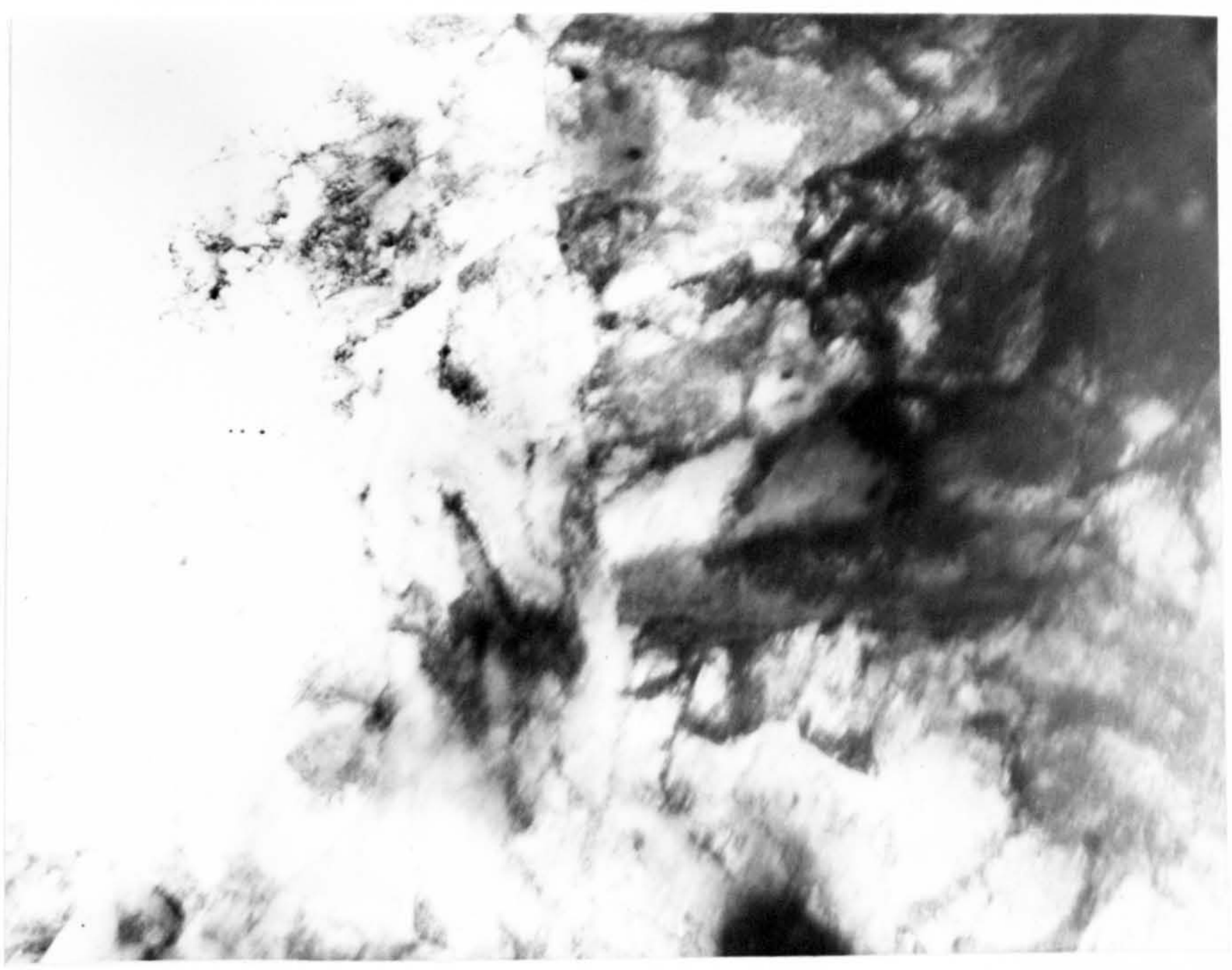

Fig. 3.40 Electron micrograph showing typical matrix area (12,000x)

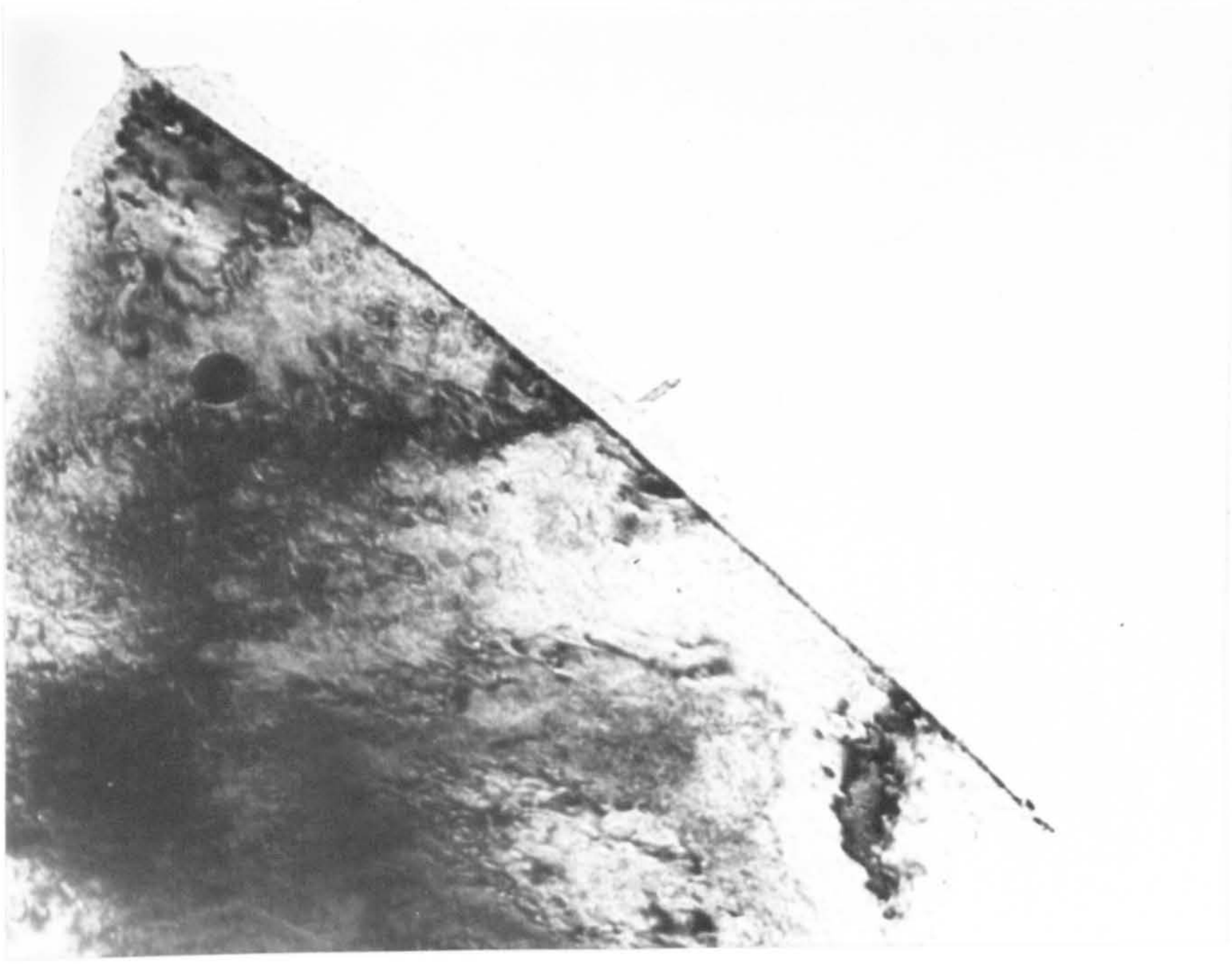

Fig. 3.41 Area indicating the presence of grain boundary precipitate in aged material (70,000x)

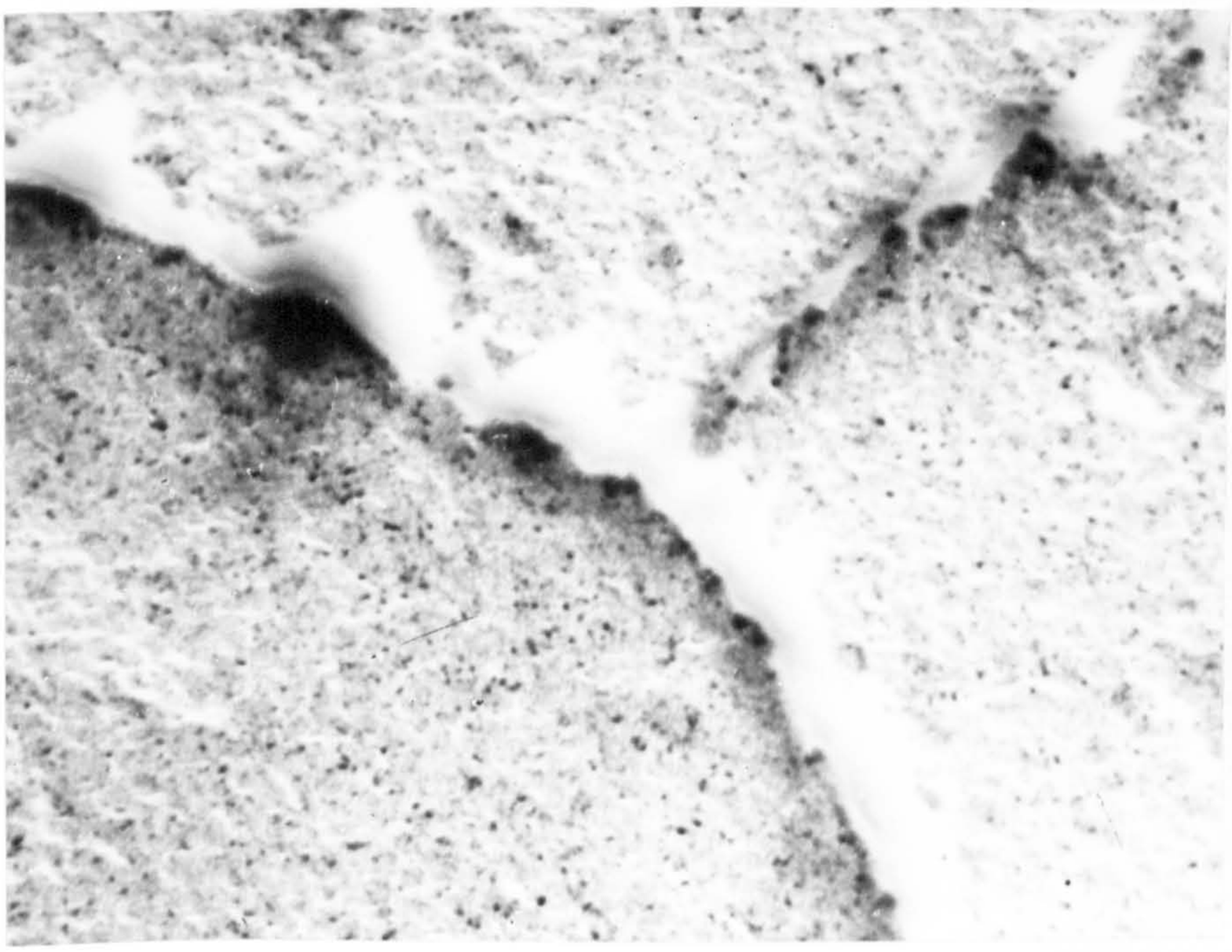

Fig.3.42 Extraction carbon replica showing a grain boundary precipitate in material aged for 48 hours at 480°C (70,000x).

Fig. 3.43 Electron micrograph showing grain boundary area (61,000x). Foil dipped and stressed in a pH 2 solution for 10 seconds.

Fig. 3.44 Electron micrograph showing random platinum deposition (20,000x). Foil dipped and stressed in a pH 2 solution for 30 seconds.

Fig. 3.45 Intergranular stress corrosion fracture surface (2,300x)

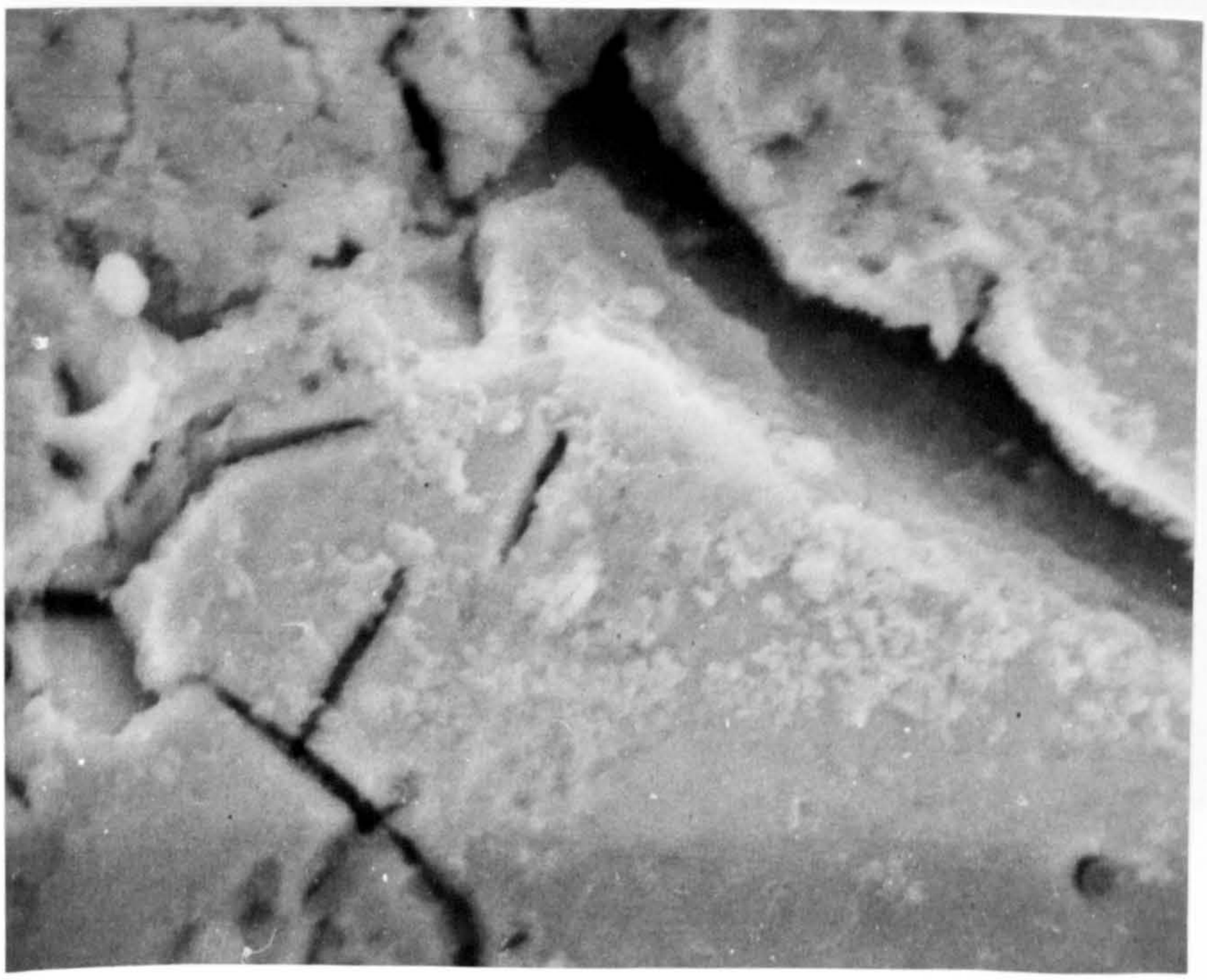

Fig. 3.46 Fracture area showing evidence of secondary transgranular cracking (2,390 x)

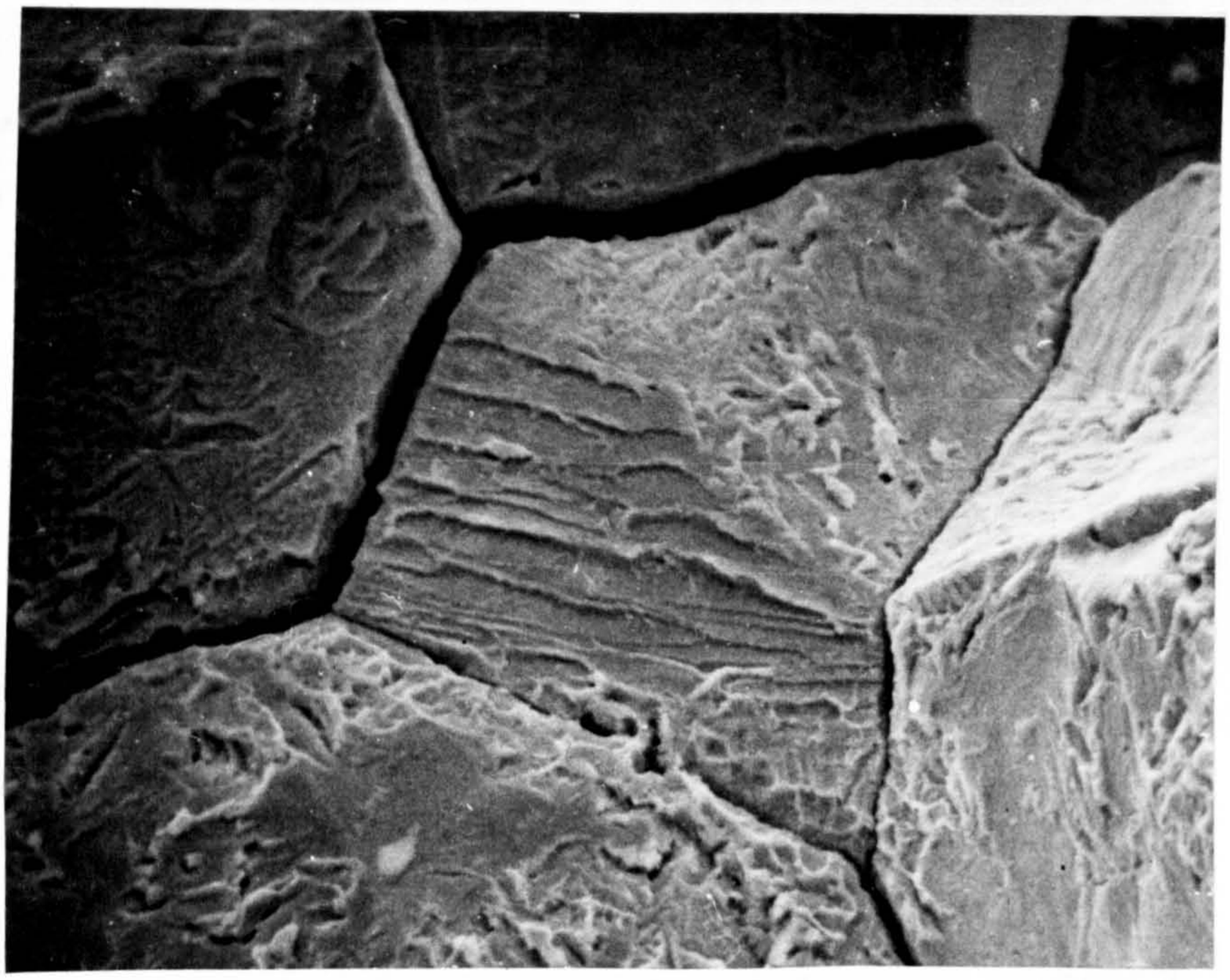

(a)

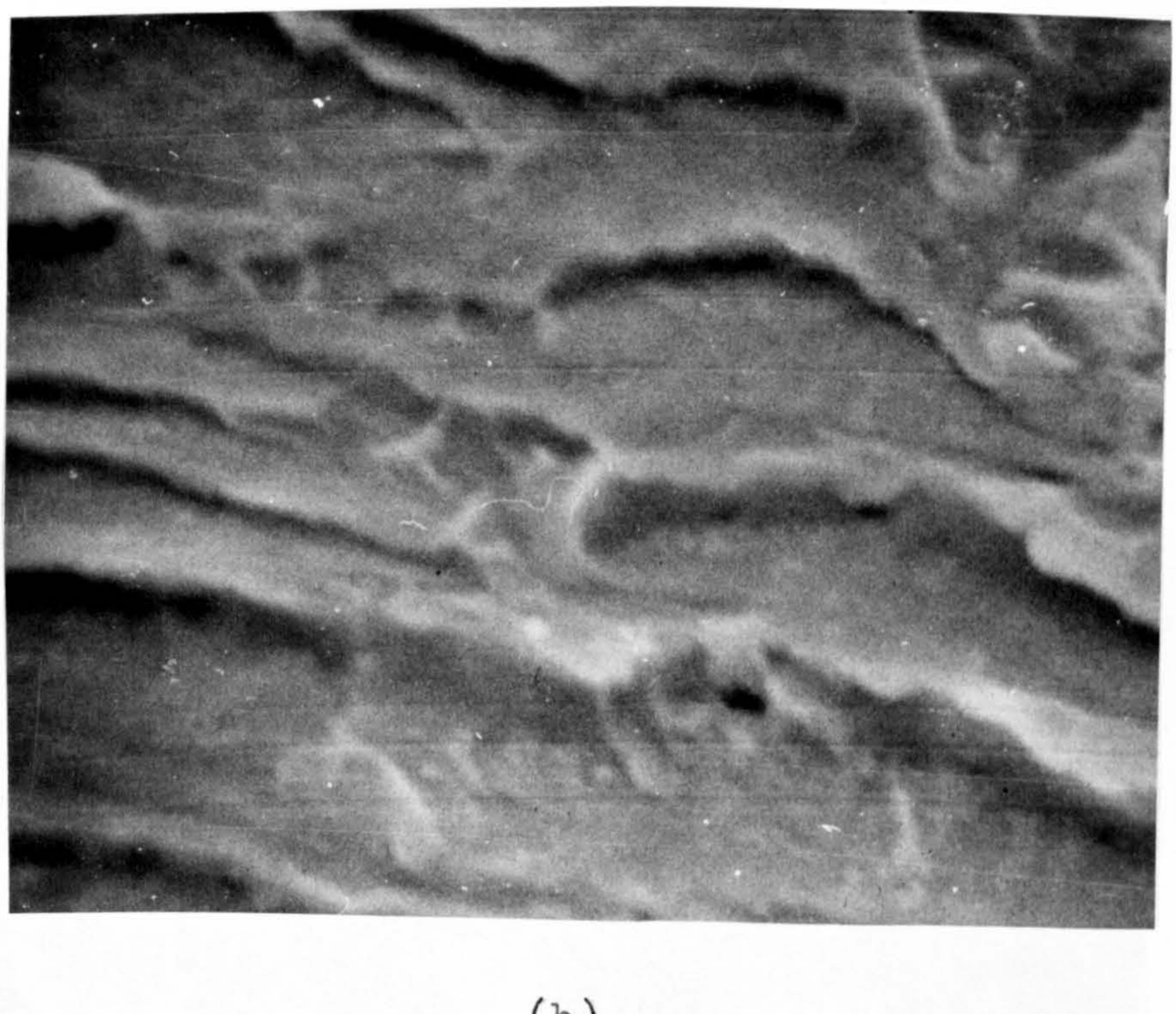

(b)

Fig. 3.47 Grain surface markings on stress corrosion areas of large grained material. (a) 1200x , (b) 6,000x.

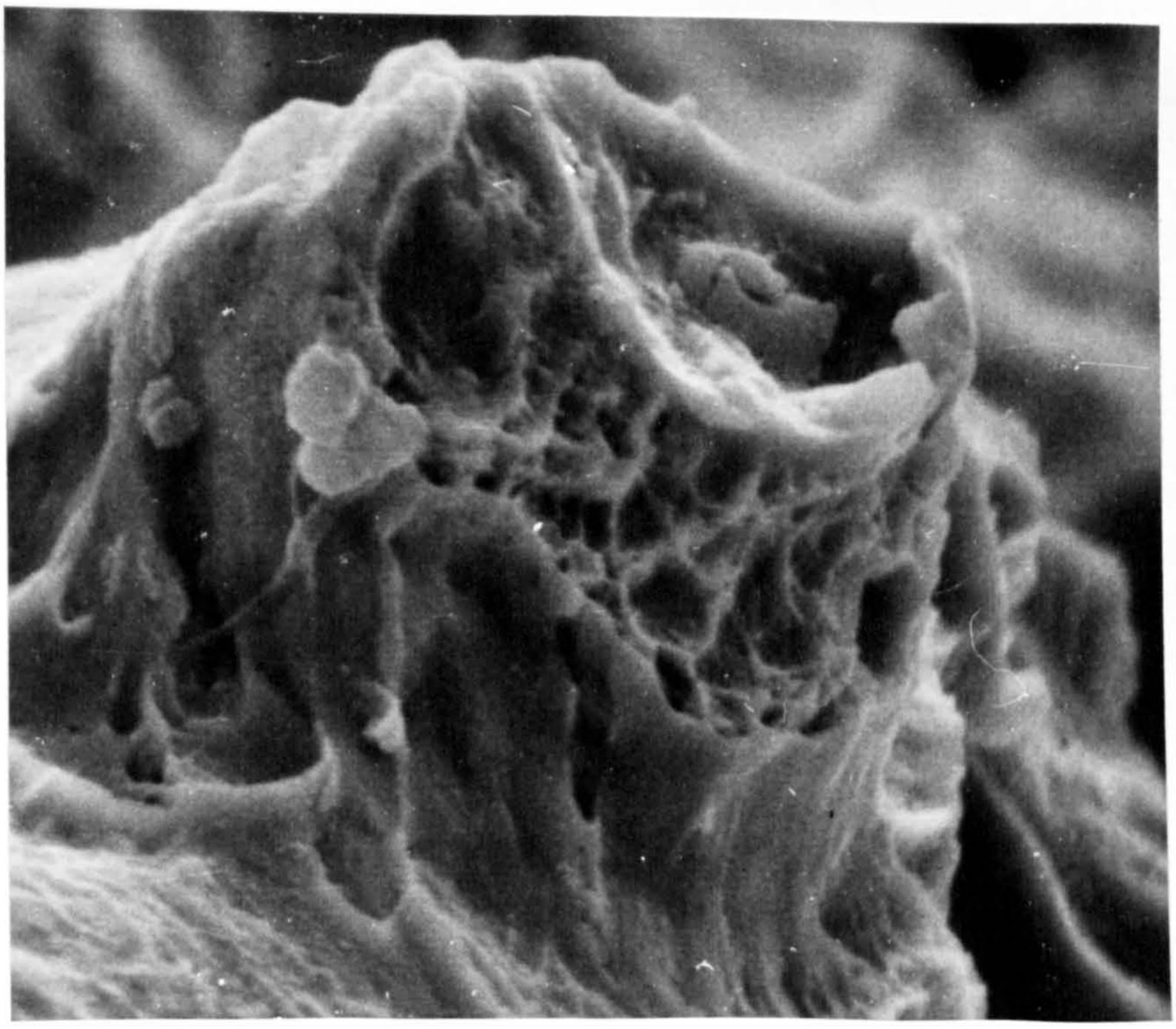

Fig. 3.48 Ductile rupture area (5,750x).

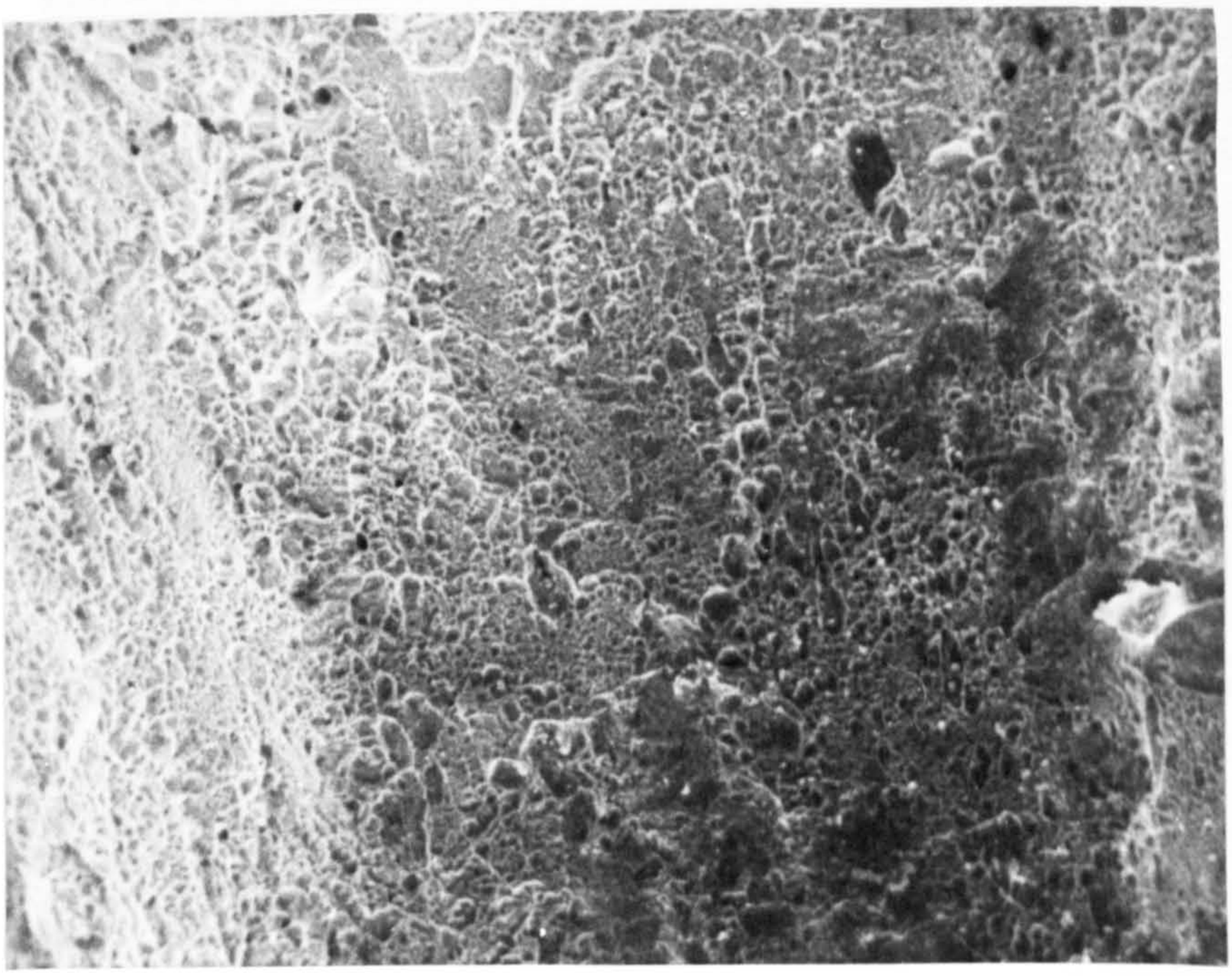

Fig. 3.49 Mechanical failure area showing evidence of shear rupture (200x).

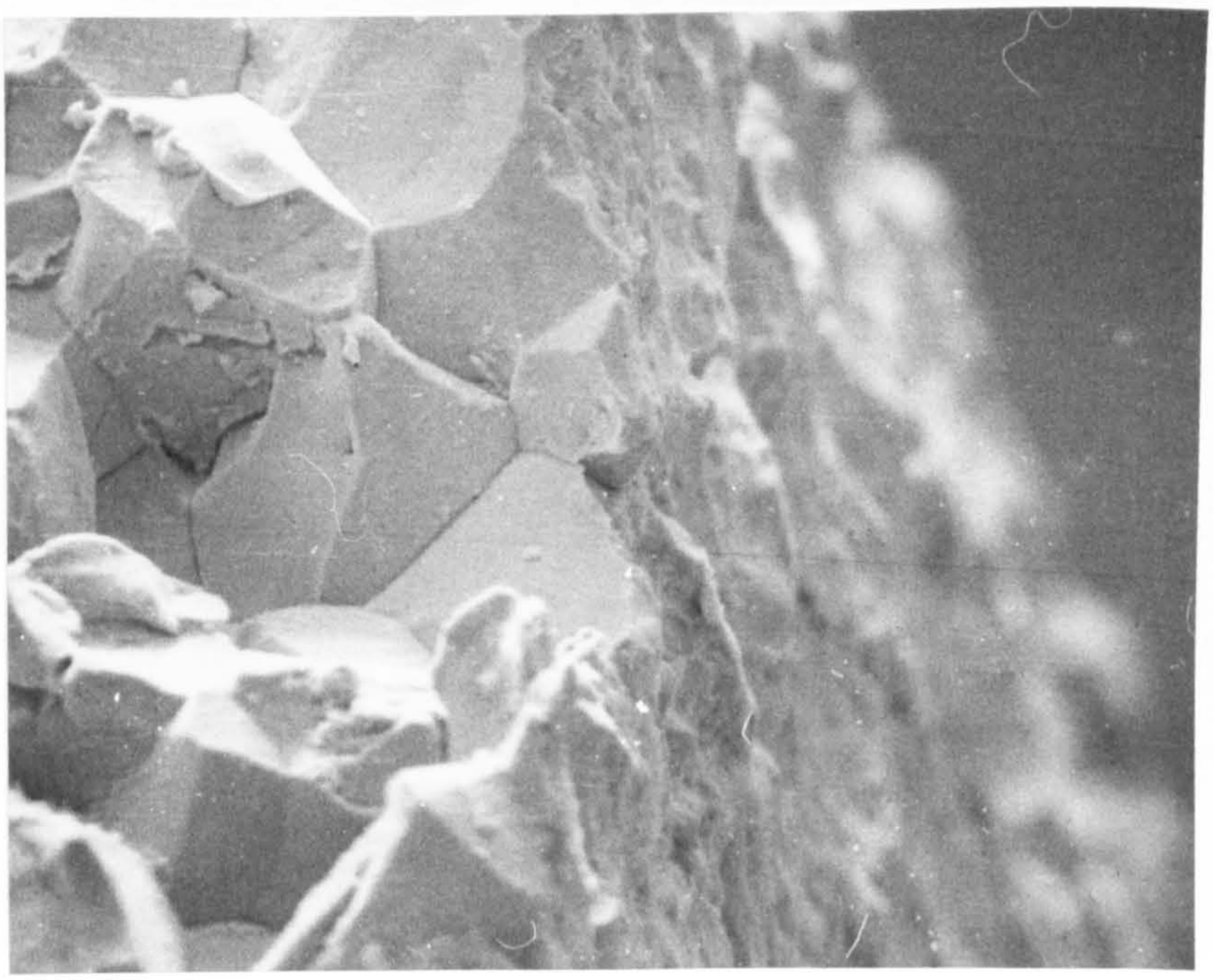

(a)

(b)

Fig.3.50 Appearance of surface fissures which lead to intergranular cracking (a - 600x, b - 6,000x).

Fig. 3.51 Crack initiation along grain boundary region. Material stressed for 15 minutes in a solution containing chloroplatinic acid. (2,350x).

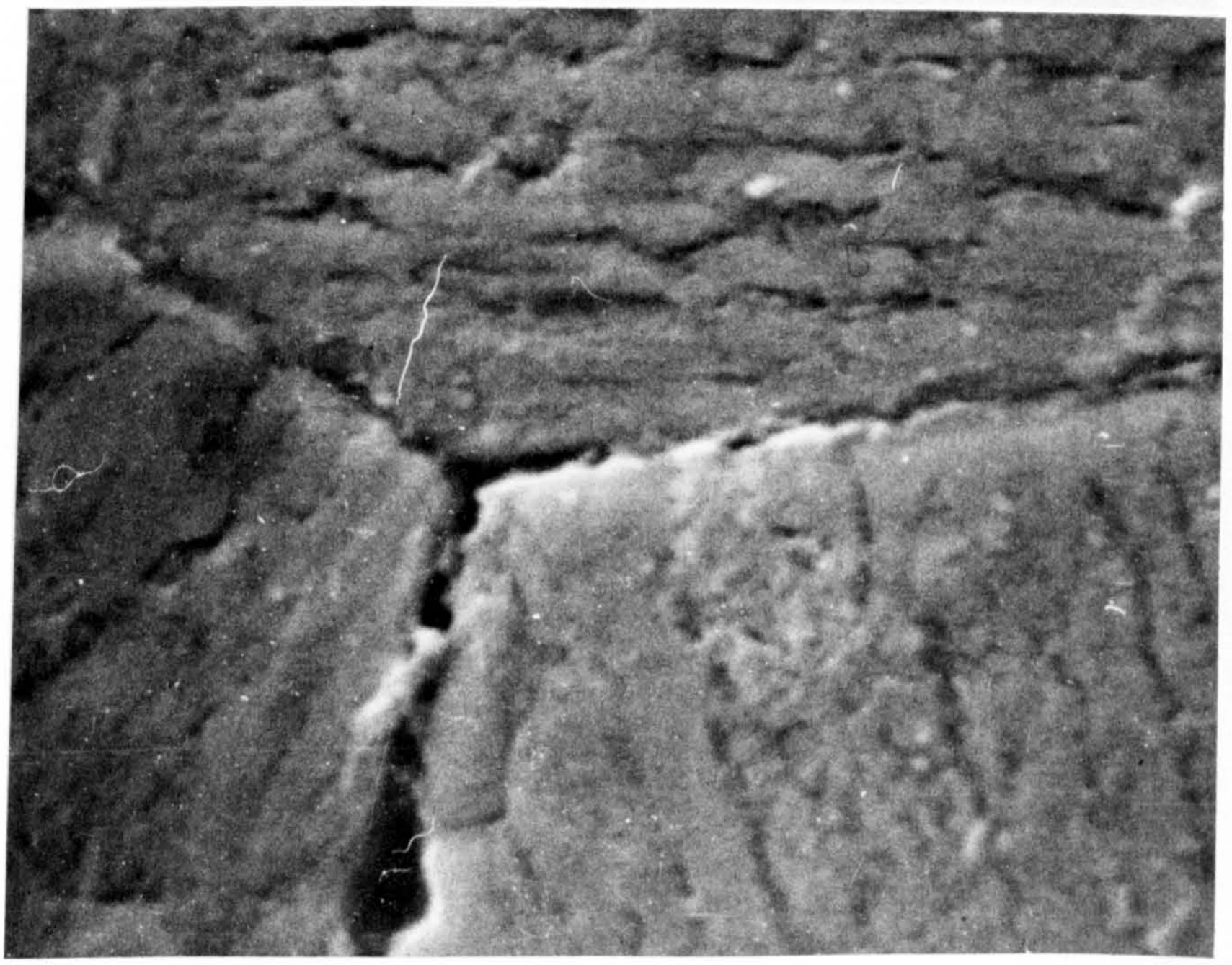

Fig. 3.52 Area showing coalescence of pits to form a continuous groove along the grain boundary. (5,750x).

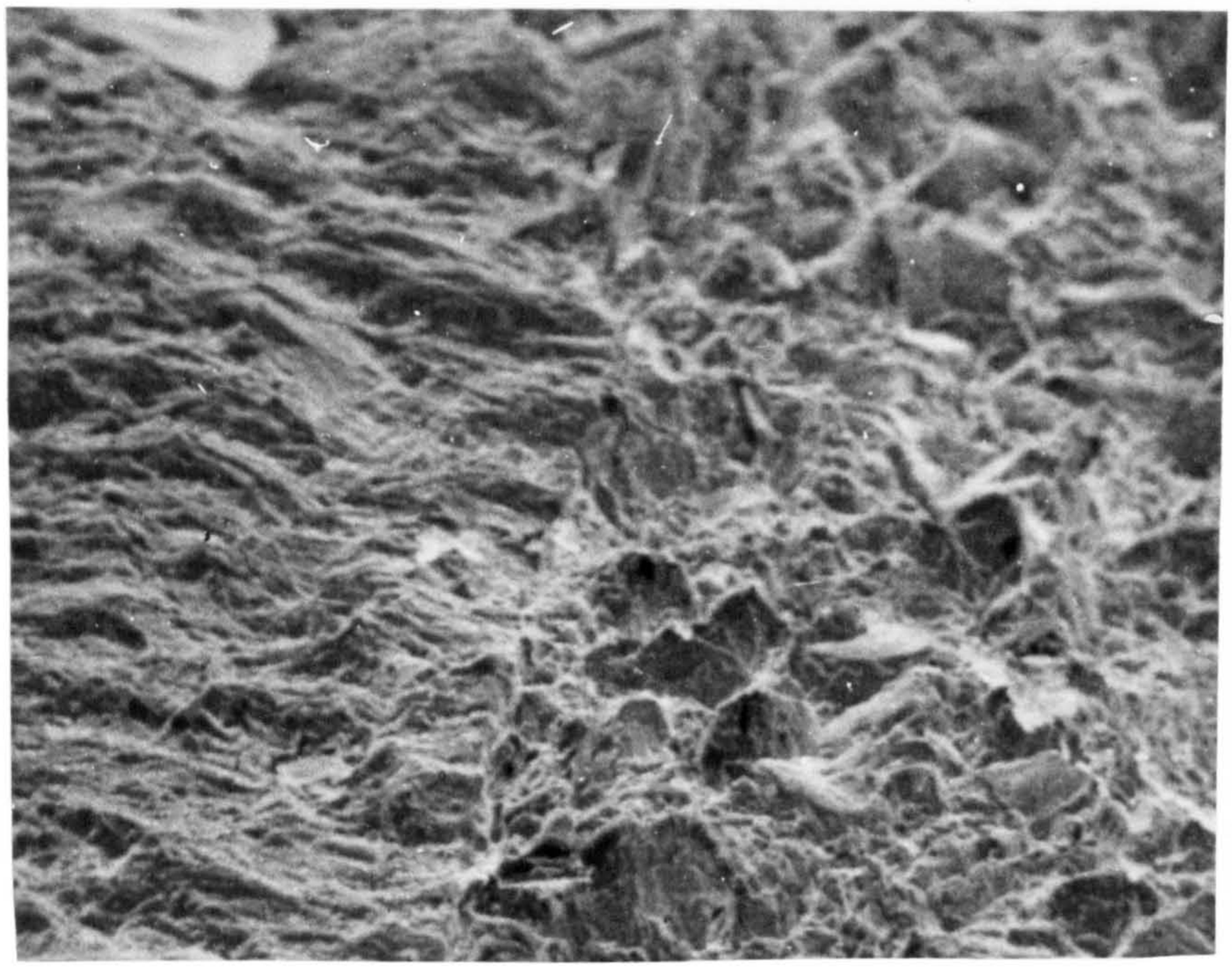

Fig. 3.53 Fracture surface showing the pre-crack and stress corrosion areas. (200x)

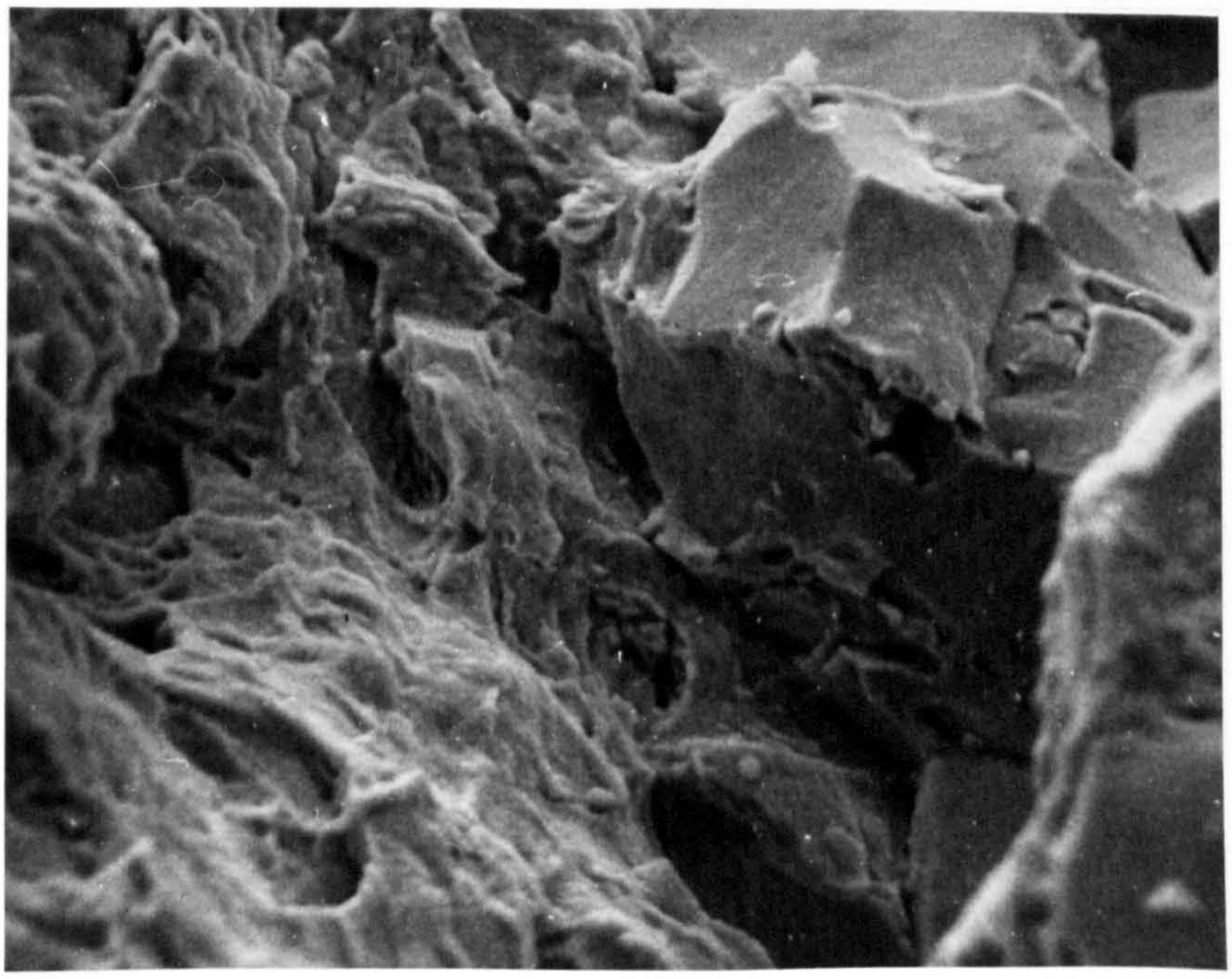

Fig. 3.54 Pre-crack/stress corrosion area in large grained material (1000x).

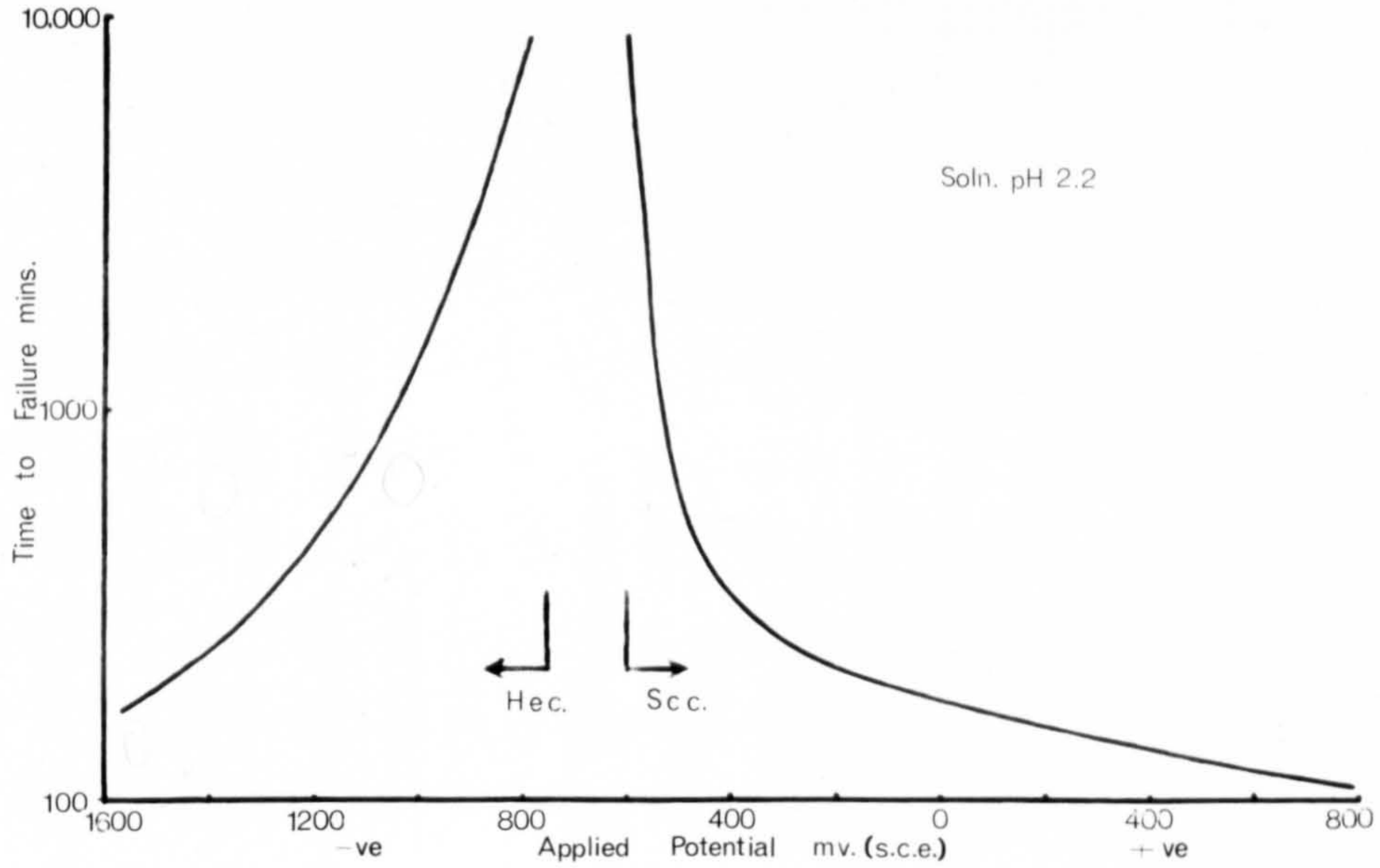

Fig. 3.55 Time to failure v.s. applied potential plot in pH 2 solution.

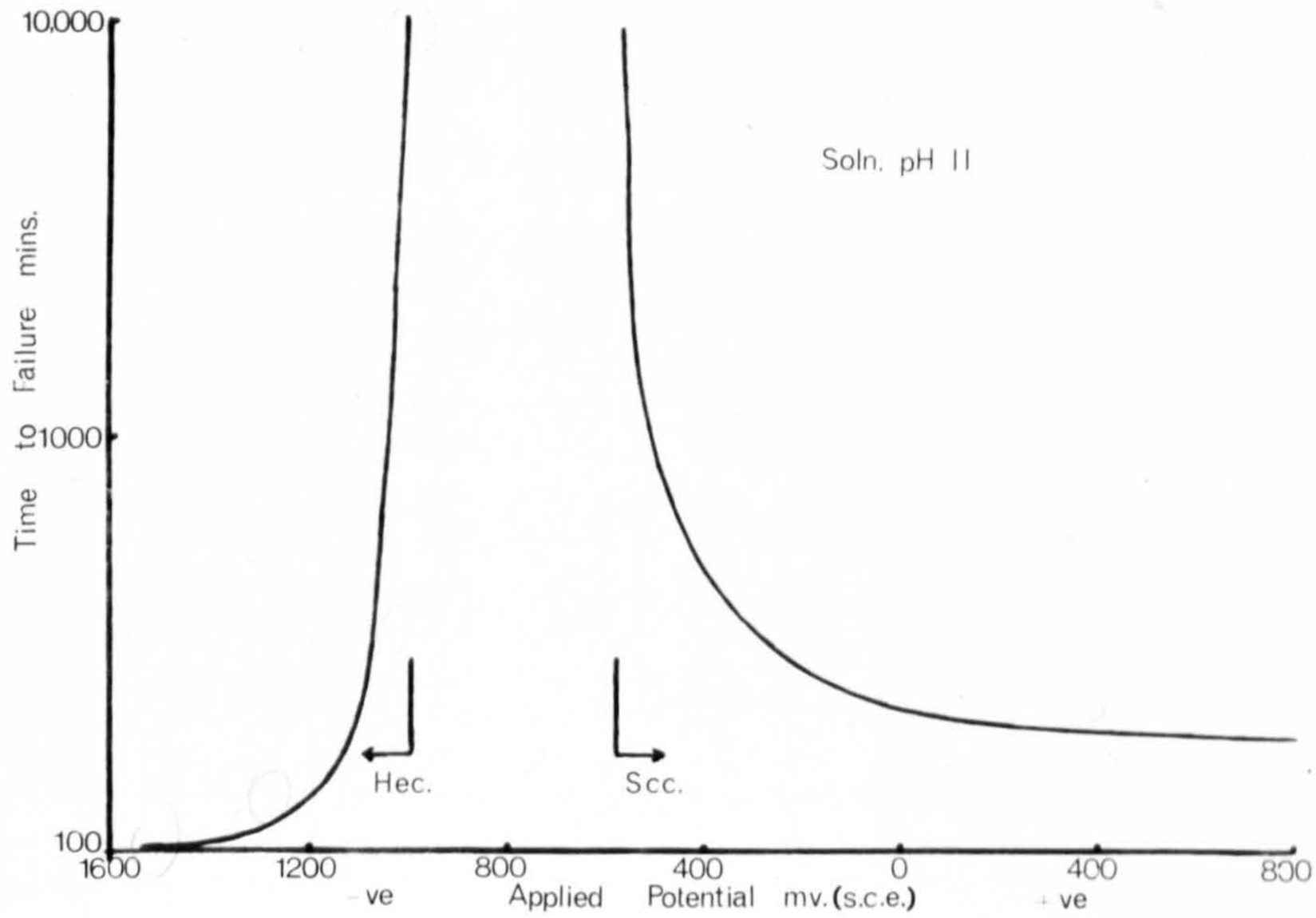

Fig. 3.56 Time to failure v.s. applied potential plot in pH 11 solution.

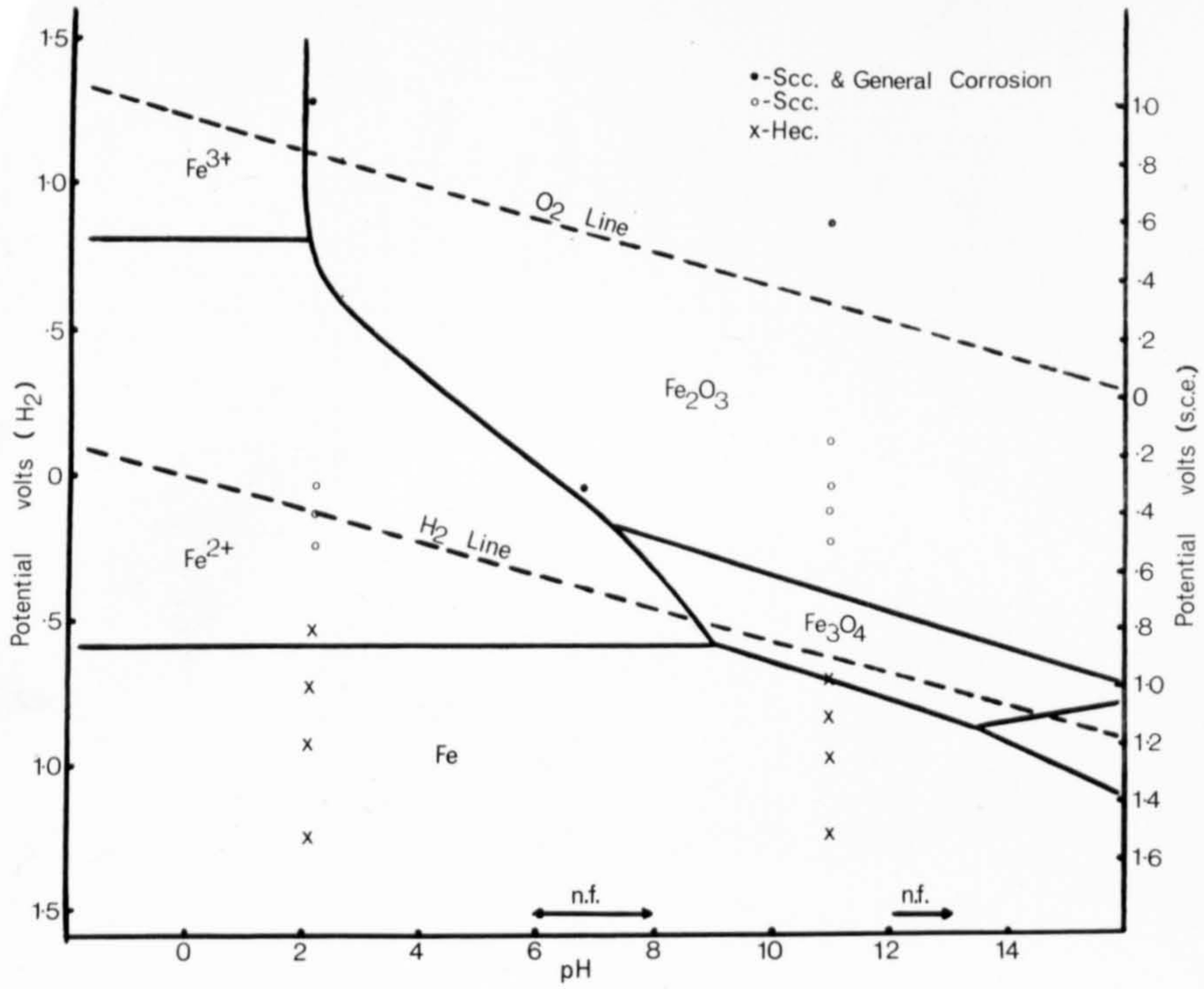

Fig. 3.57 Potential - pH diagram.

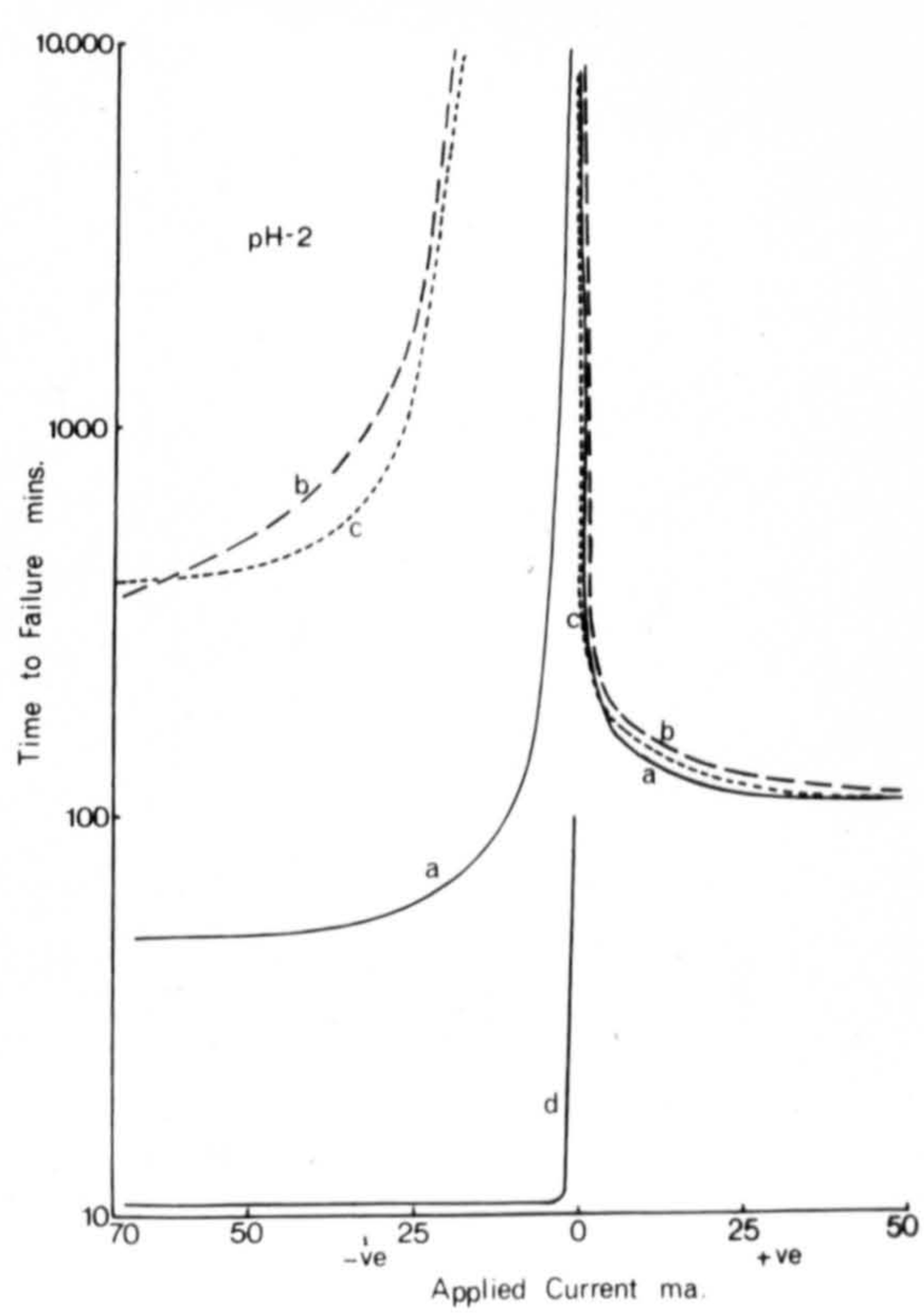

Fig. 3.58 Time to failure v.s. applied current plot for solutions of (a) pH-2 and with additions of (b) chloroplatinic acid, (c) anthraquinone, & (d) sodium arsenate.

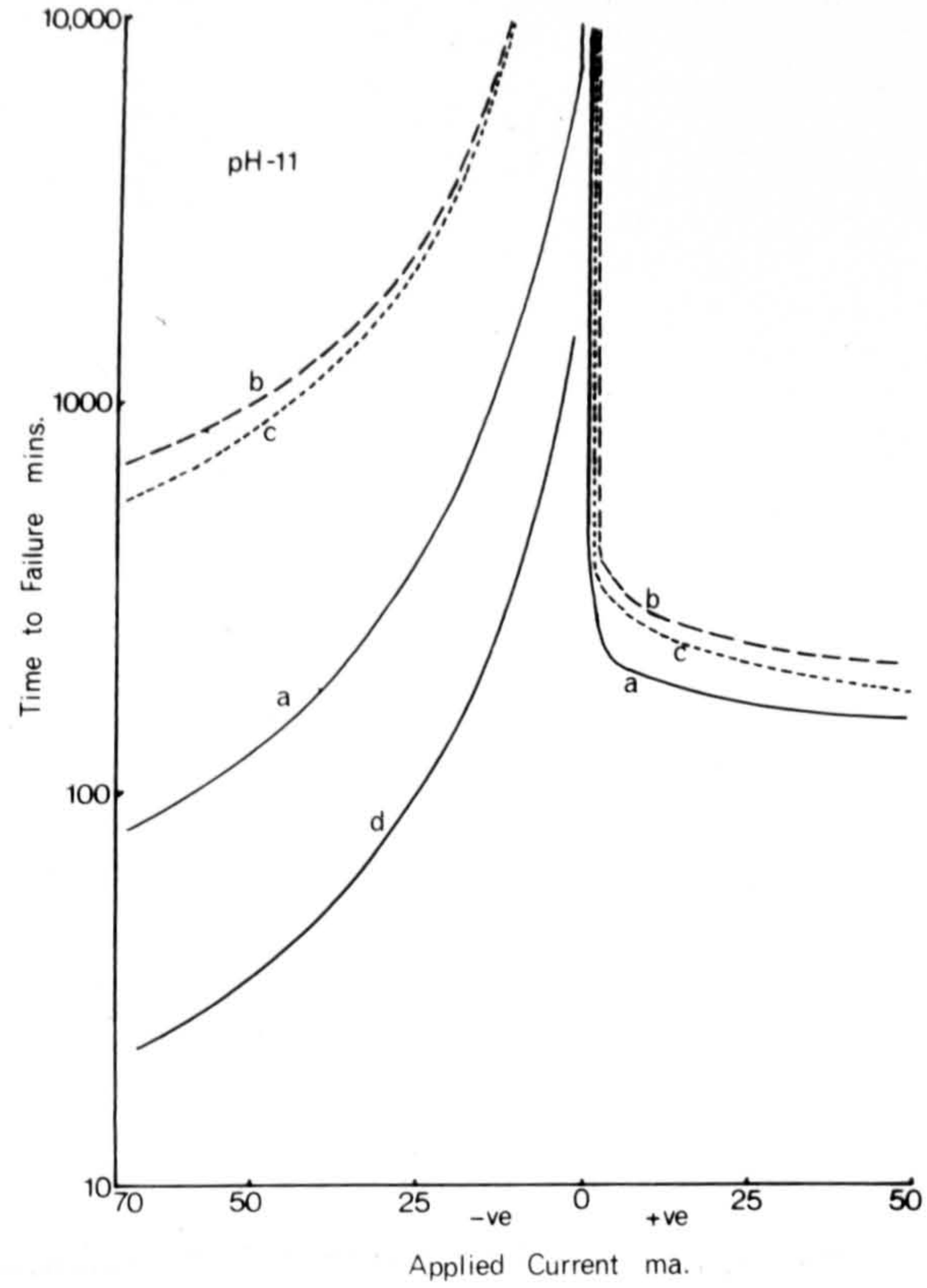

Fig : 3.59 Time to failure v.s. applied current plot for solutions of (a) pH-11 and with additions of (b) chloroplatinic acid, (c) anthraquinone and (d) sodium arsenate.

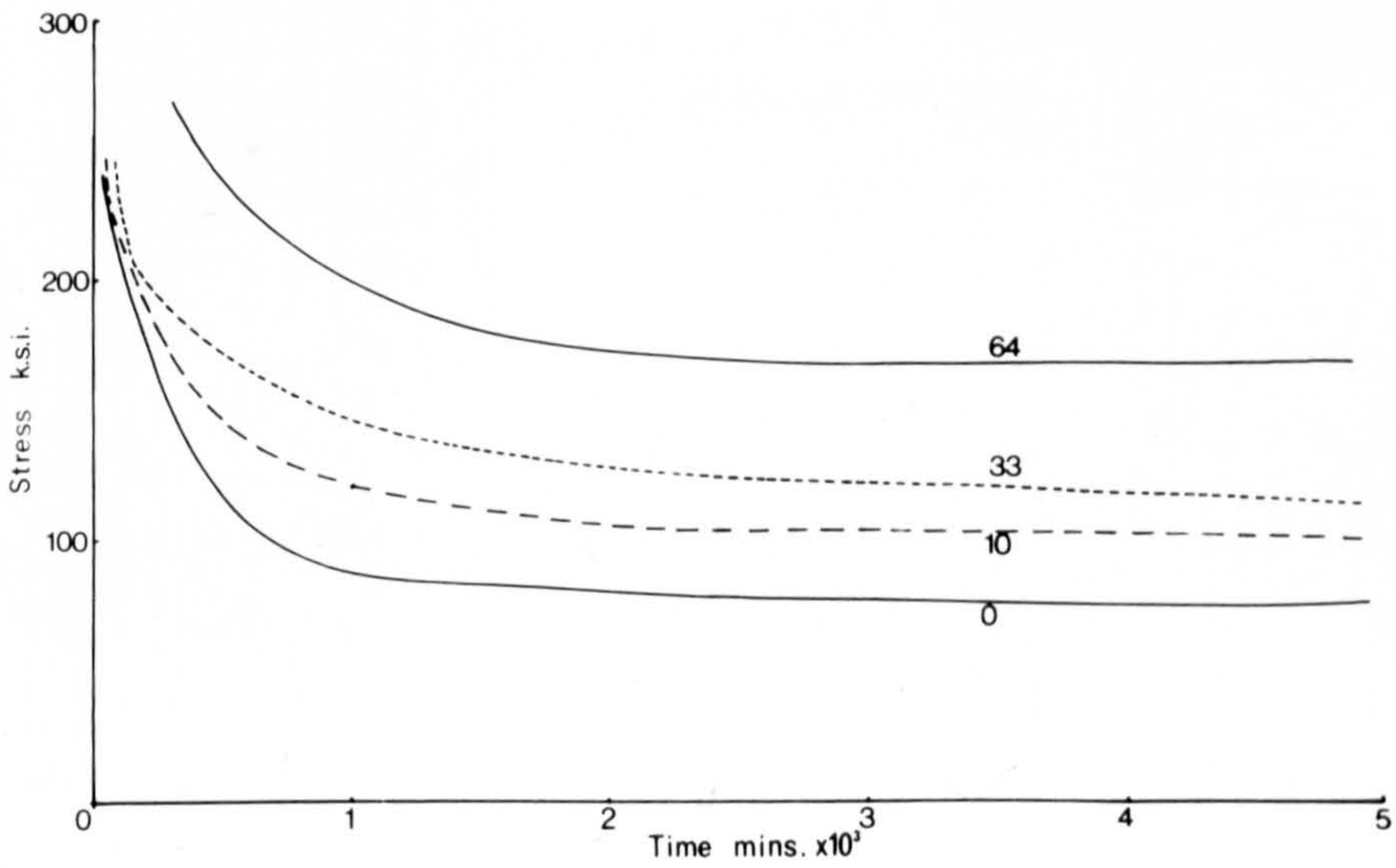

Fig. 3.60 Stress-time to failure curves for various amounts of cold working with material tested under applied cathodic currents of 50mA/cm^2

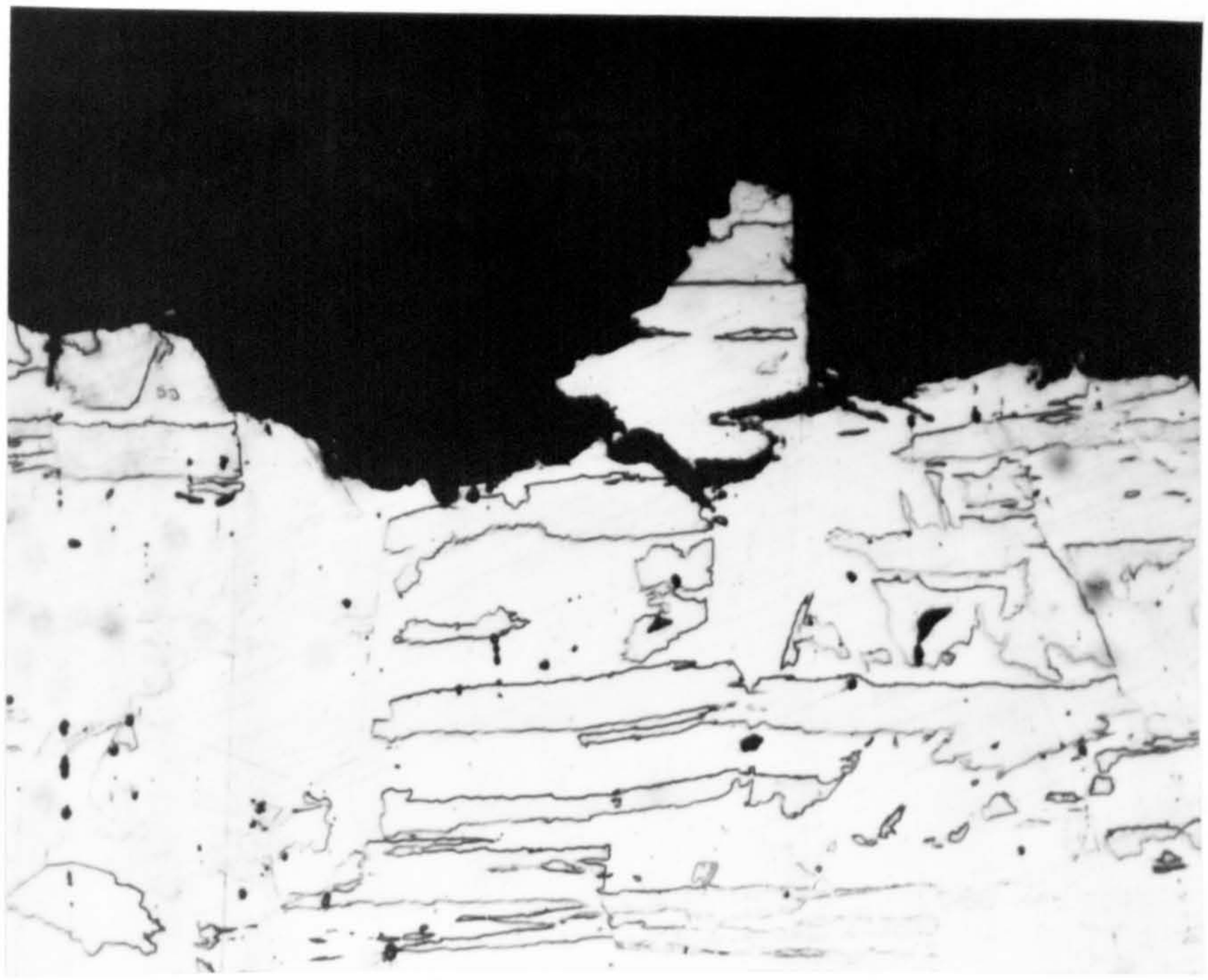

Fig. 3.61 Optical micrograph showing evidence of transgranular cracking in material which failed as a result of hydrogen embrittlement (200x)

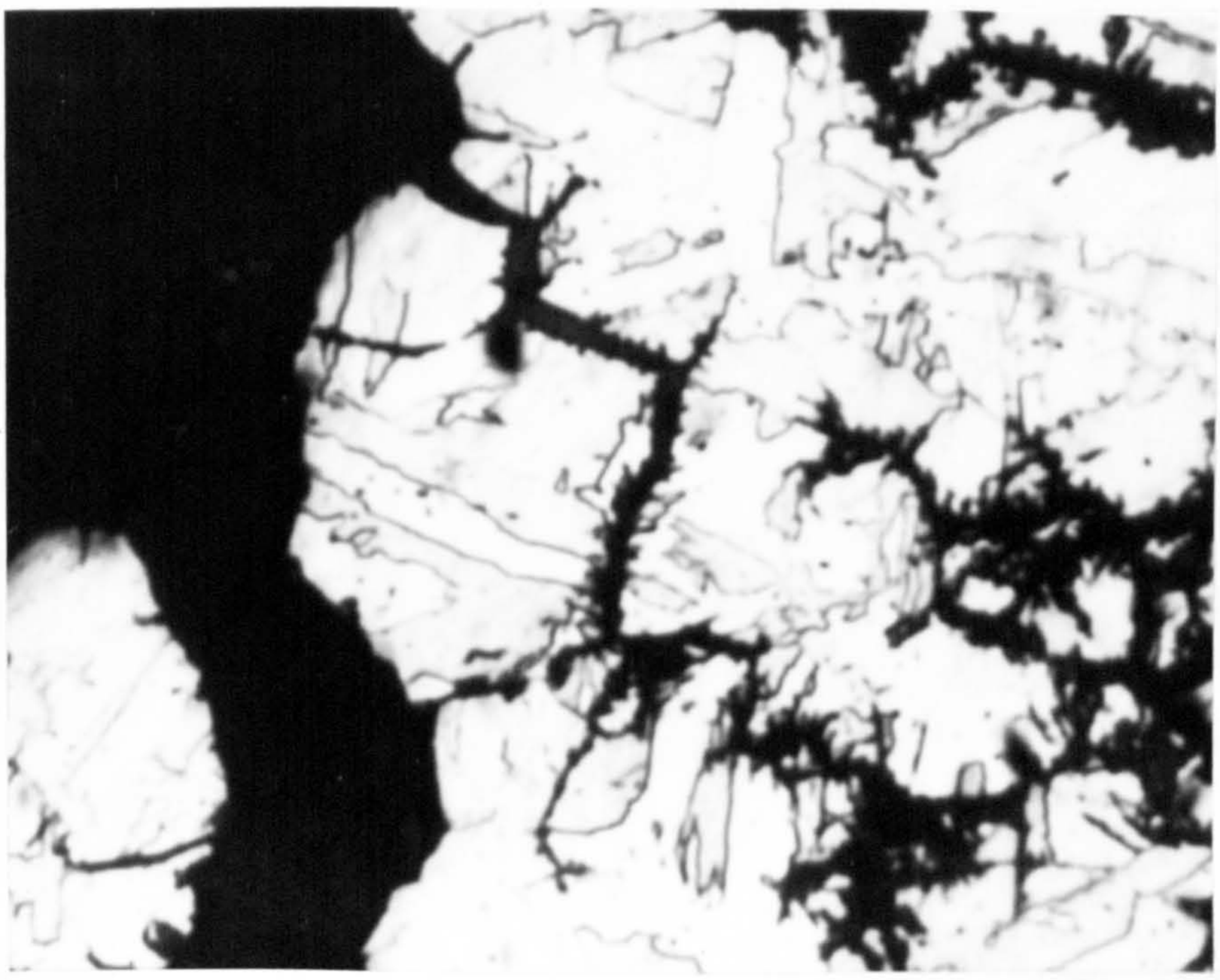

Fig. 3.62 Area showing an increase in the amount of secondary cracking towards the centre of the crack (right) (400x).

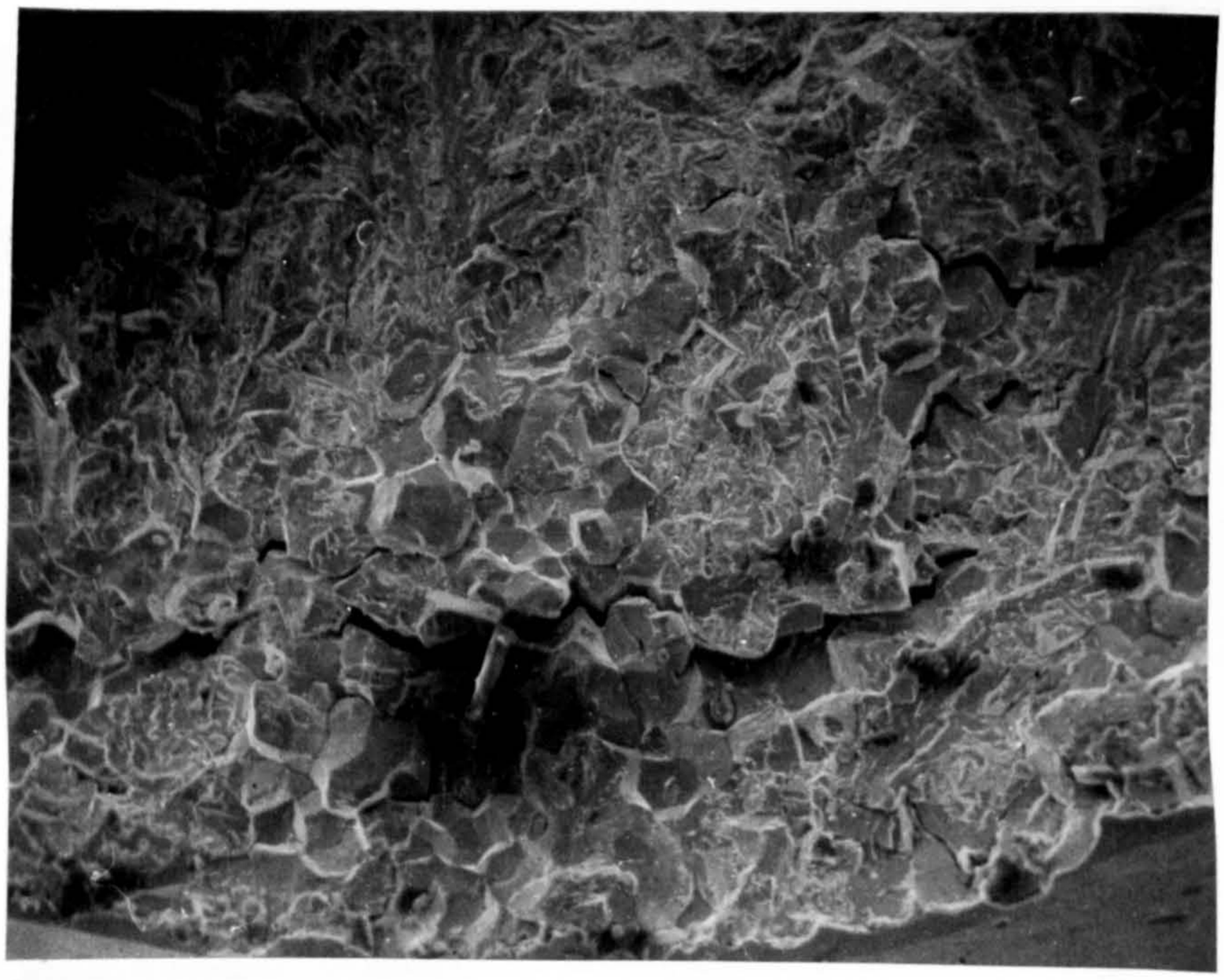

Fig. 3.63 Fracture surface showing intergranular and transgranular cracked areas (125x)

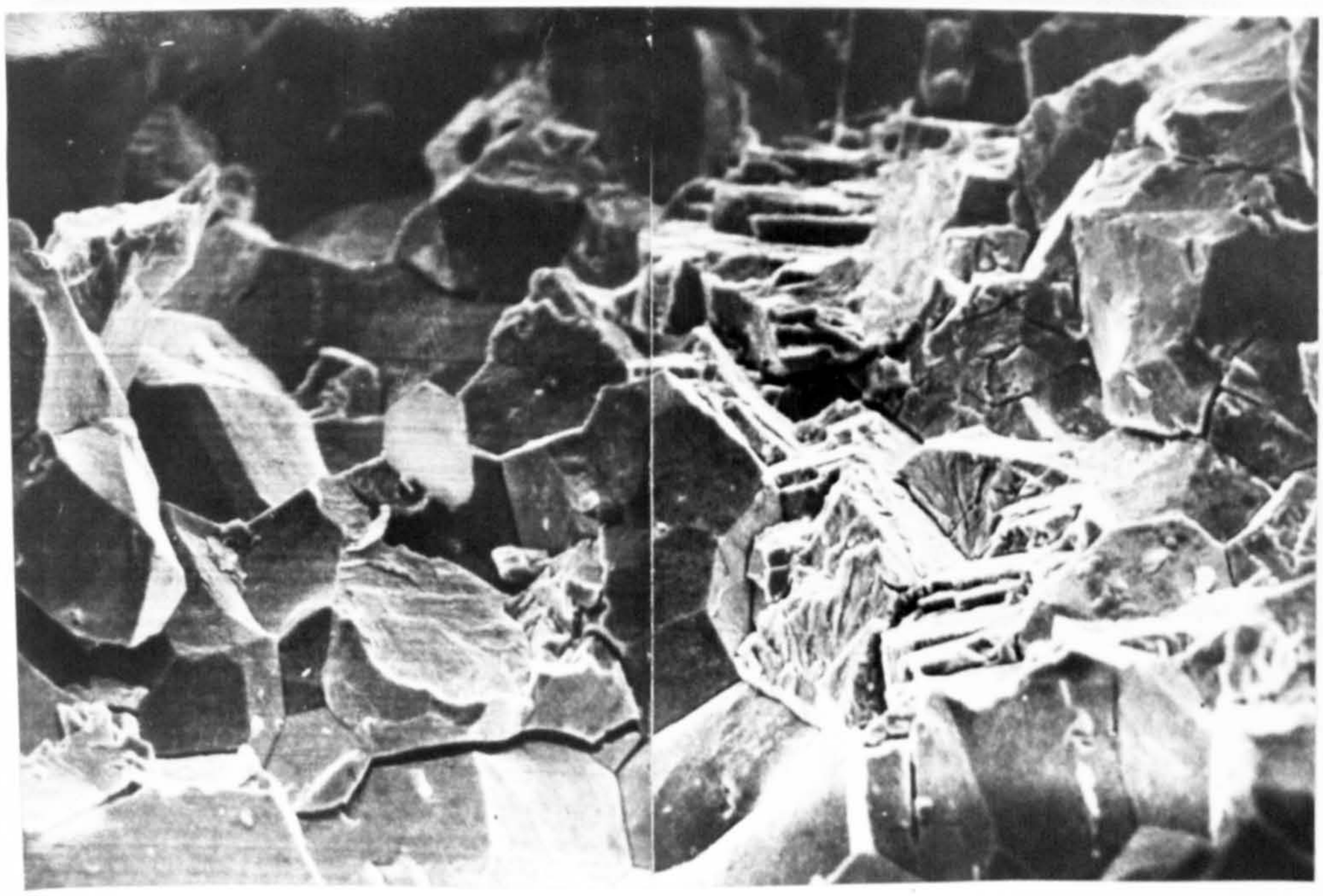

Fig. 3.64 Hydrogen embrittlement failure indicating a change from I.G to T.G. cracking towards the centre (right) of the specimen (650x).

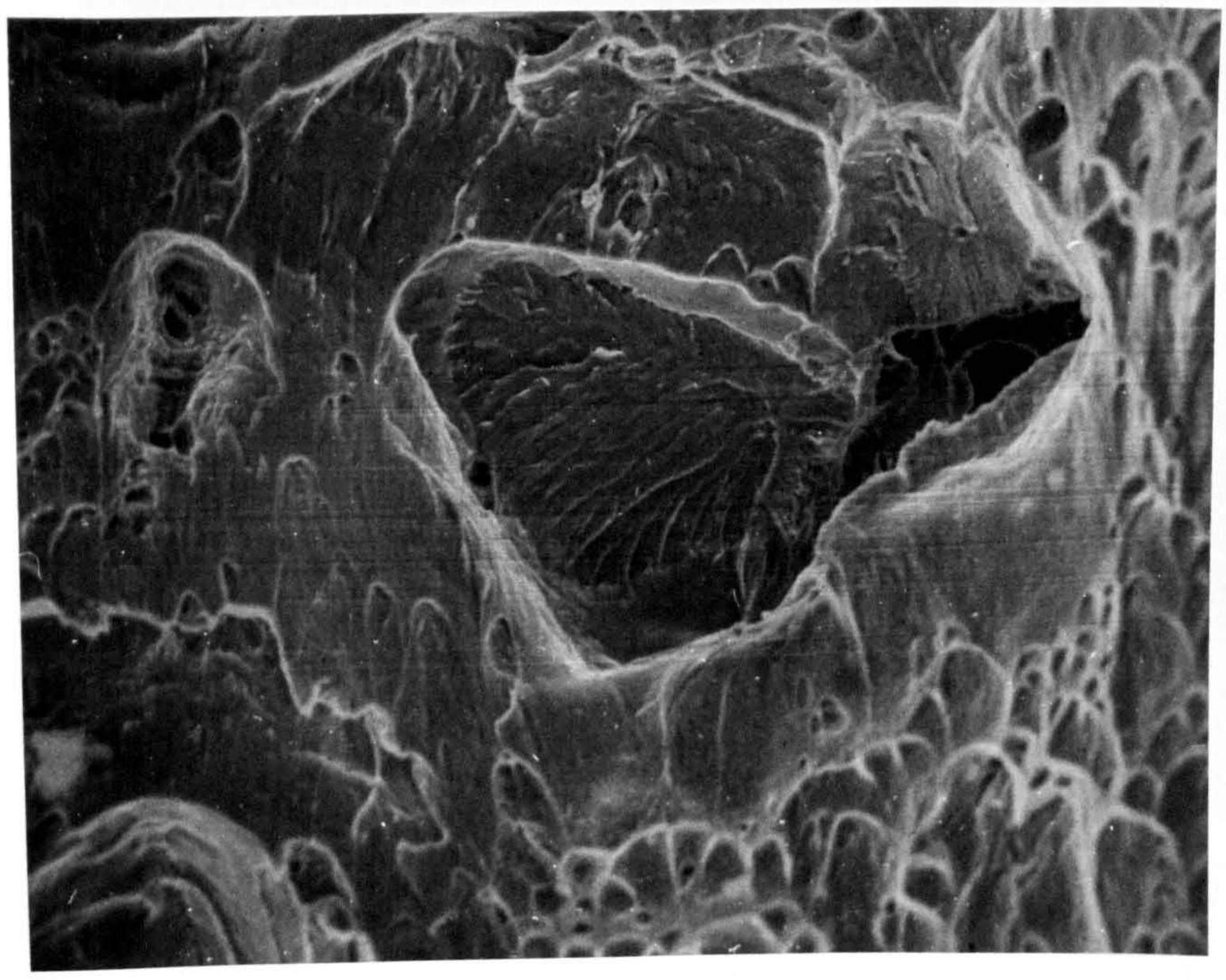

(a)

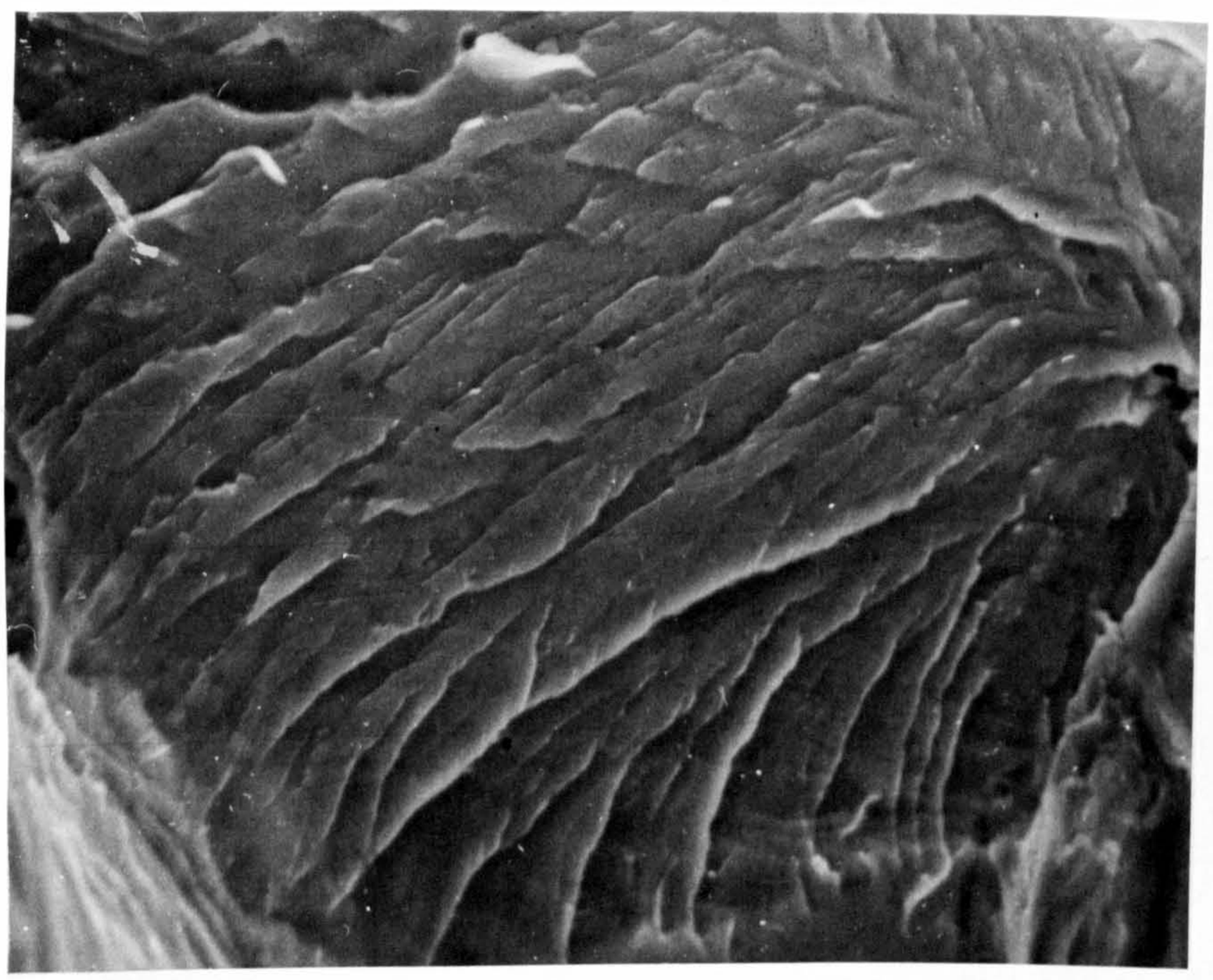

(b)

Fig. 3.65 Clevage area in a specimen embrittled in the unstressed condition (-50mA for 24 hrs.) then mechanically failed. (a, 600x & b, 2,400x.)

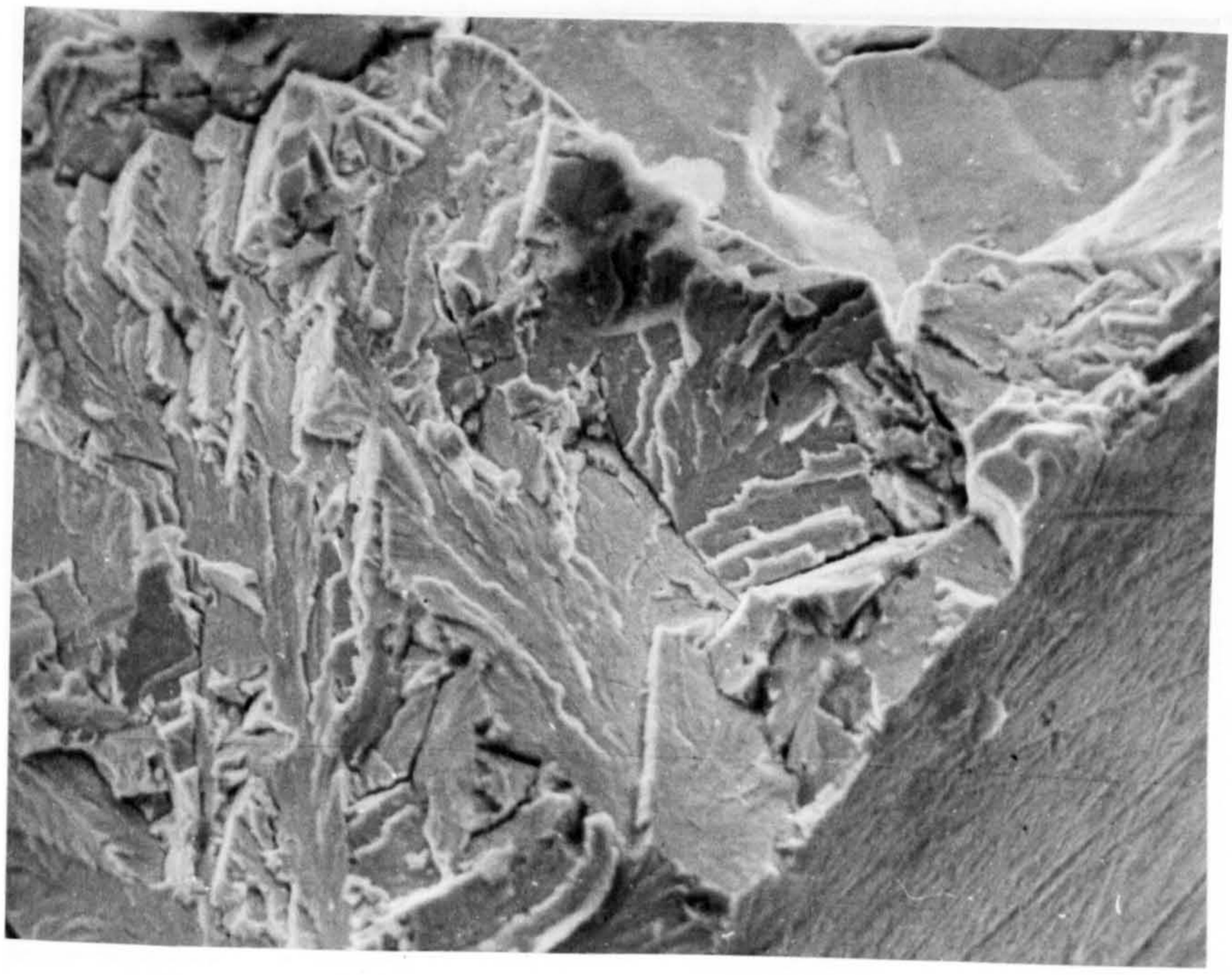

Fig. 3.66 Area of hydrogen embrittled specimen showing clevage steps and planes (640x)

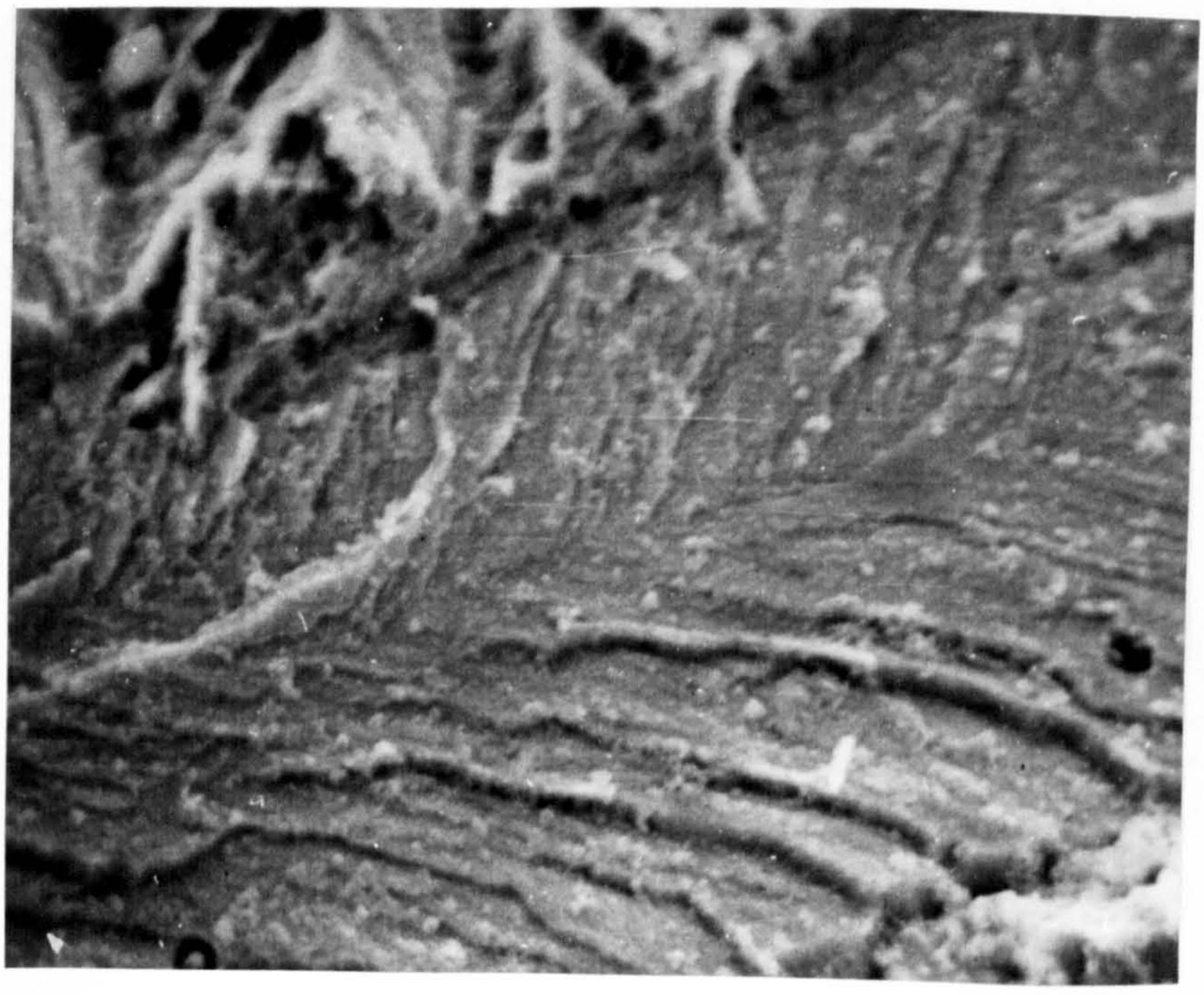

Fig. 3.67 Fracture surface showing chevron markings (2,320x).

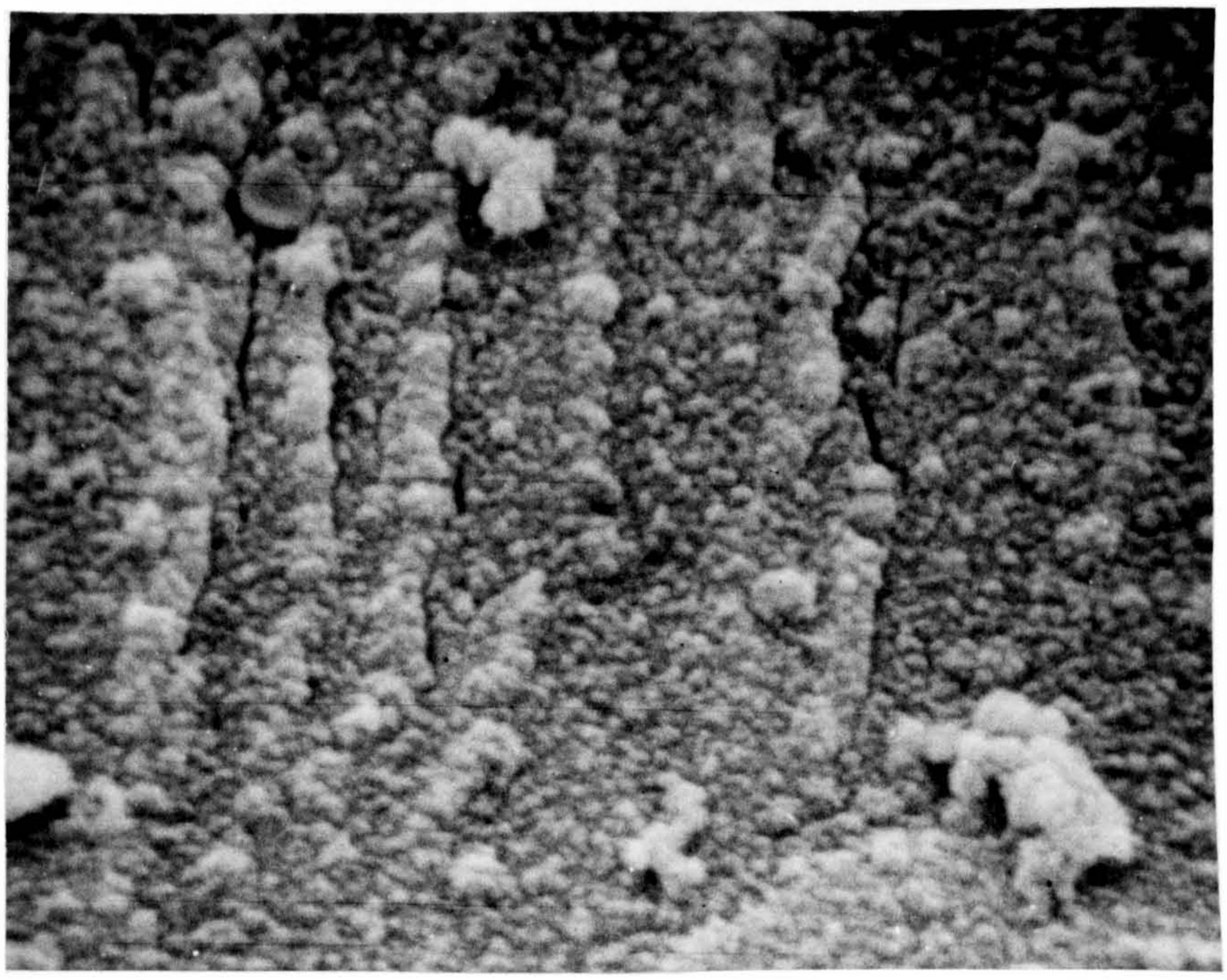

Fig. 3.68 Area of 3.67 indicating the presence of fine cracks associated with chevron marks. (11,700x)

Fig. 3.69 (a) Intergranular area of hydrogen embrittlement failure (2,500x)

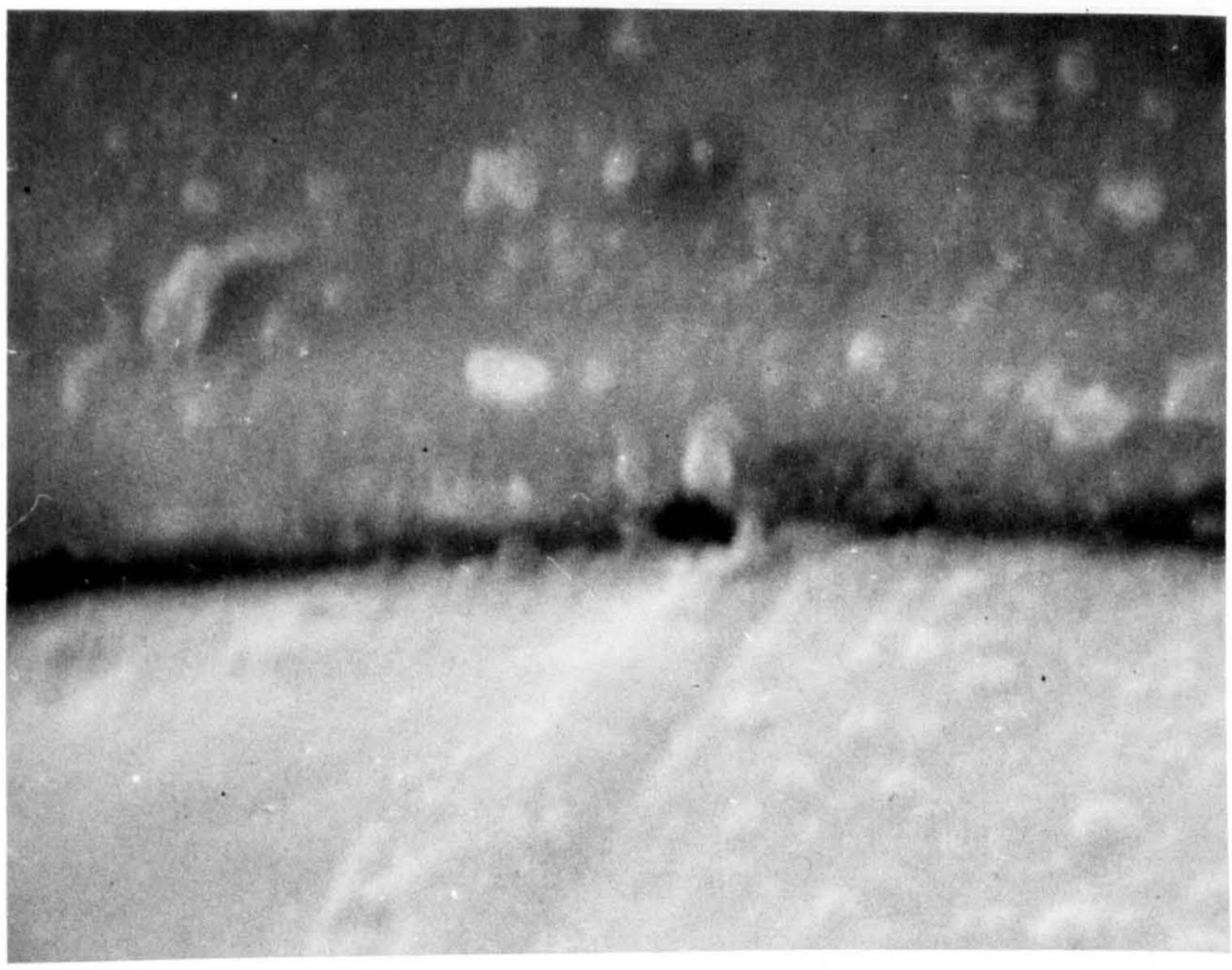

Fig. 3.69 (b) Intergranular area of hydrogen embrittled failure. (24,800)

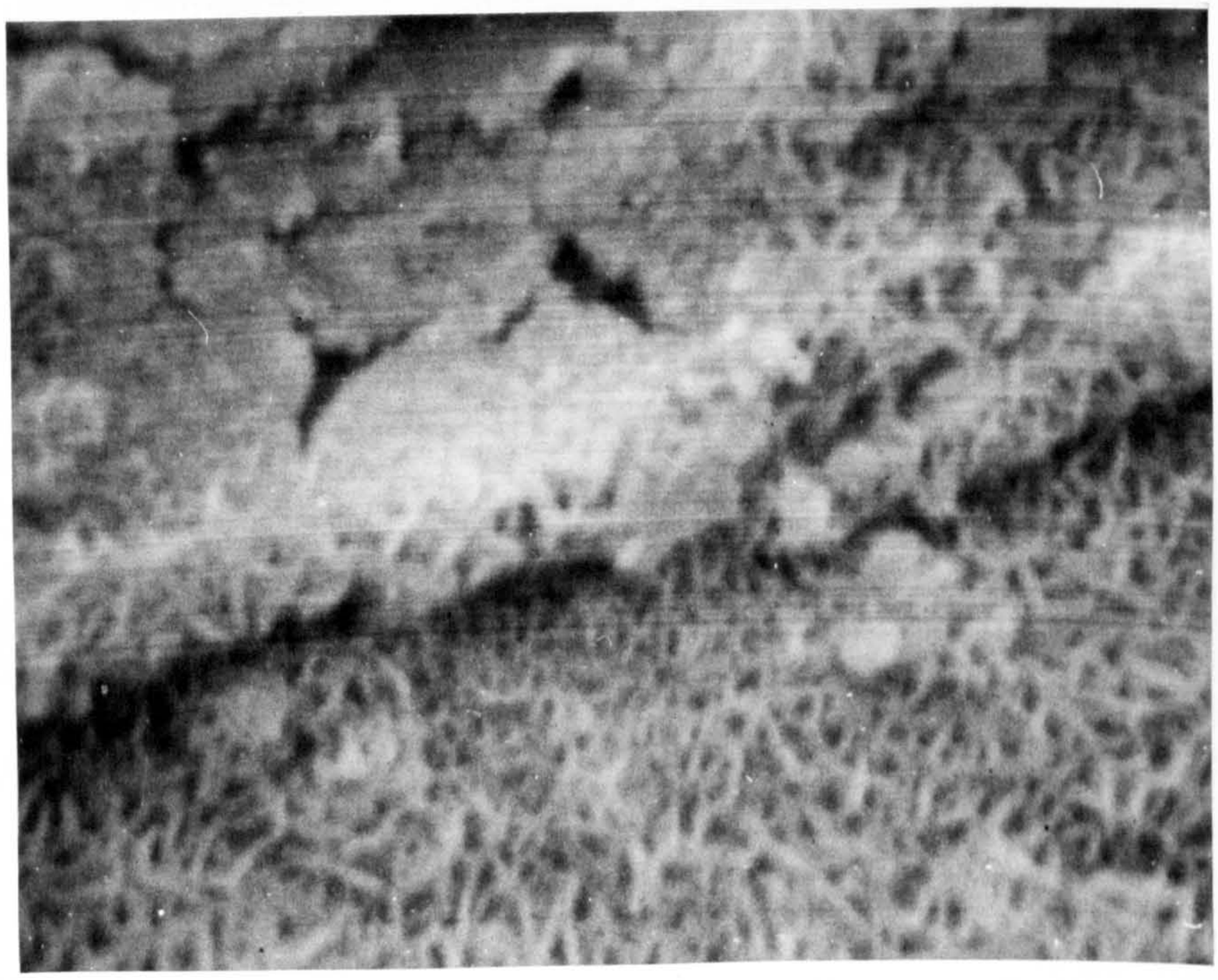

Fig. 3.70 Clevage step of hydrogen embrittlement failure (24,000)

4. DISCUSSION

In this section the results are discussed in three categories:

(a) The effect of the structural state of the material on the susceptibility towards stress corrosion cracking, with particular reference to austenitising and aging temperatures and the amount of cold work introduced into the steel.

(b) The effect of environmental factors on the cracking process. This being mainly affected by the pH, oxygen level and chloride ion concentration of the solution.

(c) The distinction between stress corrosion and hydrogen embrittlement types of cracking, which involves the relation of each type to a certain potential range under given test conditions.

(a) The structural state of the material has several effects on the susceptibility towards stress corrosion cracking in maraging steels. Results for material treated at various austenitising temperatures and aged at a fixed temperature indicate that structures having small grain sizes are less susceptible to stress corrosion cracking than those having large grains. Mechanical tensile tests indicate that all grain sizes have similar strength levels and there appears to be no obvious relationship between the strength and the threshold stress obtained with each austenitising temperature. A possible explanation may be based upon the difference in the ratio of the amount of grain boundary precipitates to the grain area produced by each treatment. Electron microscopy showed the precipitate to be more apparent in the large grained material, but no definate correlation between the amount and grain size could be produced.

All intergranular cracking in these steels occurs along the prior austenite grain boundaries, and this suggests that some form of segregation must occur during the austenitising treatment in order to decorate the grain

boundaries. Tests on unaged material, however, did not produce failure by intergranular stress corrosion cracking even on prolonged exposure, and results for steels treated at various aging temperatures indicate that the susceptibility may be associated with the precipitation reaction. The aging treatment could introduce some additional difference between the grain boundaries and the matrix, possibly by enhancing the electrochemical difference as a result of precipitation occuring in the matrix or at the grain boundaries. Treatments involving ausaging are cited to enhance the precipitation of titanium carbide at the grain boundaries during austenitising, but the results obtained in the present work indicate that no difference in susceptibility is produced by the ausaging treatment in either the unaged or aged condition. The results infer that the segregation which occurs during austenitising is only effective in decorating the grain boundaries and that the majority of grain boundary precipitation occurs during the aging treatment. Free corrosion potential measurements of titanium carbide in pH 2 and pH 11 solutions show it to be cathodic to the matrix, and if

it is precipitated in the grain boundaries this may cause the attack to be localized along the interface between the precipitate and matrix.

Measurements of crack propagation rates indicate that open crack propagation occurs at a greater rate than fine crack propagation. The latter can readily be explained in terms of electrochemical dissolution but the rate of open crack propagation would require current densities at the crack tip of several amps per square cm. Values of this order do not normally occur owing to the polarisation effects they would produce and this could suggest that some mechanical propagation may be occuring. However, this is not necessarily the case as the local corrosion rates in these solutions may be much greater than bulk corrosion rates and these may be assisted by some depolarisation effect generated by the opening crack, so providing conditions where electrochemical dissolution can sustain the rates of propagation observed. Evidence of some mechanical propagation appears to be present in certain large grained structures, but this could be a result of the large grain size involved, where several

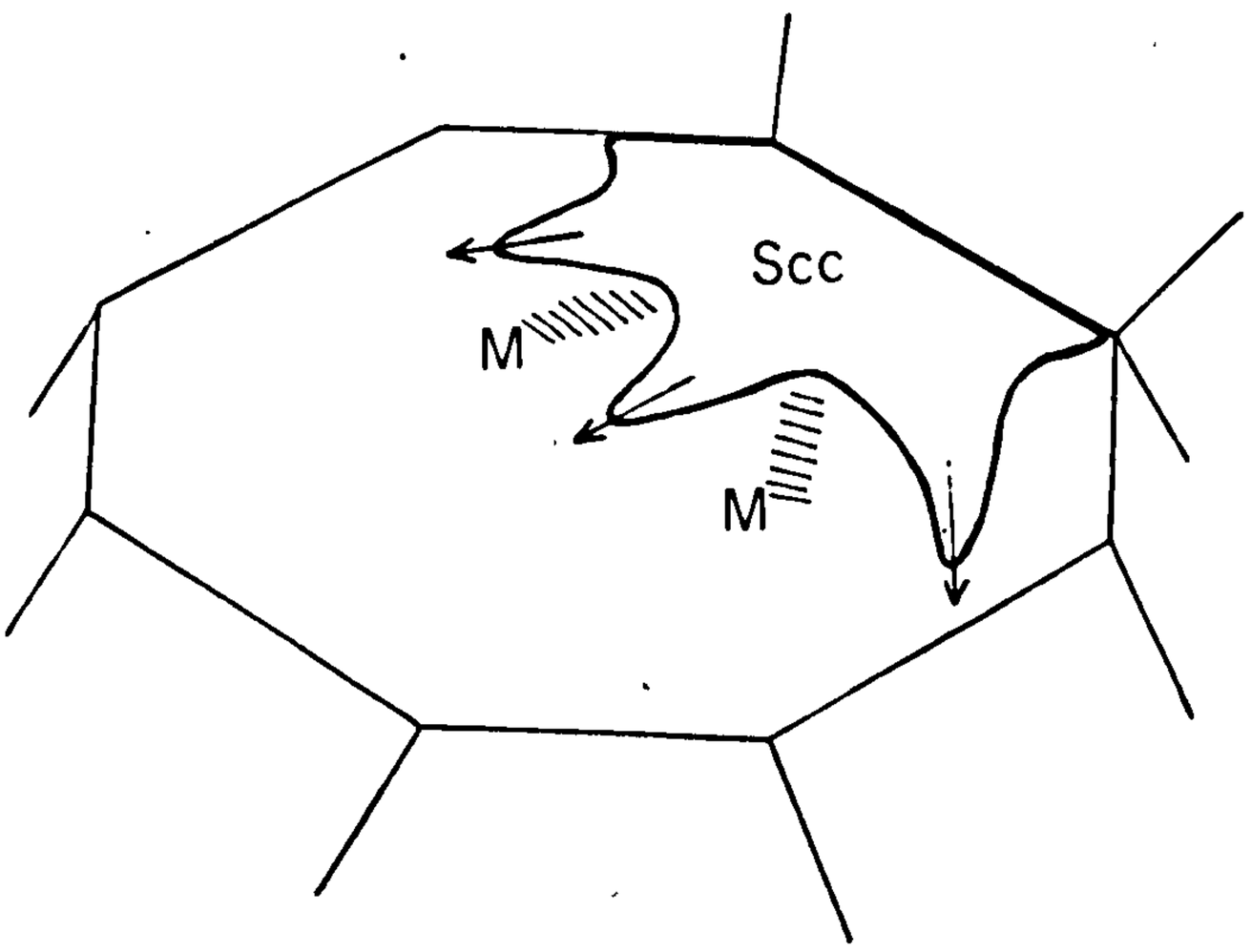

Fig. 4.1 Crack face showing possible stress corrosion (S.C.C.) and mechanical (M) areas.

points on the crack front propagate at different rates and then the area between fails by mechanical tearing to produce a single crack front (Fig. 4.1). A discontinuous electro-mechanical process is not considered to occur as no evidence of similar markings was found on any other fracture surface examined and the effect observed appears to be perculiar to one particular structure.

The effects produced by the various austenitising and aging treatments could also be explained on the basis of changes in the fracture toughness of the material with heat treatment. Values of K_{IC} and K_{ISCC} obtained (Table 6) indicate that the major effect of the heat treatments can be related to the stress corrosion factors involved. Tests on structures austenitised at different temperatures show that, although K_{IC} values vary slightly with heat treatment, the K_{ISCC} values differ considerably. This suggests that the toughness does not effect the cracking tendency to any great extent and that the major factors involved are concerned with stress corrosion effects.

T A B L E V I

Results of pre-cracked testing, in a pH - 2 solution.

Heat Treatment ^{o}C	K_{IC}	K_{ISCC}
	k.s.i.$^{3}/_{2}$	
800/350	105	60
800/480	78	50
1000/480	83	20

The cold working treatments that were carried out between austenitising and aging have effects similar to those produced by various austenitising temperatures, where the susceptibility towards stress corrosion cracking depends on the nature of the prior austenite grain boundary network. The latter is deformed by cold working and the susceptibility towards intergranular stress corrosion cracking decreases with increasing amounts of working until eventually cracking by propagation of structurally independent fissures becomes the dominant failure mechanism. Mechanical tensile test data indicate that cold working increases the strength of the material and the threshold stress results obtained indicate some dependence of the cracking process on the flow characteristics for up to 33% cold work. This appears to be a minor factor, however, as no threshold stresses could be obtained for greater than 33% working, even, with loading stresses of 90% U.T.S.

Explanation of the results can thus be considered to be related to the nature of the grain boundaries, as grain size effects cannot readily explain a change in cracking mechanism. In maraging steels a mechanism similar to that suggested

for mild steels may operate (92) where the cold working generates dislocations at grain boundaries and this allows soluble segregate to disperse away from the prior austenite grain boundaries. On subsequent aging precipitation occurs producing a final structure in which the grain boundaries differ only slightly in composition from the matrix. The resulting electrochemical difference is small and the tendency for intergranular cracking is thus less than in structures which have not been subjected to the cold working treatments.

(b) The environmental factors effect both the initiation and propagation stages of the cracking process in various ways. Work by Green et al. on maraging steel foil indicates that susceptibility towards stress corrosion cracking is pH dependent with maximum susceptibility occuring around values of pH 2 and 11. Tests on bulk material in the present work indicate failure occurs readily at pH 2 but not at pH 11, unless surface fissures are introduced prior to testing or the anodic reaction is stimulated by applied currents. The initiation process appears to be dependent on the development of surface fissures until conditions enable intergranular cracking to commence. This is supported by metallographic evidence which shows that intergranular cracks originate from surface fissures, and that tests in which material has been anodically polarised before testing, show immediate crack propagation and load relaxation. The initiation of these fissures appears to be independent of pH as specimens polarised at different pH values all show the presence of fissures to some extent. Crack propagation, however, does depend upon the pH of the solution in a similar manner to that reported by Green et al. (75,76) who suggest the effects were related to the disruptive nature of the

chloride ions in solution. Polarisation data obtained in the present work indicate that some form of passivation occurs on maraging steels in the region of pH 10 to 12, and that this passivation may be associated with nickel rich areas on the metal surface. Crack propagation in pH 11 may thus be the result of a state of partial passivation which exists at this pH and the presence of chloride ions which facilitate selective anodic attack.

The results obtained from polarisation curves indicate that the main cathodic reaction is oxygen reduction under freely corroding conditions for solutions of pH 2 and 11. The overall reaction may be expressed as,

$$O_2 \text{ (ads.)} + 2H_2O + 4e \rightarrow 4OH^-$$

which could take place by the following reactions

$$O_2 \text{ in air} \longrightarrow O_2 \text{ in solution}$$

$$O_2 \text{ in soln.} \longrightarrow O_2 \text{ (ads.)}$$

$$O_2 \text{ (ads.)} + H^+ + e \rightarrow HO_2 \text{ (ads.)}$$

$$HO_2 \text{ (ads.)} + H^+ + e \rightarrow H_2O_2 \text{ (ads.)}$$

$$H_2O_2 \text{ (ads.)} + 2e \longrightarrow 2OH^-$$

The rate of oxygen reduction depends upon the rates of the above reactions and additions of hydrogen peroxide to

solutions could increase the overall rate by providing a ready supply of oxygen at the metal surface. Polarisation results show that the addition of hydrogen peroxide to solutions produces an increase in the total cathodic current at pH 2 and 11, and the results of stress corrosion tests indicate that these additions produce a corresponding increase in the anodic reaction rates. Stress corrosion testing under stirred conditions also suggest a dependence of the cracking process on the rate of cathodic reduction of oxygen and the free corrosion potential - time curves obtained suggest that the rate controlling step may be the diffusion of oxygen from the atmosphere to the specimen surface. This could explain the fact that failure at pH - 11 could be produced in specimens which had been anodically polarised prior to testing, but not in untreated specimens. Crack propagation can occur almost immediately in material containing surface fissures and rapid failure is produced as long as there is an ample supply of oxygen. With untreated specimens, however, the oxygen supply to the cathodes does not appear to be sufficient to allow the appropriate amount of anodic reaction to occur and initiate cracking. The results thus indicate that stress corrosion

cracking in solutions of pH 11 under naturally corroding conditions is governed by the rate of supply of oxygen for the cathodic reaction. One of the possible rate controlling steps appears to be the diffusion of oxygen to the metal surface from the solution/air interface. In solutions of pH 2 the cracking process still depends on the cathodic reduction of oxygen, but not to as great an extent as in pH 11, which suggests that hydrogen ion reduction may be involved in the cathodic process. This reaction may become predominant under conditions where pH or potential drops down cracks are possible.

Potentiodynamic polarisation results indicate that additions of chloride ions to a pH 11 solution produces changes in the polarisation characteristics up to a concentration of 0.6 N after which similar curves are produced with higher concentrations. Stress corrosion tests were carried out in this range of concentrations and material was found not to fail in distilled water made alkaline to pH 11 until chloride ions were introduced. Failures could be produced for higher chloride ion concentrations up to 0.6 N, but thereafter additions appeared to produce no difference in susceptibility.

The results indicate a dependence of the cracking process on chloride ion concentration in a similar manner to that observed by other workers (75), and at 0.6N there appears to be sufficient chloride ions present for cracking to occur readily.

(c) The mechanisms of failure involving either stress corrosion cracking or hydrogen embrittlement can be related to certain environmental conditions under which failure is produced. The observation of failure times at various applied potentials show the two mechanisms to occur in the following ranges, for pH 2 stress corrosion cracking at $>-$ 600 mv and hydrogen embrittlement at $<-$ 700 mv. ; for pH 11 stress corrosion cracking at $>-$ 600 mv. and hydrogen embrittlement at $<-$ 1000 mv. Under naturally corroding conditions the free corrosion potentials of maraging steels in pH 2 and pH 11 solutions lie in the stress corrosion region, and this appers to be the failure mechanism involved. A further distinction between stress corrosion cracking and hydrogen embrittlement can be made

by observing the effects on the cracking susceptibility produced by various solution additions. The results show that additions which decreased the amount of hydrogen at the metal surface reduced the susceptibility towards hydrogen embrittlement, whereas the presence of a substance that promoted hydrogen entry produced a marked increase in susceptibility. The additions, however, produced very little change in the stress corrosion susceptibility except in certain cases where local pH changes occured. These effects suggest that stress corrosion and hydrogen embrittlement in maraging steels can be characterised as two separate mechanisms of failure by their dependence on the cathodic processes involved.

Fractrographic analysis indicates that the two medhanisms can be distinguished by the relative amounts of intergranular and transgranular cracking present. The intergranular cracking produced in hydrogen embrittlement failures was initially thought to be a result of the stress intensity of the system and that cracking would revert to transgranular when the stress intensity ahead of the crack reached a critical value. The amount of intergranular

cracking however, did not appear to be related to the loading on the system, or to initiation or propagation stages in the process. These regions of intergranular cracking always appear to occur near the surface of the specimen, and the possibility remains that this could be due to local anodic areas producing stress corrosion cracking.

In summary of the different effects produced, stress corrosion cracking would be expected to occur when specimens are tested in 0.6N. NaCl at pH 2 or 11 in the absence of applied potentials, and failure by hydrogen embrittlement may occur when testing at potentials more active than -700mv., providing that the solution conditions are such as to allow hydrogen entry into the metal. Both mechanisms may occur in the same specimen in certain cases where the pH change in a crack is of sufficient magnitude to induce a local potential drop which enables hydrogen embrittlement to occur. Under these circumstances the resulting fracture surface should show evidence of a change in fracture path from intergranular to intergranular and transgranular or to completely transgranular failure towards the centre of the specimen.

5. Proposed Cracking Mechanism

The stress corrosion cracking of maraging steels can be considered to occur in three stages, initiation, propagation, and final mechanical failure.

Crack initiation occurs by the development of structurally independent surface fissures. These are produced at random over the specimen surface, probably as a result of local breakdown of the air-formed oxide film by the presence of chloride ions in the solution (Fig. 5.1 a,b). The growth of these fissures occurs normal to the tensile axis and occasionally along the lines of maximum shear.

Crack propagation commences when a surface fissure exposes a prior austenite grain boundary, and as this is cathodic to the matrix, anodic dissolution of material occurs along the precipitate - matrix interface. Propagation between particles also occurs by anodic dissolution in a manner similar to the growth of surface fissures (Fig. 5.1 c,d,e). In the more susceptible materials this occurs along the grain boundary, but with less susceptible material sideways propagation may also occur to produce failure showing primary intergranular and secondary transgranular cracking (Fig. 5.1 f,g,h).

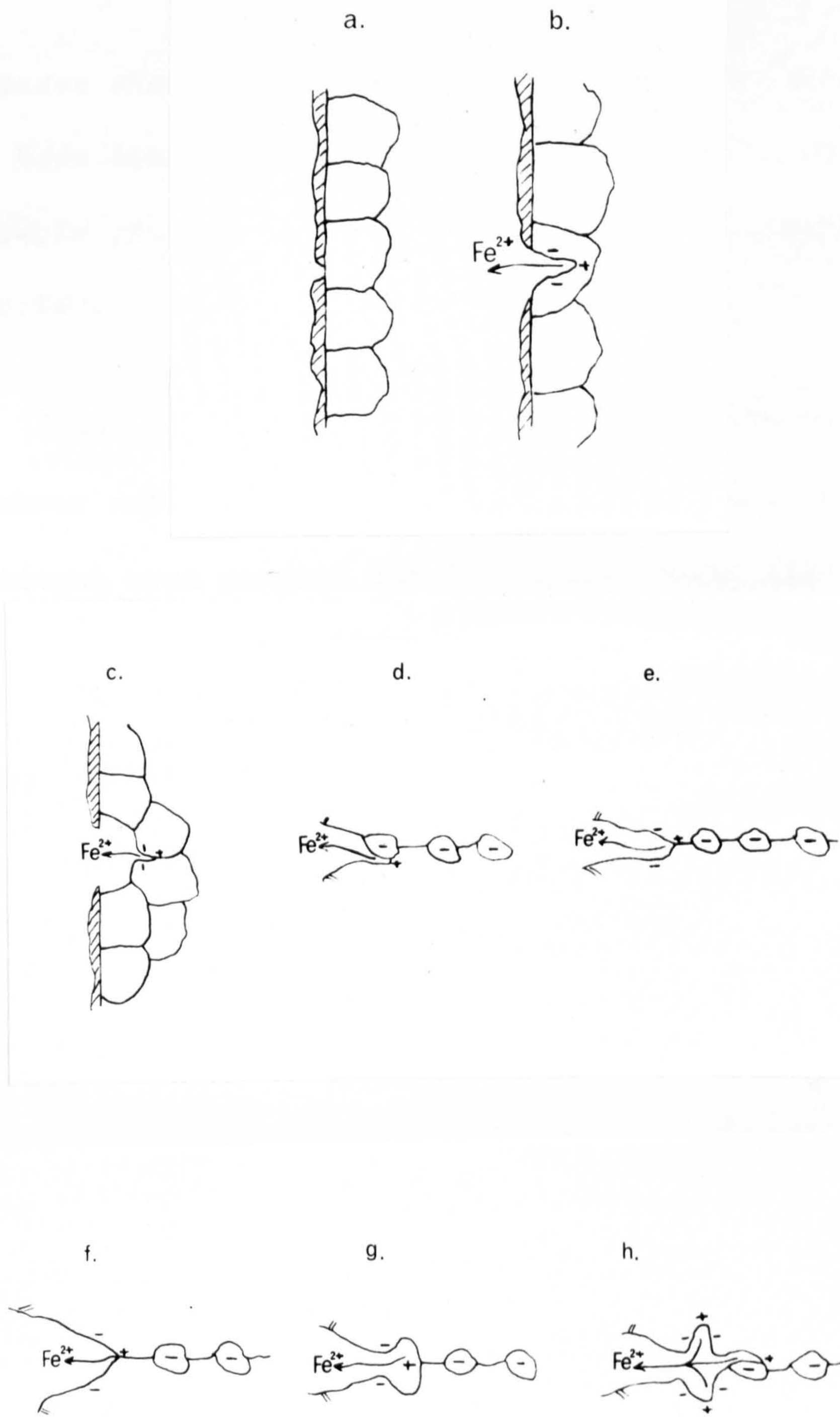

Fig. 5.1 Suggested model for crack initiation (a,b) and propagation (c,d,e) and the development of secondary cracking (f,g,h).

In cases where a predominant active path is absent or has been disrupted (i.e. by cold working), failure occurs a simple propagation of surface fissures across the specimen diameter.

Final separation occurs by mechanical ductile or shear rupture when the stress on the remaining cross sectional area reaches the UTS of the material.

-----0-----

6. CONCLUSIONS

1. Crack initiation occurs as a result of the formation of structurally independent surface fissures.

2. Crack propagation occurs along the prior austenite grain boundaries when material fails by intergranular stress corrosion cracking.

3. The susceptibility towards intergranular stress corrosion cracking can be altered by processes which produce a change in the nature of the prior austenite grain boundary network.

4. In material where the prior austenite grain boundaries are in a non-susceptible condition failure may occur by propagation of surface fissures across the diameter of the specimen.

5. The susceptibility of bulk material towards stress corrosion cracking depends on the pH of the solution.

6. In stress corrosion cracking the main cathodic reaction is that of oxygen reduction in both pH 2 and 11 solutions. With failures occuring in pH 11 solutions the rate controlling step appears to be the supply of oxygen to the specimen surface.

7. Crack propagation can be considered to be by a purely electrochemical dissolution mechanism.

8. Hydrogen embrittlement failure can be produced at potentials more active than -700 m.v. s.c.e.

9. Under naturally corroding conditions in pH 2 and 11 solutions failure will occur by a stress corrosion cracking mechanism.

---0---

REFERENCES

1. Reprint Jnl. Aeronautical Soc. Aug. 1966. A.G. Haynes
2. English Steel Publication
3. Revue de Metallurgique July 1966. A.G. Haynes
4. Metal Forming Jan. 1970. p. 15. Imrie
5. Met. Review 126. Floreen
6. J.I.S.I. Special Report 86. Stevens
7. J.I.S.I. V. 206. p.164. Wilson
8. Cobalt 33 1966. Contractor
9. T.A.S.M. V 55. p.518. Floreen & Decker
10. J.I.S.I. V 166 p.218
11. J.I.S.I. V 163 p.132. Owen & Liu
12. J.I.S.I. V 163 p.121. Jones & Phumphrey
13. Acta. Met. 1965 V 13 p.1211. Johani & Thomas
14. J.I.S.I. V 203 p.268. Sedriks & Craig
15. T.A.S.M. V 61 p.62. Peters
16. T.A.S.M. V 56 p.403. Florren & Decker
17. T.A.S.M. V 61 p.62. Peters
18. T.A.I.M.E. V 230 p.842. Floreen
19. T.A.I.M.E. V 236 p.1429. Floreen
20. T.A.S.M. V 56 p.783. Reisdorf
21. T.A.S.M. V 57 p.220. Pitler & Ansell
22. J.I.S.I. V 204 p.512. Garwood & Jones
23. T.A.S.M. V 57 p.1008. Baker & Swann
24. T.A.S.M. V 57 p.714. Floreen & Speich
25. T.A.S.M. V 60 p.528. Chilton & Barton
26. T.A.S.M. V 59 p.262. Detert
27. J.I.S.I. V 207 p.348. Bandi Lutz & Melnick
28. T.A.S.M. V 57 p.727. Hammond & Ansell
29. T.A.S.M. V 59 p.468. Marcus Schwartz & Fine
30. T.A.S.M. V 59 p.60. Mihalisim
31. J.I.S.I. V 203 p.899. Miller & Mitchell
32. J.O.M. V 14 p.710. Floreen
33. T.A.I.M.E. V 236 p.1420. Peters & Cupp.
34. T.A.I.M.E. V 236 p.1565. Miner, Jackson & Gibbons
35. T.A.I.M.E. V 239 p.1981. Peters
37. Arch. Eisen V 37 p.579. Detert
38. Acta. Met. V 5 p.169. Cahn
39. T.A.I.M.E. V 245 p.1937 Robertson & Adair
40. T.A.S.M. V 59 p.1008. Maynor & Busch
41. T.A.I.M.E. V 239 p.553. Detert
42. T.A.S.M. V 55 p.58. Decker, Eash, Goldman
43. T.A.S.M. V 60 p.418. Spaeder Brown & Murphy
44. Met. Sci Jnl. V 2 p.76. Banerjee, Hauser & Capernos
45. T.A.S.M. V 57 p.38. Floreen
46. T.A.S.M. V 59 p.71. Patterson & Richardson
47. T.A.S.M. V 60 p.125. Salmon-Cox, Birkle, Reisdorf & Pellisier

REFERENCES - CONT.

48. Eng. Fracture Mech. V1 p.55. Pellisier
49. T.A.S.M. V57 p.747 Conrad
50. Acta Met V8 p.612. Ansell & Lenel
51. Acta Met. V9 p.518. Ansell
52. A.F. Material Rep. 1965 64 390 Reisdorf Baker
53. T.A.S.M. V61 p.14. Cheng & Thomas
54. A.R.P.A. Report D6-23871 1969 Carter
55. Conf. Fundamental Aspects of S.C.C. Leckie
56. T.A.I.M.E. V242 p.31 Kirk, Covert & May
57. Corr. V20 p.93t. Davis Dreyer & Gallaugher
58. T.A.I.M.E. V242 p.1943 Parkins & Haney
59. US. Contract DA 04 495 ORD 3069 Rubin
60. J.I.S.I. V202 p.574 Scharfstein
61. Corr. V21 p.95 Dean & Copson
62. Fundamental Aspects of S.C.C. Phelps
63. 4th Int. Conf. Met. Corr. Cumha Belo, Pinard-Legry, Montuelle & Chaudron.
64. J.I.S.I. V202 p.745 Truman, Perry & Chapman
65. J.I.S.I. V172 p.149 Parkins
66. Corr. V17 p.430.t. Bhatt & Phelps
67. B.C.J. V2 p.186 Henthorne & Parkins
68. Corr. V16 p.325.t. Philps & Loginow
69. T.A.S.M. V62 p.989. Proctor & Paxton
70. 20th N.A.C.E. Conf. 1964 Setterlund
71. Corr. V 20. p.189.t. Bates & Loginow
72. T.A.S.M. V60 p.79. Ault, McDowell, Hendricks, Ronald
73. S.A.M.P.E. V4 p.32 Hasan, Sonnino & Gulbransen
74. Corr. V24. p.291. Leckie & Loginow
75. A.S.T.M. Tech Publication Green & Haney
76. Corr. V23 p.5 Green & Haney
77. Corr. V25. p.173 Tobias & Nobe
78. 3rd. Int. Naval Cong. 1969. Beifer & Syrett
79. B.C.J. V 4 p.253 Snape
80. 3rd. Int. Conf. on Metallic Corr. 1966. Bhatt & Phelps
81. Report. W.A.C.D. 56-242 1965. Fontana
82. Corr. Sci. No. 8 1968 p.359 Kennedy & Whittaker
83. C.I.T.C.E. 1956. Hoar & Hines
84. 4th Int. Conf. on Metallic Corr. 1969. Brown
85. Revue de Metallurgique 66. 11. p.741. Sonnino, Gulbramsen, Hasan & Cottey
86. Corr. Sci. 1969. V9 No. 8. p.631 Newman & Schrier
87. T.A.I.M.E. 1958 V212 p.192 Cotterell
88. Met. Prog. 85. p75. Gray & Troiano
89. T.A.I.M.E. 1962 V224 p775 Tetelman, & Robertson

REFERENCES - CONT.

90. B.C.J. 1967 V2. May, Rowlands & Bentley
91. T.A.S.M. V59 p.991. Worke & McCall
92. 4th Int. Conf. on Metallic Corr. Humphries & Parkins

The Following were also consulted for Reference

Met. Rev. 1964 V9 No. 35 p.201 R.N. Parkins
A.S.T.M. 425 Stress Corrosion Testing
The Stress Corrosion of Metals - Logan - J. Wiley
Corrosion & Corrosion Control - Uhlig - J. Wiley
Corrosion V 1 & 2 L. L. Shrier
Fracture of Structural Materials - Tetelman & McEvily
Plain Strain Fracture Toughness Testing - A.S.T.M.
Met. Rev. 129 - Brown.

ACKNOWLEDGEMENTS

The author wishes to thank Dr. R. N. Parkins for his continued interest throughout this work, Professor N. J. Petch for providing the facilities of the Department, the Science Research Council for financial support, and colleagues in the Department for their useful discussion.